Physics Modelling and Adaptive Signal Processing Filter for Online Condition Monitoring and Remaining Useful Life Prediction of Lithium-ion Battery

El-Dalahmeh, Mo'ath

School of Computing, Engineering and Digital Technologies

A thesis submitted in partial fulfilment of the requirements of Teesside University for the degree of Doctor of Philosophy

May 2023

Acknowledgements

First and foremost, I would like to praise Allah the Almighty, the Most Gracious, and the Most Merciful for giving me the patience to complete this work, Praise to God.

I would also like to express my deep, sincere gratitude towards all my supervisors, Dr Maher Al-Greer, Dr Imran Bashir and Prof. Michael Short, for their valuable input, guidance, and support. Their expertise in their respective fields and their commitment to academic excellence have been instrumental in helping me to refine my ideas and achieve my research goals. I would also like to extend my thank to Dr Maher Al-Greer, for his invaluable mentorship, expertise, and encouragement throughout the entire research process. His insightful feedback, constructive criticism, and timely support have been instrumental in shaping the direction and quality of my work.

I am also grateful to my twin brother Ma'd, who provided helpful comments, suggestions, encouragement, and collaboration in the battery research during this study. His insights, feedback, and support have been invaluable in helping me to refine my arguments and improve the clarity and coherence of my work.

My sincere thanks go to my fellow researchers and colleagues at the M7.06 office for the stimulating discussions, shared experiences, and camaraderie. I particularly want to thank Ahmed Gailani, Princewill Ikpeka, and Vishak Dudhee for their friendship, encouragement, and invaluable assistance during challenging times.

I am especially grateful for the unwavering support and friendship of Hazim, Bassem, Loay, and Obada. Your encouragement, assistance, and laughter have made this challenging journey an enjoyable and memorable experience. I am truly blessed to have you all as friends.

Finally, my deepest appreciation goes to my father and mother, whose unwavering love, support, and encouragement have been my pillars of strength and inspiration throughout my life. Their sacrifices, guidance, and prayers have been instrumental in shaping my personal and academic journey, and I owe my success to their unwavering belief in me. I warmly thank all my brothers and sisters for their constant love, support, and encouragement. Your support has been invaluable in helping me overcome the challenges and obstacles I faced during this

journey. Last but not least, I would like to express my profound gratitude and love to my fiancée, Reem. Your unwavering support, encouragement, and patience throughout this journey have been a constant source of inspiration and motivation. Your belief in me and my abilities has helped me overcome many challenges, and your love has been a guiding light throughout this journey.

Abstract

Lithium-ion batteries (LiBs) are widely used energy storage resources and provide a supply for many electrical applications, such as electric vehicles (EVs), and grids, etc. This is due to LiBs characteristics such as lightweight, high-energy density, compact size, and extended life. Despite their advantages, LiB performance is inherently subject to decreases over time due to the degradation of their electrochemical components. Moreover, in service, they may fail to supply the required energy, leading to the breakdown of the whole host application. Therefore, monitoring battery degradation and accurately predicting the remaining useful life (RUL) in LiBs has become critical to enhance performance as well as optimising battery life. It is imperative to consider various parameters and conditions, including but not limited to the consistent operating temperature, charging and discharging cycles, voltage levels, current usage patterns, state of health (SoH), and prevailing environmental factors such as humidity and pressure. Furthermore, the calibration and validation of the prediction model must align with the specific type of LiBs and their applications, employing historical data and usage statistics to optimise accuracy and reliability in predicting RUL, thereby enhancing both performance and optimisation of battery life. For this reason, this thesis focuses on accurately estimating the RUL of LiBs by developing a framework of a model-based battery coupled with a novel adaptive filter technique.

The thesis presents a novel approach for predicting the RUL of LiBs using the Smooth Particle Filter (SPF) Based Likelihood Approximations algorithm. The proposed algorithm provides various advantages over the classic Particle filter method, including the capability to handle complicated nonlinearities and uncertainties in battery behaviour. Hence, the majority of methods necessitate special consideration to enhance the estimation's convergence rate and stability. The intrinsically noisy estimation is the fundamental obstacle in predicting the likelihood functions and derivatives. Consequently, there is an urgent need for a comprehensive and adaptable battery model, coupled with a precise nonlinear estimation algorithm, to address these challenges and improve battery RUL prediction. The results showed that the proposed algorithm can predict the RUL of LiBs with high accuracy and convergence rate compared to the classic PF algorithm, making it a promising tool for battery management systems.

Moreover, an improvement to the proposed Physics based informed SPF algorithm for RUL prediction of LiBs framework is presented by simultaneously considering multiple degradation mechanisms. This includes losses of active materials of the positive and negative electrodes and the loss of lithium inventory. The proposed approach uses a half-cell model to estimate degradation parameters from voltage and capacity measurements. This allows for quantifying the degradation mechanisms and predicting the capacity fade trend based on the estimated parameters. Unlike traditional capacity-based prognostics, which rely solely on the empirical capacity fade trend, the proposed approach offers a more comprehensive and accurate way to predict battery RUL. To ensure a reliable framework, accurately and rapidly estimating the initial parameters of the degradation model is crucial to prevent the gradient error from increasing during the prediction process. With this consideration, this thesis proposes a new hybrid approach that integrates data-driven and model-based approaches to enhance the accuracy of online prognostic health management prediction within the current framework. The proposed framework employs a Neural Network (NN) to model and monitor battery degradation trends while also determining the initial values of the degradation model under varying operating conditions. The results show that the proposed hybrid framework is more accurate and improves the convergence rate compared to the traditional capacity prognostic framework.

Contents

List of Figures

List of Tables

Nomenclature

ANN	Artificial Neural Network
ARIMA	Autoregressive Integrated Moving Average
CNN	Convolutional Neural Network
CVAE	Conditional Variational Auto-encoder
DL	Deep Learning
DNN	Deep Neural Network
ECM	Equivalent Circuit Model
EKF	Extended Kalman Filter
EM	Empirical Model
EMPF	Extended Mutated Particle Filter
EoS	End of Service
GHPF	Gauss-Hermite Particle Filter
GPR	Gauss Progress Regression
HPPC	Hybrid Pulse Power Characterisation
KAF	Kernel Adaptive Filter
KF	Kalman Filter
LLI	Loss of Lithium Inventory
LORPF	Linear Optimisation Resampling Particle Filter
LSTM	Long Short Term Memory
MCMC	Markov Chain Monte Carlo
ML	Machine Learning
NLLS	Non-Linear Least Squares
P2D	Pseudo-2-Dimensional Model
PBM	Physics Based Model
PDE	Partial Differential Equation
PDF	Particle Density Function
PF	Particle Filter

RAPF	Regularised Auxiliary Particle Filter
RBPF	Rao-Blackwellized Particle Filter
RMSE	Root Mean Square Error
RNN	Recurrent Neural Network
RUL	Remaining Useful Life
RVM	Relevance Vector Machine
SCKF	Spherical Cubature Kalman Filter
SEI	Solid Electrolyte Interface
SGM	Sliding Window Grey Model
SOC	State of Charge
SOH	State of Health
SPM	Single-Particle Model
SVM	Support Vector Machine
SVR	Support Vector Regression
UDDS	Urban Dynamometer Driving Schedule
UKF	Unscented Kalman Filter
UPF	Unscented Particle Filter

Chapter 1 Introduction

1.1 Motivation of the Proposed Research

Nowadays, reliance on lithium-ion batteries (LiBs) has increased enormously. They are used as energy storage units in several fields, such as electrical transmission systems, smart grids, and portable electronic devices, due to their long life span, high energy density, and low-self discharge [1]. However, due to the degradation mechanism of their electrochemical ingredients, LiB performance diminishes with operating time, increasing internal resistance and diminishing capacity and power [2]. These degradation phenomena cause a failure to meet energy requirements, which could lead to burning or battery explosion and significant economic losses [3]. To avoid this failure, accurate online monitoring of Prognostic Health Management (PHM) is critical to the functioning of the Battery Management System (BMS) and thus to guaranteeing that LiBs operate reliably and safely.

BMS can ensure that the battery operates within safe limits, prevent damage due to overcharging or over-discharging, and provide early warning of any issues. The BMS can also help maximise the battery's energy and power delivery capabilities by balancing the charge across cells and monitoring the state of charge (SoC) and health of each individual cell.

Figure. 1.1 depicts a lithium-ion battery pack from a Toyota Prius vehicle damaged by fire [4]. The reason for the failure is believed to be strongly associated with a faulty BMS, which caused some of the individual battery cells to undergo a thermal runaway event. From Figure. 1.1, a reliable BMS is of utmost importance when it comes to safety-critical battery applications, especially in electric vehicle systems, where a battery failure of the aforementioned nature can directly put the passenger’s lives at risk. The significance of a reliable BMS is also evident in battery-powered portable electronic devices, where consumer convenience and safety are top priorities for battery system designers as shown in Figure 1.2. A robust BMS offers additional benefits, such as prolonging the battery's service life by operating it under favourable conditions and avoiding operation beyond the manufacturer's recommended limits.

Figure 1. 1 Example of a Fire damaged vehicle and battery cells in Toyota Prius vehicle [4].

Figure 1. 2 Functions of BMS.

BMS is responsible for various hardware and software operations to ensure the battery always remains in a safe condition. The battery monitoring system is a central component of the BMS and conventionally performs several critical tasks [5], including:

- Monitoring battery voltage, current, and temperature to ensure the battery operates within safe limits.
- Controlling battery charging and discharging to prevent overcharging, over-discharging, and overheating.
- Balancing the charge levels of individual cells or modules to ensure even wear and extend battery life.
- Provide fault detection and diagnostics to alert the user or system in case of abnormal battery behaviour or malfunctions.
- Implementing safety measures, such as thermal management, insulation, and fusing, to prevent fire, explosion, or electrical hazards.

1.2 The Challenge of Battery RUL Prediction

Despite the importance of RUL prediction, it remains a challenging task. There are several challenges in accurately predicting the RUL of LiBs. One major challenge is the lack of historical data [6]. Batteries in real-world applications are subject to a wide range of operating conditions and usage patterns, making it difficult to collect sufficient data for accurate prediction [7]. Additionally, the aging process of batteries is complex and affected by many factors, such as temperature, SoC, and usage history. Therefore, predicting RUL accurately requires a comprehensive understanding of the degradation mechanisms and the ability to model and analyse the complex data [8]. Another challenge is the changes in future aging. Aging is a dynamic process, and the future aging of a battery is affected by both its current state and its future usage conditions [9]. Accurately predicting the future aging of a battery requires the ability to model and analyse the complex data and incorporate the uncertainties in future usage conditions.

To address these challenges, researchers have been developing new methods for RUL prediction. One approach is to use physics-based models that incorporate the fundamental physics of the battery chemistry and structure [10]. These models can provide a more accurate prediction of the degradation mechanisms and RUL. Another approach is to use data-driven models, such as Bayesian method, neural networks, and machine learning algorithms [11], to analyse the large amounts of data collected from batteries in real-world applications. These models can identify patterns and trends in the data to predict RUL accurately.

There are also opportunities in the development of RUL prediction methods. The increasing use of LiBs in a variety of applications, from electric vehicles to grid storage systems, provides a wealth of data for analysis and model development [12]. The rapid advancements in computing power and data analysis techniques provide new tools and opportunities for more accurate and efficient RUL prediction [13].

1.3 Contribution

This thesis is focused on online battery modelling and identification techniques, which lead to the development of a framework-based battery status monitoring system. Below is a summary of the contributions developed in this thesis:

- **Enhance the RUL Prediction of Lithium-ion (LiB) Batteries**: By smoothing the Particle filter (PF) with a combination of Likelihood Approximations and a second-order degradation model. The proposed Smoothing Particle Filter (SPF) algorithm improves the RUL prediction's accuracy by selecting the proposal distribution and resampling weights based on current parameter estimates, effectively addressing the issue of particle impoverishment and uncertainty in the degradation model parameters. This contribution is crucial in improving the performance and reliability of RUL prediction for LiBs compared to the conventional PF method. The SPF method exhibits an impressive reduction in absolute prediction error, improving accuracy by approximately 14 cycles, equating to an 11.2% improvement in the total battery

lifecycle, which is set at 125 cycles. Furthermore, in relative terms, the SPF method substantially decreases the relative error by 0.112, representing an 82.35% reduction. The computational complexity of predicting the RUL for the batteries via the proposed SPF method involves intricate calculations, requiring the sequential processing of non-linear dynamics through kernel smoothing and resampling techniques; this complexity often entails a substantial computational burden but yields a robust mechanism for tracking the multifaceted degradation processes inherent in LiBs systems.

- **Integration with Reduced Ordered Single Particle Model (ROM):** By utilising the ROM, the coefficients for three main degradation phenomena (active material loss in positive and negative electrodes, and loss of lithium inventory) can be extracted. These parameters are directly correlated with RUL predicting of LiBs. The proposed physics-based predictive framework provides more accurate early predictions of the late-stage fading trend than the conventional capacity-based prognostic framework. The degradation parameters obtained from the single particle model are then fed into a SPF algorithm, which is adopted due to its robustness, simplicity, and computational efficiency compared to other particle filters. The deployment of the physics-based model informed SPF for RUL prediction of LiBs resulted in a considerable decrease in absolute error from 55 to 8 cycles (~85% improvement) and substantial reductions in RMSE from 0.0083 to 0.003 (~64% improvement) and RE from 0.0229 to 0.0035 (~85% improvement). The proposed solution accurately represents the degradation coefficients and capacity decay of LiBs when a suitable mathematical model is available.
- **Hybrids RUL Prediction and Parameter Estimation:** The current limitations of online RUL prediction techniques lie in their inability to account for capacity degradation variations across different battery cells and operating conditions, which can lead to inaccurate predictions. This work proposes a hybrid approach to enhance the accuracy of online RUL forecasting by integrating both data-driven and model-based approaches. The proposed framework utilises a NN to model and monitor battery degradation trends, while also accounting for the degradation model's initial values

under varying operating conditions. This approach addresses the limitations of the existing framework and offers a more accurate and reliable method for online RUL prediction. The novel hybrid approach engendered a substantial enhancement in the prediction of lithium-ion battery lifespan, reducing the absolute error by approximately 59 cycles (~93%) and lowering the Root Mean Square Error from $0.0532\ to\ 0.0209$ (~61%) compared to the traditional empirical model framework. These advancements signify a considerable stride in LiB health management, potentially catalysing increased efficiency and reliability in their usage across various sectors.

1.4 Aim and Objectives of the Thesis

Accurate prediction of the RUL in LiBs is a key aspect of managing their health, in order to promote reliable and secure systems, and to reduce the need for unscheduled maintenance and costs. To this end, the main aim of this thesis is to develop framework of a model-based of the battery integrated with a new adaptive filter algorithm to accurately predict the RUL of LiBs. The proposed SPF algorithm is based on the Sequential Monte Carle algorithm. According to the literature review, many approaches are proposed to predict the safety cycle life of the batteries. Particular attention is given to model-based RUL approaches by modelling the degradation of the battery through mathematically models and corresponding parameters.

In order to quickly and accurately predict the RUL of LiBs, a new SMC adaptive algorithm known as the SPF Based Likelihood Approximations algorithm is proposed. Most approaches require particular attention to improve the convergence rate and stability of the estimation. The key challenges of the prediction of the likelihood functions and derivatives are an inherently noisy estimation. Therefore, to mitigate the problems, a general and flexible battery model with an accurate non-linear estimation algorithm is urgently needed for battery RUL prediction. A significant conclusion from the work is that the SPF can achieve more precise prediction performance and improve the convergence rate compared to the standard PF algorithm. In addition, an enhancement of the proposed framework is suggested by simultaneously

considering multiple degradation mechanisms, including the losses of active materials of the positive and negative electrodes and the loss of lithium inventory. Unlike traditional capacity-based prognostics that exclusively relies on the empirical capacity fade trend, the proposed approach leverages a half-cell model to:

1. Estimate degradation parameters from voltage and capacity measurements to quantify the degradation mechanisms.
2. Predict the capacity fade trend based on the estimated parameters. The concept of this framework is presented in the thesis, and the advantages it delivers are discussed.

Furthermore, to achieve a robust framework, the initial parameters of the degradation model should be estimated quickly and accurately to avoid increasing the gradient error during the prediction process. With this issue in mind, this thesis proposes a hybrid approach to improve the accuracy of online prognostic health management prediction in the existing framework by integrating data-driven and model-based approaches. The proposed framework utilises the NN to model and track battery degradation trends, and it also degrades the initial values of the degradation model's transactions under different operating conditions. The following objectives were accomplished to meet this aim:

1. To identify the gap in the literature and develop a new adaptive scheme; therefore, a comprehensive literature review was conducted on the latest state-of-the-art life cycle prediction techniques for LiBs (Addressed in Chapter 2).
2. To develop a novel algorithm to improve the performance of the prediction process. This objective was achieved by fully investigating and developing the proposed new method on estimating the RUL of LiBs based on SPF. This method appears to be more effective than a traditional method like the PF and UPF. Comparison of the various methods are performed based on a dataset from the Prognostics Centre of Excellence NASA using non-linear characteristics degradation properties (Addressed in Chapter 3). This objective was achieved through the following tasks:

Task 1: Design an adaptive prognostic empirical model. The task is to identify the parameters that affect battery degradation and develop a model that can accurately predict the battery's future performance.

Task 2: Implement the SPF based on the experiential data. The model should learn from the historical data to identify patterns, trends, and anomalies.

3. To develop a RUL prediction algorithm based on estimation of parameters of a Single Particle Model (SPM) that could be implemented using vehicle charging data. The developed model will be integrated with the proposed SPF in point 2 (Addressed in Chapter 4). This objective will be achieved through the following tasks:

Task 1: Develop an SPM that describes the behaviour of the battery during charging. The SPM should consider the charging profile and the properties of the battery, such as the capacity, internal resistance, voltage limits, and the formation of the Solid Electrolyte Interphase (SEI) layer on the cathode.

Task 2: Correlate the parameters of the SPM with the state variables of the SPF algorithm; these parameters can be identified by applying specially designed current excitations to the battery. The SPM based capacity simulation process is taken as the observation equation in the SPF algorithm framework.

4. Develop a hybrid prediction technique based on the adaptive filter method and a machine-learning algorithm to investigate the effect of the initial guesses of model parameters on the prediction results to identify the optimum initial parameters by using the Machine Learning (ML) algorithm. A deep neural network with algorithms, and pre-trained models (Addressed in Chapter 5). This objective will be achieved through the following tasks:

Task 1: Extract the initial parameters. The model should learn from the historical data to identify patterns, trends, and anomalies. The model should be able to adapt to changing conditions and incorporate new data.

Task 2: Develop an NN model and integrated with SPF algorithm to monitor and predict system performance. The model should be integrated with real-time data and provide alerts and notifications when anomalies or failures are detected.

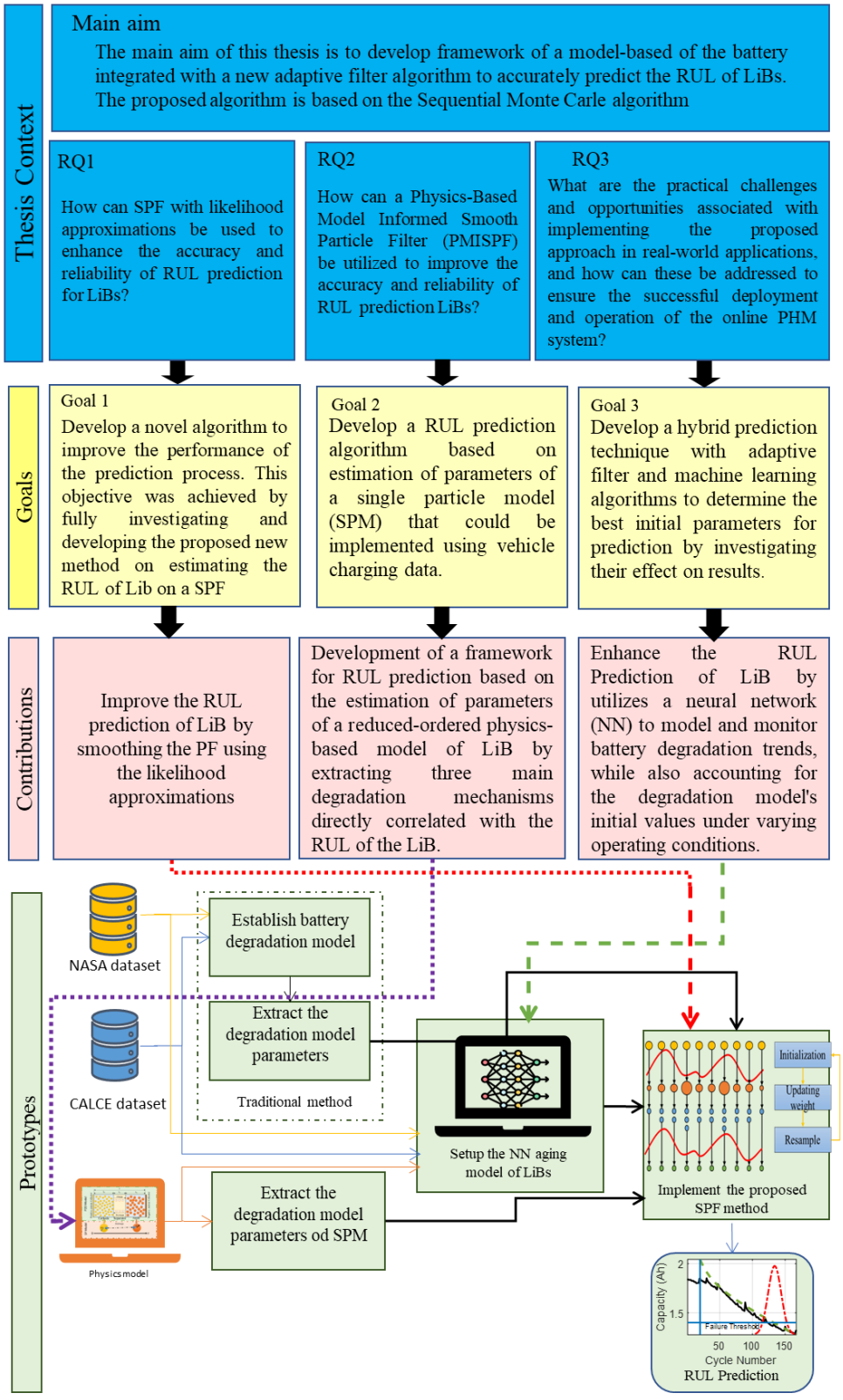
Thesis Context
Main aim
The main aim of this thesis is to develop framework of a model-based of the battery integrated with a new adaptive filter algorithm to accurately predict the RUL of LiBs. The proposed algorithm is based on the Sequential Monte Carle algorithm
RQ1
How can SPF with likelihood approximations be used to enhance the accuracy and reliability of RUL prediction for LiBs?
RQ2
How can a Physics-Based Model Informed Smooth Particle Filter (PMISPF) be utilized to improve the accuracy and reliability of RUL prediction LiBs?
RQ3
What are the practical challenges and opportunities associated with implementing the proposed approach in real-world applications, and how can these be addressed to ensure the successful deployment and operation of the online PHM system?
Goals
Goal 1
Develop a novel algorithm to improve the performance of the prediction process. This objective was achieved by fully investigating and developing the proposed new method on estimating the RUL of Lib on a SPF
Goal 2
Develop a RUL prediction algorithm based on estimation of parameters of a single particle model (SPM) that could be implemented using vehicle charging data.
Goal 3
Develop a hybrid prediction technique with adaptive filter and machine learning algorithms to determine the best initial parameters for prediction by investigating their effect on results.
Contributions
Improve the RUL prediction of LiB by smoothing the PF using the likelihood approximations
Development of a framework for RUL prediction based on the estimation of parameters of a reduced-ordered physics-based model of LiB by extracting three main degradation mechanisms directly correlated with the RUL of the LiB.
Enhance the RUL Prediction of LiB by utilizes a neural network (NN) to model and monitor battery degradation trends, while also accounting for the degradation model's initial values under varying operating conditions.
Prototypes
NASA dataset
CALCE dataset
Establish battery degradation model
Extract the degradation model parameters
Traditional method
Physics model
Extract the degradation model parameters od SPM
Setup the NN aging model of LiBs
Initialization
Updating weight
Resample
Implement the proposed SPF method
Capacity (Ah)
2
1.5
Failure Threshold
50
100
150
Cycle Number
RUL Prediction

Figure 1. 3 Overview of the context, goals, contributions, and prototypes.

1.5 Publications and Awards

1.5.1 Publications

1. **M.o'ath. El-Dalahmeh,** M. Al-Greer, M. d. El-Dalahmeh, and I. Bashir, "Physics-based model informed smooth particle filter for remaining useful life prediction of lithium-ion battery," Measurement, vol. 214, p. 112838, 2023/06/15/ 2023.
2. **Mo'ath. El-Dalahmeh**, M. Al-Greer, M. d. El-Dalahmeh, and M. Short, "Smooth particle filter-based likelihood approximations for remaining useful life prediction of Lithium-ion batteries," *IET Smart Grid,* 2021.
3. M. d. El-Dalahmeh, M. Al-Greer, **Mo'ath. El-Dalahmeh**, and I. Bashir, "Capacity estimation of lithium-ion batteries based on adaptive empirical wavelet transform and long short-term memory neural network," *Journal of Energy Storage,* vol. 70, p. 108046, 2023/10/15/ 2023.
4. M. d. El-Dalahmeh, M. Al-Greer, **Mo'ath. El-Dalahmeh**, and M. Short, "Time-frequency image analysis and transfer learning for capacity prediction of lithium-ion batteries," *Energies,* vol. 13, no. 20, p. 5447, 2020.
5. **Mo'ath. El-Dalahmeh**, M. Al-Greer, M. El-Dalahmeh, and I. Bashir, "Online Hybrid Prognostic Health Management Prediction Using a Neural Network and Smooth Particle Filter for Lithium-ion Batteries," in *2022 57th International Universities Power Engineering Conference (UPEC)*, 30 Aug.-2 Sept. 2022 2022, pp. 1-6.
6. M. El-Dalahmeh, I. Bashir, M. Al-Greer, and **Mo'ath. El-Dalahmeh**, "Lithium-ion Batteries Capacity Degradation Trajectory Prediction Based on Decomposition Techniques and NARX Algorithm," in *2022 57th International Universities Power Engineering Conference (UPEC)*, 30 Aug.-2 Sept. 2022 2022, pp. 1-6.
7. A. Gailani, R. Mokidm, **Mo'ath. El-Dalahmeh**, M. El-Dalahmeh, and M. Al-Greer, "Analysis of Lithium-ion Battery Cells Degradation Based on Different Manufacturers," in *2020 55th International Universities Power Engineering Conference (UPEC)*, 1-4 Sept. 2020 2020, pp. 1-6.

8. M. El-Dalahmeh, J. Lillystone, M. Al-Greer, and Mo'ath. El-Dalahmeh, "State of Health Estimation of Lithium-ion Batteries Based on Data-Driven Techniques," in 2021 56th International Universities Power Engineering Conference (UPEC), 31 Aug.-3 Sept. 2021 2021, pp. 1-6.
9. M. El-Dalahmeh, P. Thummarapally, M. Al-Greer, and **Mo'ath. El-Dalahmeh**, "Time and Frequency Domain Health Indicators for Capacity Prediction of Lithium-ion Battery," in *2021 56th International Universities Power Engineering Conference (UPEC)*, 31 Aug.-3 Sept. 2021 2021, pp. 1-6.

1.5.2 Awards

- Best Paper Award "Online Hybrid Prognostic Health Management Prediction Using a Neural Network and Smooth Particle Filter for Lithium-ion Batteries"; 57th International Universities Power Engineering Conference (UPEC).
- Best Poster Award "Physics-Based Model Informed Smooth Particle Filter Based Likelihood Approximation for Remaining Useful Life Prediction of Lithium-ion Battery; 2nd World Energy Storage Conference (WESC 2022) Jointly with the 7th UK Energy Storage conference.

1.6 Thesis outline

Chapter 1-Introduction: This chapter introduces the discussion of the motivation for the research and highlights the importance of battery RUL prediction. After discussing the reasons behind the research work, this chapter identifies the challenges of battery RUL prediction. Then, this work's aim, objectives, and thesis contribution have been presented.

Chapter 2-Battery Lifetime Prognostic Technologies: This chapter shows the operation principles of LiBs and battery modelling, followed by details on degradation mechanisms. In addition, it provides a detailed analysis of battery lifetime prognostic technologies. It also focuses on the recent advances in model-based, data-driven, and hybrid approaches to battery

degradation prediction. Various methods are discussed in detail, highlighting their advantages and limitations, and a comparison of these approaches is presented.

Chapter 3 -Battery Lifetime Identification Using Smooth Particle Filter Technique: This chapter introduces a new online RUL prediction for LiB using SPF-based likelihood approximations method integrated with an empirical degradation modelling approach. The first parts of the chapter introduce the theoretical background method of the Bayesian techniques and the implementation procedures for the PF and the proposed SPF algorithms. Capacity degradation modelling for LiBs based on the experimental data collected by PCoE- NASA is demonstrated in Section 3.4.2. Then, from section 3.5 onwards, the proposed framework results are discussed.

Chapter 4-Physics-Based Modelling for Monitoring Battery Lifetime: **This chapter** proposes a new physics-informed SPF framework for RUL prediction to improve the RUL prediction framework of LiBs analysis performed in Chapter 3. The first part of this chapter provides details on the degradation mechanism modelling, such as the SEI layer formation of solid-phase LiB dynamics, loss of active material, and lithium plating. Following this, extract the three main degradation mechanisms is presented. In addition, Chapter 4 compares the empirical degradation approach with the physics-based approach. Robustness and stability analysis of the proposed framework is also discussed.

Chapter 5- Online Hybrid Prognostic Health Management Prediction: This chapter presents a novel hybrid battery identification technique that can be applied to any BESS to adaptively identify the battery's degradation parameters in real time. The first parts of the chapter introduce the proposed framework that utilises the NN method to model and track battery degradation trends. In addition, identifying the initial values of the degradation model's transactions under different operating conditions is discussed. Then, from section 5.5 onwards, the comparison results are discussed.

Chapter 6-Conclusions and Future Work: This chapter provides the conclusions drawn from the study and the significant contributions that it has been made to knowledge. It also outlines the limitations of the research and proposes suggestions for future work.

Chapter 2 Advances in Battery lifetime Prognostics

'This chapter illuminates the functional tenets of LiBs and the intricacies of battery modelling before delving into understanding their fade processes. Moreover, it furnishes an in-depth review of technologies used for estimating battery lifespan. The spotlight is also on the latest breakthroughs in forecast models derived from inherent battery behaviours, insights gleaned from collected data, and a blend of both for predicting battery deterioration. An exhaustive discussion about diverse methods, underscoring their strengths and potential constraints, is articulated, and a comparative overview of these methodologies is exhibited.'

2.1 Introduction

Battery lifetime prognostics have become increasingly important in recent years, as the use of batteries continues to grow in various industries. These technologies allow for accurate predictions of battery degradation over time, enabling better management of battery performance and reducing maintenance costs. With battery-powered devices becoming more prevalent, the development and implementation of such technologies are critical for ensuring efficient and reliable operation. The use of battery lifetime prognostic technologies involves the collection of performance data from batteries, which is then analysed using various algorithms and models. These technologies can predict battery degradation based on factors such as usage patterns, environmental conditions, and manufacturing defects, allowing for early detection of faults and timely maintenance or replacement. By enabling accurate predictions of battery life, battery lifetime prognostic technologies can help optimise battery utilisation and reduce maintenance costs. They also facilitate the development of more robust battery management systems, which can significantly extend the life of batteries and reduce the environmental impact of battery disposal. The importance of battery lifetime prognostic technologies is particularly relevant in industries that rely heavily on battery-powered equipment and systems, such as transportation, telecommunications, and renewable energy. In these applications, the reliability and efficiency of battery-powered systems are critical to their operations, and any failure or downtime can have significant financial and environmental consequences.

This chapter introduces a discourse on the operational principles of LiBs, and subsequently assesses various types of LiB models and their advantages for predictive health monitoring. Furthermore, the impact of internal battery degradation factors on battery lifespan is examined. A thorough evaluation and examination of LiB storage systems' prognostic lifetime is then conducted, with emphasis placed on recent advancements in model-based, data-driven, and hybrid methods. Consequently, this chapter highlights how the study bridges a gap in the existing literature.

2.2 Lithium-ion Battery Fundamentals

A LiB is an electrochemical storage device that can store chemical energy and convert it into electrical energy when needed. Despite significant technological improvements, the basic working principle of current electrochemical cells like LiB has remained the same since Alessandro Volta developed the voltaic pile in 1800 [14]. However, only internal parts such as electrodes, separators and electrolytes have been improved, progressing from metal discs, paper, and brine to more advanced materials.

Figure 2.1 depicts a LiB's components, including the separator, positive electrode (cathode), and negative electrode (anode). Both electrodes are made of porous material to store lithium ions within their crystal structure. A microporous separator material sits between these two electrodes to provide electrical isolation. The LiB's components are soaked in an electrolyte solution that allows lithium ions to move freely between the two electrodes. When a LiB is discharging, electrons released from the anode electrode flow to the external circuit, while ions travel through the electrolyte to be intercalated in the cathode electrode material. When a LiB is charged, the process is reversed, and the inverse mechanism occurs. Electrical current is conducted via the current collectors at both electrodes during charge and discharge, as shown in Figure 2.1.

The performance of LiBs mainly depends on the materials used to form the electrodes and electrolytes. Although most negative electrodes are typically made of graphite, silicon is a promising alternative; in contrast, for the positive electrode, various lithium metal oxides can be used to make the cathode, such as lithium manganese oxide (LMO), nickel manganese cobalt (NMC), nickel cobalt aluminium (NCA), and lithium cobalt oxide (LCO). A conductive binder is used to adhere the anode and cathode components to the current collector sheets, which are made of metal. The electrolyte is comprised of salt dissolved in a solvent such as ethylene carbonate. In most cases, the anode, separator, and cathode are rolled, stacked, and then combined into cylindrical, prismatic, or pouch cases to form the electrochemical cell that is produced when these three components are combined. When referring to battery

terminologies, these are specific terms used to describe aspects such as battery design, construction, performance, and usage. In this section, the keywords used in this thesis are defined, to support understanding of the subsequent derivation and development of useful equations for the testing and validation of the suggested battery monitoring methods (See Appendix A).

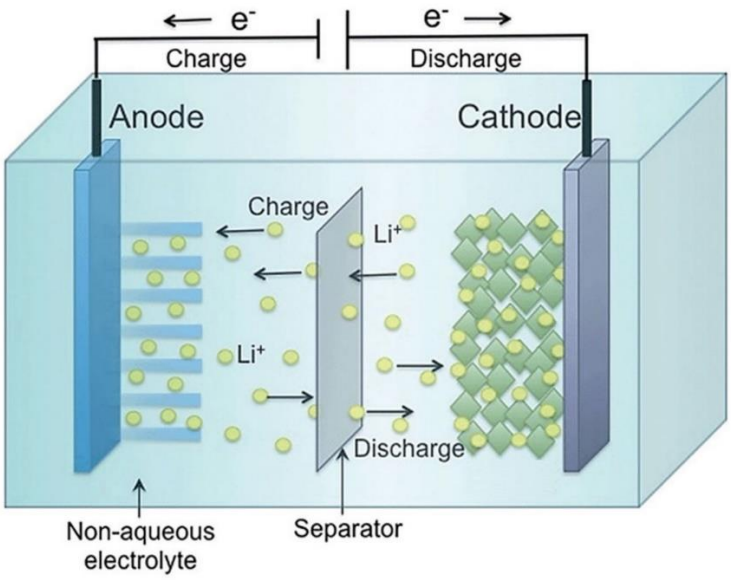

Figure 2. 1 Structure and operating principle of a lithium-ion cell [15].

2.3 An Overview of the Lithium-ion Battery Modelling Approaches

A LiB model is used to represent the behaviour of a battery and can be employed to predict the current and future internal status of the battery, such as SoC and SoH. Modelling the behaviour of LiB is important for designing and optimising these systems. There are different types of battery models, each with their own advantages and disadvantages. The most commonly used battery models are equivalent-circuit models (ECM) and physics-based models (PBM) [16,

17]. All these models have their own strengths and weaknesses, and the choice of which model to use depends on the specific application and the level of detail required. In practice, a combination of models is often used to achieve the best results.

The ECM of a LiB is a simplified representation of the battery that can be used to predict its behaviour under different conditions [18]. The model consists of a series of electrical components, such as resistors and capacitors, that are connected in such a way as to mimic the behaviour of the real battery [19].

The most basic ECM for a LiB consists of a single resistor and capacitor in series, representing the battery's internal resistance and the charge stored in the battery, as shown in Figure 2.2. This model consists of a voltage source in series with a resistance and capacitance. The voltage source represents the open-circuit voltage (OCV) of the battery, which depends on the SoC. The resistance represents the total internal resistance of the battery, including the resistance of the electrodes, the electrolyte, and current collectors. The capacitance represents the double-layer capacitance of the electrodes, which is related to the ability of the electrodes to store lithium ions. More complex models may include additional resistors and capacitors to represent various aspects of the battery's behaviour, such as temperature and ageing effects [20]. ECMs are useful for various applications, including designing and optimising BMS, predicting the performance of battery-powered devices, and understanding the factors that affect the performance and life of LiB [21].

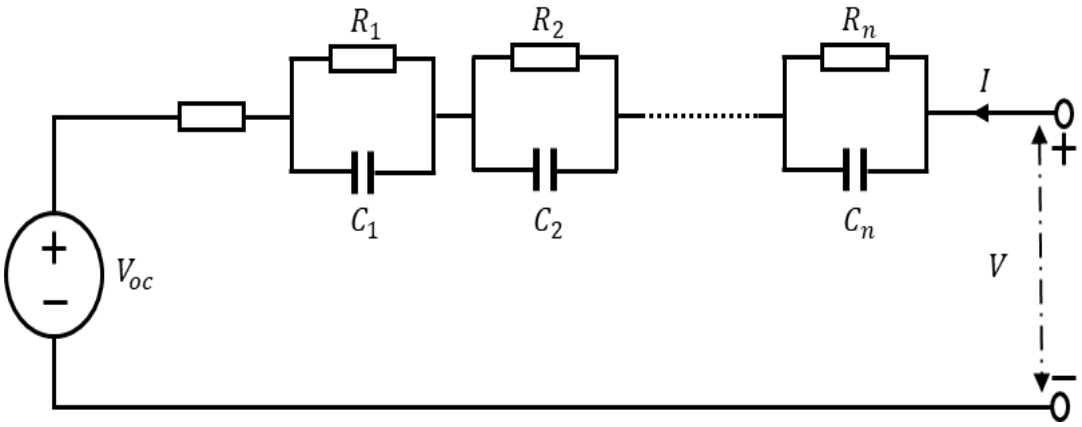

Figure 2. 2 Battery equivalent electrical circuit model.

A PBM for a LiB typically couples Partial Differential Equations (PDEs) for the electrochemical reactions at the electrodes and transport equations for the ions and electrons within the battery. These are then solved numerically using techniques such as finite element or boundary element analysis [22]. These equations can be combined with those of continuum mechanics to model the mechanical deformation of the electrodes, separator, and other components of the battery. Additionally, the model must consider the thermal behaviour of the battery, as its temperature can affect the rate of the electrochemical reactions and the mechanical behaviour of the materials [23]. The model can be used to predict the battery's performance under different conditions, such as different discharge rates or temperatures, and can help to optimise the design of the battery. The most popular PBMs are the Pseudo-2-Dimensional (P2D) model, which was developed in [24]. It simulates lithium transport and diffusion into two dimensions: inside a solid particle, and along the thickness of a cell. This makes it possible to have a concentration gradient over the thickness of an electrode, dependent on the electrolyte transport, as well as a gradient inside the particle, dependent on solid diffusion. However, due to its complex algebraic requirements and other mathematical features, the utilisation of the P2D model is computationally intensive. Therefore, it is neither optimal nor suitable for degradation simulations, which must model the whole battery life [25]. One of the simplest PBMs is the Single-Particle Model (SPM) [26], derived by omitting the 'thickness' dimension, i.e., by assuming electrolyte movement and migration, and fast

electrical conductivity in the electrodes and electrolyte [27]. However, using the SPM introduces simplifications and limitations, discussed in Section 2.5.2.3.

Models of battery deterioration or lifetime can be utilised to predict the RUL of a battery under various operating situations. There are several ways to classify battery degradation models, but one common method is based on the model's level of detail and complexity. These models can be empirical, physics models or data driven [28]. Empirical degradation models are based on experimental data and use simple mathematical equations to describe the relationship between certain inputs (e.g., current, temperature) and outputs (e.g., capacity, voltage). Empirical models are easy to use and understand, but their accuracy may be limited by the quality and scope of the data used to develop them. Physics degradation models are added to, or coupled with; the PBMs mentioned above to improve model accuracy and describe specific ageing mechanisms. They use more complex mathematical equations and require more input data, but they can provide more accurate predictions of a battery's performance over its lifetime. Data-driven models use ML techniques to extract patterns from large datasets of battery performance data. They can be more accurate than empirical models but require a large amount of data to train and can be difficult to interpret. Most examples of these models are reviewed in Section 2.5.

2.4 Battery Degradation

The internal characteristics of a LiB are complicated and exhibit nonlinear behaviour with a dynamic electrochemical system that changes over time. The performance and lifetime of a LiB continuously degrade with increasing charging and discharging cycles. There are several reasons for battery deterioration, including physical (e.g., temperature and mechanical stress) and chemical processes (e.g., side reactions). The most common battery degradation mechanisms are depicted in Figure 2.3. Various degradation mechanisms contribute to the battery's deterioration, which can be categorised into two primary degradation modes: (1) LLI resulting from the consumption of lithium ions by side reactions; and (2) LAM resulting in a

reduction in storage capacity. The sub-sections below review the principles of the main degradation mechanisms considered.

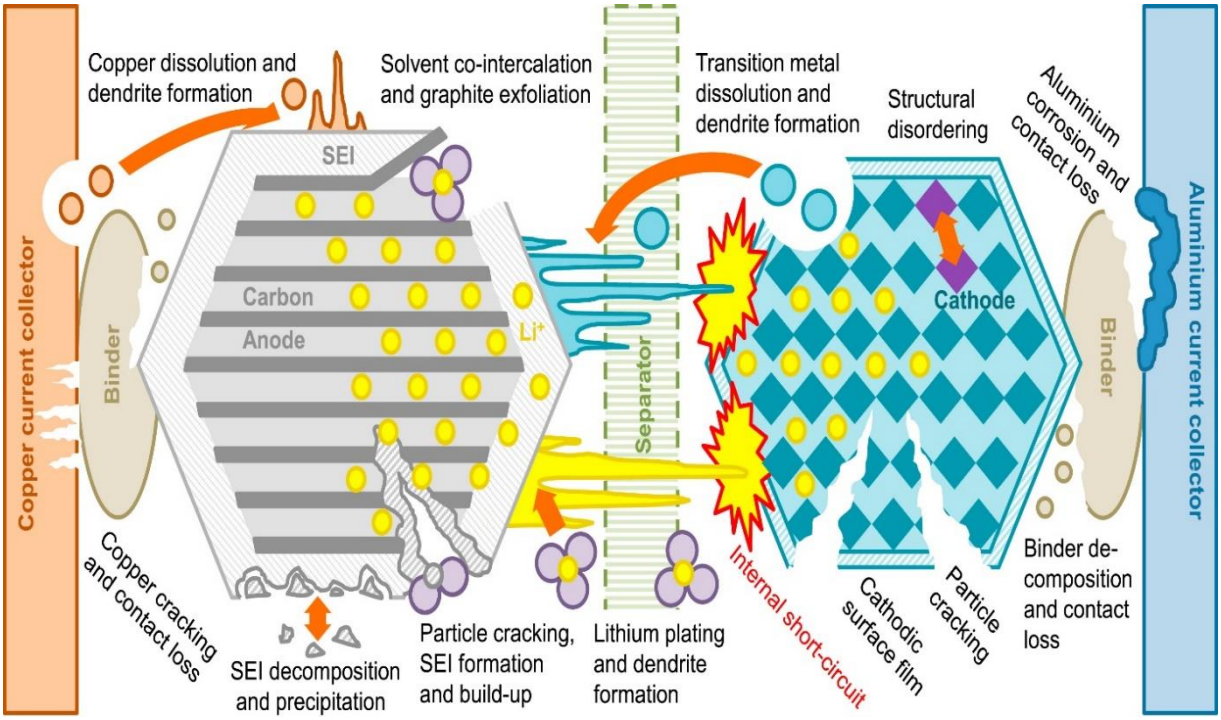

Figure 2. 3 Main Degradation Mechanisms in Lithium-Ion Batteries [29].

2.4.1 Solid-Electrolyte Interphase Layer

The formation of a SEI layer is the most pertinent degradation mechanism in LiB with graphite anodes [30]. At the graphite anode, the lithium ions react with parts of the electrolyte to form solid products that settle on the graphite surface; passivating the surface reduces the side reaction. As a result of imperfect isolation, the layer persists in expanding and consuming lithium ions. The cell's capacity decreases since these ions no longer contribute to the main intercalation process.

Studies [31-34] provide a comprehensive review of the formation of the SEI and the reactions that simultaneously occur. The authors of [35] noted that the growth rate of the layer

depends on the cell voltage and temperature; the SEI layer is significantly impacted by the material characteristics of the electrodes, electrolytes, and additives used. According to [36], the SEI layer thickness can be measured in the tens of nanometres, increasing cell impedance by around $10 - 100\ \Omega\ \mathrm{cm}^2$.

The SEI layer can potentially affect other types of degradation mechanisms, such as LAM and LLI. In related chemical processes, gases can be generated [37], and the SEI layer can block pores in the anode. Isolating active material in pores can reduce the active surface area, aiding other modes of deterioration, such as lithium plating.

2.4.2 Growth of Cracks on the Electrode's Surface

The process of lithium intercalation results in changes in the volume of the host material. When a cell cycles, it experiences alternate status of tension and compression due to the alternating strain caused by the cell's expansion and contraction [38]. Phase transitions in the electrode material can also cause volume changes and resultant pressures.

Crack development is frequently brought on by alternating stress cycles (e.g., in metal fatigue). If the SEI layer develops fractures, it can break apart, allowing the electrolyte to come into contact with a fresh graphite surface [39]. Consequently, a new layer of SEI is produced on these surfaces, accelerating the rate at which the SEI side reaction consumes lithium ions [40]. Solvent co-intercalation can also cause cracks, leading to the same consequence [41].

2.4.3 Loss of Active Material (LAM)

LAM is a phenomenon that can affect either the positive or negative electrodes. This mode categorises methods which lead to a decrease in the amount of material accessible for electrochemical action, leading to lithium-ion loss. Several mechanisms of degradation can cause LAM. For instance, the authors in [42] described how pores in the positive electrode become blocked by the gaseous carbon dioxide (CO_2) and SEI layer, preventing lithium ions

moving from the positive into the negative electrode material. However, these lithium ions are forced into a side reaction that promotes the formation of the SEI layer.

Additionally, the electrical contact between the active material and the current collector may be lost [30]. This frequently occurs analogous to the process described in the previous section regarding surface cracks; however, cracks grow within the electrode in this case. This results in the material breaking off or losing contact with the binder [40], preventing the lithium from (de)intercalating, as no electrons can reach the current collector and vice versa. Therefore, the material is passivated [43].

2.4.4 Lithium Plating

On the anode electrode side of the LiB, lithium plating is an undesirable side reaction that occurs when lithium ions are reduced to metallic lithium rather than intercalating into the anode crystal structure [44]. In addition, the production of dendrites is made possible by the deposition of metallic lithium on the negative electrode. This phenomenon occurs when the potential of the local anode falls below 0 V [45]. Lithium plating can be localised in the presence of graphite anode surface heterogeneity, but can also be caused by slow diffusion processes, slow intercalation kinetics, and high SEI film resistances in the anode, caused by low temperatures or high current rates [41].

The plating side reaction, similar to the SEI layer, takes lithium from the primary intercalation reaction and this leads to the loss of lithium inventory, resulting in decreased cell capacity [46]. When plated lithium is present, it can cause excessive development of the SEI layer. Because dendrite growth may lead to internal short circuits and an exothermic reaction can induce thermal runaway, this also poses a safety issue.

2.5 Classification of RUL Prediction Techniques

The battery health predictor is an essential component of BMS which gives information about the time the battery system has left to perform its intended functions. Monitoring battery degradation, forecasting battery status, and improving maintenance have therefore become

important focal points in LiB engineering research, to improve battery performance and reliability. To do so, an accurate estimate of a battery's RUL and SoH is required. Various techniques for battery capacity estimation have been developed to enable the prediction of future changes in SoH as a function of usage history. Battery RUL prediction cannot exist independently, as it requires the SoH estimator's information to function correctly; Figure 2.4 depicts their relationship [47].

In general, predictive methods can be split into three state-of-the-art paradigms of RUL predictions for LIB, such as [47]: model-based, data-driven, and hybrid methods (see Figure 2.5). The model-based approach requires the development of an ageing physics-based model and an empirical ageing model to construct the capacity fading path for LiB. In contrast, the data-driven approach does not require an ageing model and can instead learn from the ageing data to predict changes in battery health. The third, hybrid approach is developed to integrate the best features of both previous approaches. The benefits and drawbacks of these methods are compared below.

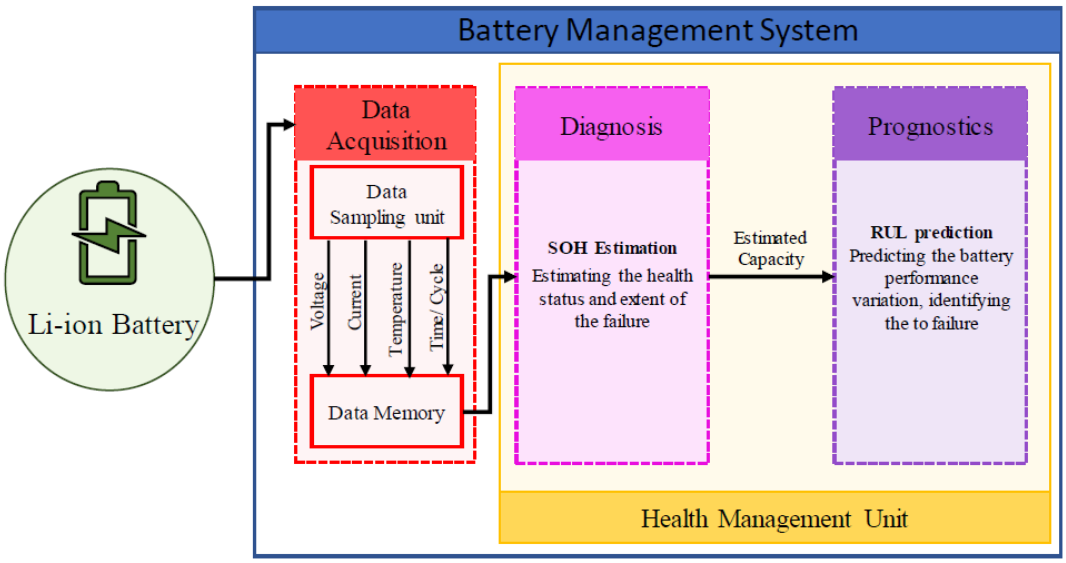

Figure 2. 4 BMS health diagnostics and prognostics algorithm framework.

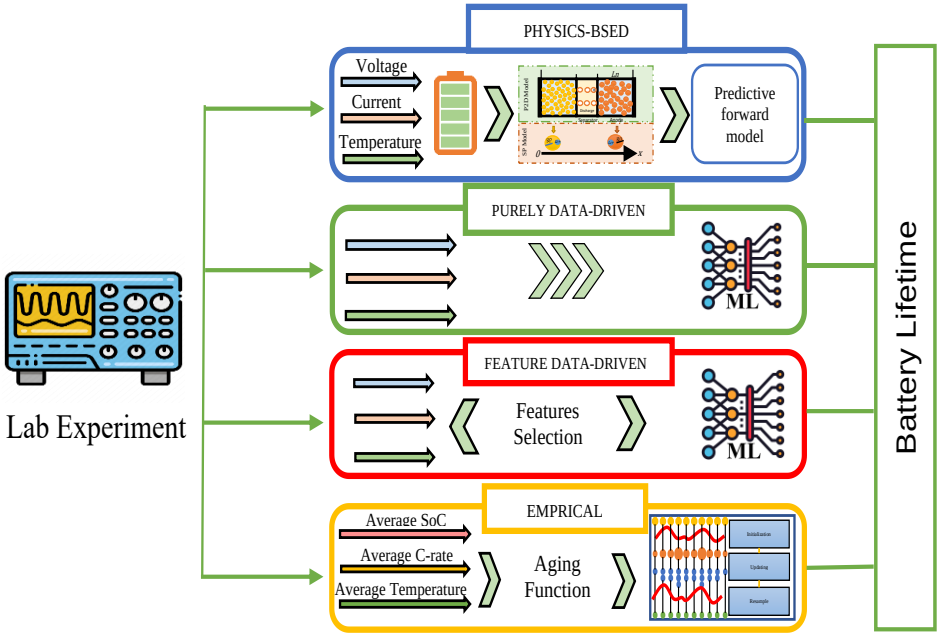

Figure 2. 5 Different approaches to battery RUL prediction.

2.5.1 Data-driven Approaches for RUL Prediction

Data-driven systems directly forecast the deterioration trajectory of a battery based on historical monitoring data, even though its causes and propagation rules are unknown [48]. Furthermore, this approach develops a mathematical model or derives weight parameters based only on training data, as opposed to adopting a particular physics-based model [8]. The data-driven techniques have been subdivided into purely data-driven and feature data-driven, as shown in Figure 2.4.

2.5.1.1 Purely Data-Driven Methods

Purely data-driven methods take directly measured data, such as voltage, current, impedance and temperature, as input for machine learning models [49, 50]. Data-driven techniques have shown significant promise in estimating the present SoH of the battery. So far, limited application to date can be found of data-driven techniques for the prognostics of LiBs, possibly due to certain limitations they face. For instance, the deep long short-term memory networks method was proposed in [51] to estimate the capacity and predict RUL based on experimental voltage-time sensor data, but accuracy was impacted due to a lack of training data, possibly due to a shortage of data. Although each cell contains hundreds of cycles which can be used as training data for an SoH estimate, the lifecycle of each cell is only a point in time in data per cell [8]. Another drawback of data-driven techniques is that the models for large sets of purely data-driven approaches rely on raw data as input, thus making the applicability to lifetime estimation more complex, since extensive, inclusive, unbiased, and good quality data are needed to train the models [52]. According to [13-15], a ML model can be trained to learn how much capacity fading happens over a short interval of time, depending on the existing capacity, current, or temperature during the period in question. This method is called forward simulation [47, 52, 53]. Thus, the RUL can be forecast by combining the capacity fades for each of these periods and looking at where the resulting trajectory crosses the failure threshold of the End of Service (EoS) (80% of nominal capacity).

2.5.1.2 Feature-Based Data-Driven Methods

To solve the limitations of purely data-driven techniques, research focus has shifted to feature-based data-driven methods. With feature extraction data-driven models, a pre-processing step is included which extracts certain features from capacity, current and voltage data that inform the physical behaviour of the cell [54]. This step is called the feature extraction step. These features are then employed as inputs to ML algorithms [55]. For example, a probabilistic prediction approach for a LiB lifecycle was proposed in [56] by merging the Bayesian Least Squares Support Vector Regression (LS-SVR) and the wavelet neural network to predict the diminishing capacity of a LiB. The authors in [19] proposed a Hybrid Pulse Power Characterisation (HPPC) evaluation of the first-order Randle's technique for prediction of a battery's SoH using a three-layer back-propagation neural network. The proposed strategy required a great deal of time to collect the necessary data because of the lack of a physical interpretation of model parameters. Another example in [57] is a simple, regularised linear regression model, demonstrating that characteristics derived from differences between successive cycles may provide highly accurate lifetime predictions. In [58], the authors used more features and a more efficient ML algorithm to increase the accuracy of this method (lower prediction error with fewer cycles). Data-driven techniques, such as the statistical model [59], autoregressive (AR) model [60], Gaussian process regression (GPR) [61], NN support [49], and vector machines [62], have frequently been employed for battery RUL prediction. Nevertheless, such approaches tend to depend strongly on the measurement data employed in the simulation, and the findings on prediction are less precise than those produced from model-based approaches [13].

2.5.2 Model- Based Approach for RUL Prediction

Model-based approaches are comprised of a mathematical model, empirical model, and algebraic equations and include a wide range of ageing data measured under operational laboratory conditions. Using model-based methods, battery degradation behaviour can be determined using a physics or regression model, and the results can then be extrapolated to

predict how well a battery will perform. For long-term forecasts, the physics model demonstrates more accurate prediction outcomes than the empirical model, which lacks prediction accuracy and leads to a significant error. Accordingly, empirical models are associated with filtering techniques [63]. These can update the parameters of the model as part of the diagnostic process to ensure accurate long-term RUL prediction. The following sub-sections describe the categories of model-based methods.

2.5.2.1 Equivalent Circuit Model (ECM)

ECM is developed by analysing batteries' chemical and physical processes. This analysis leads to the identification of combinations of circuit elements that produce a similar electrical behaviour as batteries. Therefore, methods of circuit analysis can be utilised to develop mathematical models that characterise the LiB's dynamic response and degrading behaviour [64]. The formation of the SEI layer causes the internal resistance to increase progressively over time. Electrochemical Impedance Spectroscopy (EIS) data can be utilised to detect ECM parameters and battery RUL can be predicted using a regression model [65]. The author in [66] developed a framework for predicting RUL using the internal resistance growth model and the PF method for updating model parameters. Based on the internal resistance development model, several strategies for enhancing the performance of the filtering algorithm have been presented. For instance, in [67], the authors proposed a Mutated Particle Filter (MPF) designed for enhanced battery RUL prediction accuracy by overcoming particle diversity loss, also referred to as sample impoverishment. Nonetheless, the proposed MPF algorithm randomly produces mutated particles without a feedback mechanism. As a result, an enhanced MPF algorithm was presented in [68], which employed a dynamic feedback mechanism to explore the posterior space more efficiently and resource-effectively. This method also took into consideration prior information concerning the high-likelihood area. In another illustration, a Regularised Auxiliary PF (RAPF) was constructed to estimate and then update the parameters of the model that depict the evolution of exponentially increasing resistance [69]. The proposed RAPF improves particle diversity by standardising the empirical distribution, and it is made more resilient by using a rejection resampling strategy. The authors in [70] used the Linear

Optimisation Resampling PF (LORPF) with the Sliding-window Grey Model (SGM) to forecast the RUL of LiBs. The suggested SGM-LORPF resolved the problem of inconsistent samples and enhanced the traceability of the PF method. The SGM-LORPF-based technique showed improved prediction accuracy for LiB. However, EIS tests take a great deal of time in real-time applications, and the necessary equipment is not always accessible. EIS serves as a vital sign for lithium-ion battery health, but traditional methods are offline and need manual input. To monitor battery health in real-time, this work [71] presents a cutting-edge approach using a fractional-order equivalent circuit model (FOECM) for online EIS estimation. First, using current and voltage measurements, the model's parameters are figured out with a recursive least-squares technique and a fractional-order state variable filter. These parameters then help estimate the battery's EIS under various aging conditions. Next, a regression model from the EIS spectrum shows the battery's degradation trend regarding internal resistance growth. Finally, the regression model is used in a particle filtering framework to predict the battery's RUL, which is reasonably satisfactory compared to RUL based on measured EIS data.

2.5.2.2 Empirical Model

The empirical model is constructed by analysing the correlation between large amounts of data obtained from experimental or observational studies [72]. The capacity fade curve may be used to monitor battery degradation by depicting how the capacity declines as a function of equivalent cycle numbers, charge throughput, or time. Building an empirical capacity decline model parametrised by operating conditions is the most straightforward approach to RUL prediction [64]. This may depend on several parameters, including number of cycles and charge throughput.

Two empirical models were developed for battery RUL prediction: the weighted (Ah) ageing model and the event-oriented ageing model [73]. In the weighted (Ah) ageing model, the LiB is considered to have failed when its cumulative weighted Ah value exceeds a certain threshold. In the event-oriented ageing model, the RUL is obtained by analysing the influence on the lifetime induced by each event and then adding up all of the events [74]. An empirical internal

resistance model was built by selecting time, temperature, and SoC during battery testing as model parameters; this model can be utilised for calendar and cycle-life prediction across a temperature range of $40℃ - 70℃$ [75, 76]. Similarly, several health indicators, such as the discharged voltage and internal resistance [77], the rate of temperature change [78], and the battery discharge curve [79], were used to build empirical models. With model-based methods, mathematical ageing models which capture long-term battery degradation dependencies are required. Because of the mathematical simplicity, wide validity, and high flexibility, RUL can be predicted [80].

Most studies in the literature have utilised a model that is generally linear, exponential, or polynomial [74, 81, 82]. Model-based approaches are also associated with advanced Bayesian, KF and PF, respectively [83]. These can update the parameters of the model as part of the diagnostic process to ensure accurate RUL prediction. The best candidate for solving linear system problems with Gaussian noise is the KF [84]. A linear model of capacity degradation linked with two filters has also been proposed to estimate the RUL in [85]; however, the process of battery degradation is often non-linear, and this is where different KF algorithms, such as an unscented KF or extended KF [86], may address the above-mentioned issue. According to [87], most errors in the process of predicting RUL derive from several sources when obtaining data, and thus, total noise often does not show Gaussian behaviour. In this context, therefore, the application of a KF algorithm leads to divergence. However, the method of health diagnosis includes solutions for non-Gaussian non-linear system-based problems. For this reason, studies have tended to consider PF algorithms, which give solutions for both non-linear and non-Gaussian issues [88]. Several papers have employed PF to determine the failure points of LiB. For example, in [89, 90], a method was proposed to predict failure using the exponential model and classical PF. In addition, a second-order polynomial was presented in [74], which contains fewer parameters than the exponential model; this model is less accurate than the exponential model. For instance, the proposed enhanced PF method in [91] uses an enhanced particle method to reduce the impact of these problems on state estimation. An evolving fuzzy predictor is also adopted and fused into the enhanced PF structure to deal with the lack of new battery measurements during the prognostic period. This helps to improve the accuracy of RUL

prediction by providing a more accurate estimate of the current state of the battery. The authors in [35] presented a long-term RUL prediction scheme based on Kernel Adaptive Filter (KAF) for the LiB. The UKF algorithm was used to improve prediction accuracy while dealing with noisy data. While the UKF-based model produced satisfactory results, its operational complexity meant it needed scarification methods to reduce time and spatial complexity.

In general, PF suffers from two main problems: particle degeneracy and particle impoverishment. The latter is due to the fact that a PF has a resampling phase that can reduce particle degeneracy, and this may also result in a loss of sample particles [92]. Accordingly, other types of PF used to solve these problems have been considered. For example, an unscented PF (UPF) was presented in [93] to improve the sampling and reshaping of classical PF. The authors in [94] presented a scheme for battery capacity estimation based on the estimated capacity using a Gauss-Hermite PF (GHPF) algorithm to predict the failure limit for the uncertainty in the RUL prediction. The Markov Chain Monte Carlo (MCMC) method was applied in [95] to solve sample problem impoverishment in a UPF algorithm. Regularised particle filters have also been used in the re-sampling phase to enhance classical PF accuracy, as presented in [96]. A Rao-Blackwellized PF (RBPF) was suggested in [97] to limit the distribution of likelihood into a subspace of the state distribution of likelihood in the state space sample. The authors in [98] integrated the neural networks radial basis with a PF for the end-of-discharge prediction for a LiB.

In [99], the authors proposed an improvement in the accuracy of the residual life prediction theory by dividing the method into two parts. First, the degradation model was extracted using the NN technique under different operating conditions. Second, the parameters of the NN model were updated with the Bat-PF. The Bat technique is used to push the particles to areas of high probability to optimise particle distribution and further reduce PF impoverishment and degeneracy. A second-order Central Difference (SCD-PF) algorithm was introduced in [100] to improve the performance of the classic PF for RUL prediction of LiB. Most previous improved algorithms have extensively reduced the problems faced by the classical PF algorithm in terms of particle decomposition and sample diversity deficiency and thus obtained

a strong result for LiB RUL prediction. Nevertheless, issues with particle degradation and particle diversity deficiency remain difficult for RUL prediction. For this reason, this work aims to improve the RUL prediction of LiBs by smoothing the PF using the Likelihood Approximations scheme [101]. The proposed SPF algorithm improves the accuracy of RUL prediction by choosing the proposal distribution and the resampling weights, depending on certain current parameter estimates, thus overcoming the problem of particle impoverishment and uncertainty in the degradation model parameters. However, this approach has some implementation limitations. First, the quantity of data needed to extrapolate typical operating circumstances is relatively large. Second, this technique cannot simply characterise the changes from one cell to another due to the difference in manufacturing or heterogeneous temperatures within a single package or current distribution. Lastly, an approach using an evidence-based ageing model fails to include physical degradation mechanisms, and thus it could not capture the knee points (i.e., changes in degradation, in the capacity fade curve). The rate of degradation is possibly because of an alteration in the core mechanism (e.g., an increase in SEI, which then leads to lithium plating). It is complex to assess, particularly with basic empirical degradation models [89, 102].

2.5.2.3 **Physics-Based Model**

To overcome the above-mentioned limitations, several works have proposed the addition of a physical understanding of battery degradation mechanisms to achieve accurate and reliable RUL predictions at various degradation stages to enhance the predictive approach in the model-based prediction algorithm. For example, the authors in [103] focused on using physics-based models to predict the RUL of LiBs -based on a Non-linear Least Squares (NLS) algorithm. The authors considered multiple aging mechanisms that affected the battery performance and used a half-cell model to estimate the battery capacity. By tracking degradation parameters and considering the characteristics of these parameters over time, the authors were able to provide an online-based RUL prediction for the batteries. The work was carried out using eight batteries, and the findings were compared to the traditional approach to confirm their validity. However, filter-based techniques such as PF could be considered in future research work to

improve performance. The PF is well-suited for systems where the observations are noisy or uncertain, as it provides a probabilistic estimate of the system's state. The work in [104] developed a method to predict how much a battery's capacity will decrease. This approach uses five physical models that consider factors like temperature, how much charge the battery has, and how much current flows through it. These models predict how much the battery's capacity has decreased in the past. The output of these models is then fed into an artificial intelligence algorithm (LSTM) that predicts how much the battery's capacity will decrease in the future. However, this second algorithm can only make predictions based on the battery's past capacity decreases and does not explicitly consider the specific operational conditions (like temperature) that the battery was subject to in the past. The method cannot be adjusted for different operating conditions during battery cycles. In [105], the author proposed a Simplified Electrochemical Model (SEM) based PF framework for LIB RUL prediction. Similarly, to estimate the RUL, the authors in [106] used an improved Single-Particle Model (SPM) coupled with an Auxiliary Sampling Importance Resampling (ASIR) PF to develop a prediction system based on parameter estimation (PE), in which vehicle charging data was utilised. Recent research [107] introduced several degradation trend mechanisms for estimating the capacity and RUL of an implantable-grade LiB. One proposed framework includes the loss of active materials in positive and negative electrodes and a loss of lithium inventory. In the physics-based prognostic approach, three critical trends for degradation are used to enhance the prediction: the Loss of Lithium Inventory (LLI), the active material Loss on the Negative Electrode ($\mathrm{LAM_{NE}}$), and active material Loss on the Positive Electrode ($\mathrm{LAM_{PE}}$). Post-mortem analyses of aged LiBs have identified these mechanisms as significant causes of capacity loss. Specifically, this predictive approach tracks changes in the active masses of the positive and negative electrodes ($\mathrm{m_p}$ and $\mathrm{m_n}$, respectively) and the Lithium Inventory Indicator (LII) degradation parameters. Analysing the half-cell curve can provide an estimate of these three degradation characteristics [108]. This examines the voltage capacity (VQ) curves and the differential voltage ($\mathrm{dV/dQ}$) curves. Since the authors in [108] introduced half-cell curve analysis as a non-destructive way to assess the health of a battery cell, it has become extensively employed in LiB research. Qualitative analysis of half-cell curves was used to rebuild a full-

cell curve by changing the degradation parameters in half-cell curves of the PE and NE. Once the half-cell model parameters have been changed, the fitting of the rebuilt full-cell curve to the simulated VQ and dV/dQ full-cell curve is achieved by altering the model's parameters to gain a more dependable prediction of the degradation parameters. Model-based methods are also related to filter technology tracking and update the three estimated degradation parameters from experimental data to choose an appropriate method and representation.

2.5.3 Hybrid Approaches for RUL Prediction

One major drawback of data-driven approaches is that they may provide erroneous predictions or even incorrect outcomes if they are fed incomplete or biased training data [109]. Model-based techniques, however, are less adaptable than data-driven ones since they need specialised expertise to develop physical models [110]. However, the latter methods are more stable and resilient because they require fewer data and are less affected by external uncertainty. In recent years, hybrid techniques combining model-based and data-driven methods to produce accurate forecasts have been a hot topic of study in battery RUL prediction, seeking to capitalise on the relative strengths of both approaches [111]. In general, hybrid methods can be divided into two groups based on their objectives: (1) enhancing the efficiency of filtering techniques; (2) producing future observation data.

2.5.3.1 Enhancing the Efficiency of Filtering Techniques

All the predictive approaches mentioned above depend on the design of the experimental degradation model on specific operational requirements or batteries with particular materials. For real-time RUL prediction, LiB often works under less-than-ideal operating conditions, and so the estimated initial model parameters may be inaccurate, leading to unstable and inaccurate RUL prediction [3]. Moreover, inappropriate initial values can slow the convergence of the algorithm and lead to divergence. It is thus essential to have a robust and flexible model that

can adequately track the capacity degradation trends and extract model parameters under different operating conditions.

To this end, hybrid approaches based on integrating basic predictive methods have become increasingly attractive due to their ability to extract a fading capacity model and track degradation model parameters. For example, [112] used the RVM technique to measure noise in a battery capacity fading dataset. The PF is fed these transactions to update them and estimate the remaining life. The authors in [81] proposed the Dempster-Shafer theory to set the initial parameter value of the PF algorithm, which increases the speed convergence and improves accuracy in early battery life predictions. The NN was proposed in [113] to produce as much training data as possible and convert these into deterioration models using data prospecting techniques. These were then linked to the PF algorithm as measurement and case transmission functions. The authors avoided utilising an empirical model into the PF algorithm, despite its high computational complexity and load. The accuracy of the suggested technique depends on the amount of training data simulated by the ensemble NN model. Similarly, [99] presented a Bat method to resample PF particles to improve MLP+PF hybrid performance. However, most previous hybrid approaches have significantly reduced the problems experienced by the online life expectancy threshold by identifying the initial values of degradation parameters with artificial intelligence techniques. As such, they have obtained robust and reliable predictive models.

2.5.3.2 Producing Future Observation Data

As mentioned above, the empirical ageing model's state variables must be updated during long-term prediction. This is typically accomplished through a filtering method. However, the update function of the filtering algorithm for long-term RUL prediction relies on future measurements, such as future battery capacity, which are not currently accessible [64]. Therefore, in the absence of future measurements, the filtering algorithm can only predict the future trend by repeatedly solving the state equation based on the most recent information gathered, and the model parameters remain the same throughout the forecast process. The

missing future observation data contain the degradation information, and the lack of this data will lead to errors in the prediction of RUL [114].

Two different methods are used in the literature to solve the above problem. In more recent research [115], the work described above was expanded, and the optimised prediction results after filtering were utilised to update the Nonlinear Degradation Autoregressive (ND–AR) training data, resulting in additional improvements to the prediction accuracy. An alternative method is using data-driven algorithms (e.g., RVM) to predict the future residual sequence. The prediction error series was used by the authors in [116] to adjust the unscented PF output results and by those in [86] to revise the unscented KF state variables. The techniques mentioned above are utilised to adjust the final output or the model parameters based on the prediction error. This leads to more reliable forecasts.

2.6 Summary

Based on this comprehensive literature review, key research gaps and priorities in RUL prediction of LiBs have identified three main knowledge gaps, which this thesis seeks to address by refining existing methods and introducing innovative solutions to enhance prediction accuracy and applicability in real-world scenarios.

- Previous improved algorithms (Section 2.5.2.2) have extensively reduced the problems faced by the PF algorithm in terms of particle decomposition and sample diversity deficiency and obtained a strong result for LiB RUL prediction. Nevertheless, issues with particle degradation and particle diversity deficiency remain difficult for RUL prediction. Thus, the key contribution of the current work is to improve the RUL prediction of LiB by smoothing the PF using the likelihood approximations scheme [101], combined with a second-order degradation model (addressed in Chapter 3).

- The developed methods for RUL prediction face two challenges. First, most approaches are mainly based on traditional empirical degradation models without considering

degradation mechanisms. Second, the stability of the standard PF method is greatly constrained by a lack of particles and uncertainty in the degradation model parameters, which are, in turn, constrained by the availability of sufficient and reliable data. Consequently, this can lead to inaccurate RUL prediction. Therefore, the present research proposes the development of a framework for RUL prediction based on the estimation of parameters of a reduced-ordered physics-based model of LiB by extracting three main degradation mechanisms directly correlated with the RUL of the LiB. These degradation mechanisms are LAM in positive and negative electrodes and LLI (addressed in Chapter 4).

- Online RUL prediction may lack the ability to describe capacity degradation, given the variability in decline between cells and others under different operational conditions. As such, this can result in inaccurate RUL prediction. The current work thus proposes a hybrid approach to improve the accuracy of online forecasting in the existing framework by integrating data-driven and model-based approaches. The proposed framework utilises a NN to model and track battery degradation trends, and it also degrades the initial values of the degradation model's transactions under different operating conditions (addressed in Chapter 5).

- Suppose a new or different battery dataset is used instead of those referenced in the thesis in the methods proposed in Chapters 3 and 4. Adjustments would then be required for each method based on the estimated initial model parameters. For real-time RUL prediction, LiBs often operate under less-than-ideal conditions. Consequently, the estimated initial model parameters may be inaccurate, leading to unstable and inaccurate RUL predictions [3]. Therefore, it is crucial to have a robust and flexible model that can accurately track capacity degradation trends and extract model parameters under varying operating conditions (This solution is addressed in Chapter 5).

Chapter 3 Battery Lifetime Identification Using SPF Technique

'In Chapter 2, a comprehensive review is given of the enhancements made to existing algorithms that have significantly lessened the complications the PF algorithm encounters, particularly regarding particle disintegration and the deficit of sample diversity. These modifications have resulted in robust outcomes for predicting the RUL of LiBs. Nevertheless, issues with particle degradation and particle diversity deficiency remain difficult for RUL prediction. For this reason, this chapter unveils a novel online method for RUL prediction of LiBs utilising an approach based on SPF for approximating likelihoods. The proposed SPF algorithm can accurately estimate the unidentified parameters of the degradation model and predicting the degradation status by resolving the optimisation issue at every iterative step instead of solely proceeding with a gradient step. This typically results in more rapid convergence, eliminates instability problems, and enhances the precision of predictions.'

3.1 Introduction

Accurate predictions of RUL for LiBs are a key aspect of managing their health, promoting reliable and secure systems, and reducing the need for unscheduled maintenance and costs [110]. Recent work on RUL prediction has largely focused on refining the accuracy and reliability of the RUL prediction. However, the complex nature of battery degradation processes and the lack of accurate models make battery lifetime identification a challenging task [64]. In recent years, PF algorithms have shown great potential for RUL prediction by representing the probability distribution of the system state using a set of particles. However, there are several challenges associated with the use of PF algorithms for RUL prediction of LiBs [117].

One of the main challenges is the complexity of the degradation processes in batteries. LiBs exhibit various degradation mechanisms, including capacity fade, power fade, and impedance rise, which can interact in complex ways [118]. Accurate modelling of these degradation mechanisms is essential for effective RUL prediction using PF algorithms [119]. Another challenge is the selection of appropriate state variables for the PF algorithm. The state variables used to represent the probability distribution of the system state must capture the relevant degradation mechanisms and be informative enough to enable accurate RUL prediction [83]. However, selecting too many state variables can result in increased computational complexity, while selecting too few state variables can result in an inadequate representation of the system state. Finally, PF algorithms can be computationally expensive, particularly when dealing with large data sets or complex models. The efficiency of particle filter algorithms can be improved by using various techniques, such as resampling, importance sampling, and Markov Chain Monte Carlo methods [70, 120].

For this reason, this chapter introduces a new online RUL prediction for LiB using SPF based likelihood approximations method. The proposed algorithm can accurately estimate the unknown degradation model parameters and predict the degradation state by solving the

optimisation problem at each iteration rather than only taking a gradient step, which tends to lead to rapid convergence, avoids instability issues and improves predictive accuracy.

This chapter provides background information on LiBs, their degradation mechanisms, and the challenges associated with predicting RUL. Section 3.2 explains a new approach for RUL prediction using SPF-based likelihood approximations. The theoretical background and the procedures of implementation for the PF and the proposed SPF algorithms are set out in Section 3.3. Section 3.4 demonstrated the experimental datasets published by PCoE NASA; a second-order degradation model was created to explore the degradation of LiB, utilizing non-linear characteristics and non-Gaussian capacity degradation. Maximum error analysis and prediction relative and absolute error comparison are presented in section 3.5. Obtained results are presented and discussed in Section 3.6. Finally, conclusions and discussion are summarised in Section 3.7.

3.2 Empirical Model for Predicting RUL

The primary research methodology focuses on the study of statistical analysis of data using the proposed SPF method. In general, the investigation in this study follows the framework RUL prediction process, as shown in Figure 3.1. As depicted in Figure 3.1, experimental capacity degradation datasets were used as input data for a curve-fitting toolbox to extract the empirical model that best describes the battery's capacity degradation. Then, a second-order exponential degradation model was developed, and degradation model parameters were utilised as input data for the SPF algorithm to validate the effectiveness and stability of the proposed method.

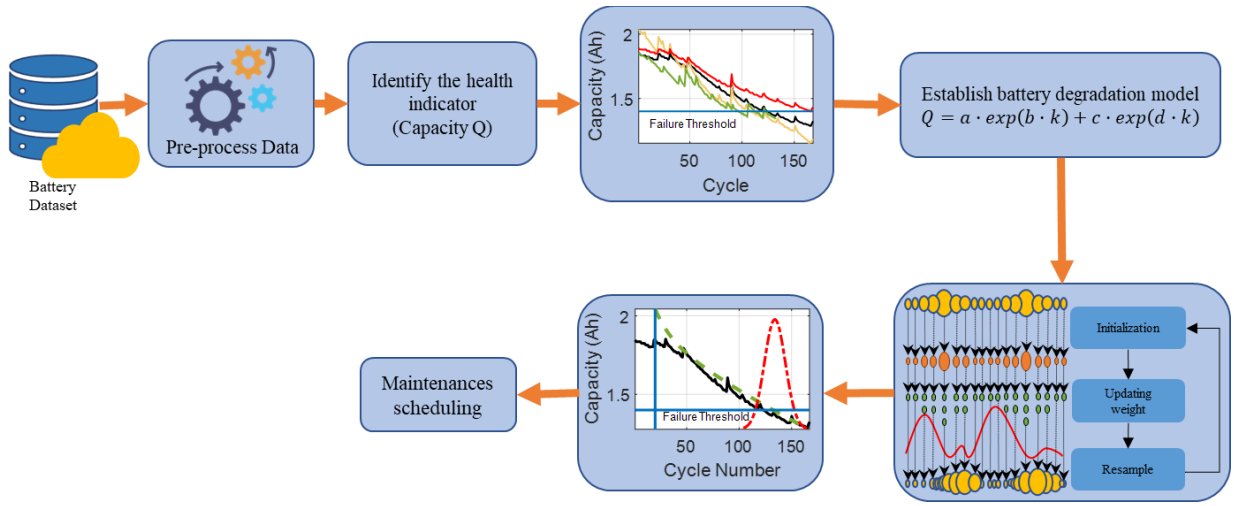

Figure 3. 1 Generic block diagram of RUL prediction.

3.3 Theoretical Background-Methodology

3.3.1 Bayesian Filtering Methods

Bayesian inference is a method of statistical inference that utilises Bayes' theorem to update the probability of a hypothesis as more data becomes available [121]. This inference method is particularly useful in problems with uncertain or incomplete information, where it can be used to incorporate prior knowledge and make probabilistic predictions about the system's state [122-124]. The estimation procedure can follow one of two models [125]. The first model assumes that the parameters are estimated by minimising the sum of squares of the residuals between the observations and predictions model. This method assumes that the parameters are non-random and constant during the observation window, and the observations are only affected by random noise [126]. The technique is called non-Bayesian because it does not involve the computation of the posterior probability distribution of the parameters given the observations [127].

On the other hand, the second model considers the parameters' uncertainty by incorporating prior knowledge about the probability distribution of the parameters [128]. The method uses

Bayes' theorem to compute the posterior probability distribution of the parameters given the observations. This posterior distribution represents the updated belief about the parameters after considering the new data. Parameter estimation using the second model is called Bayesian estimation [129]. Prior beliefs are used as a starting point for Bayesian estimation, and the first belief statement comprises an indicator based on a prior probability distribution. A prediction can be made based on the initial belief and a likelihood function describing the event [130]. The core idea behind recursive Bayesian estimation is as follows [130-133]:

1. Begin with some prior belief statements.
2. Use the prior belief and a dynamic model to make a prediction.
3. Obtain a posterior belief using the observation model.
4. Declare the posterior belief as the new prior belief and return to 2.

Figure 3.2 depicts the classification of Bayesian filters for both Gaussian and non-Gaussian circumstances. Gaussian filters are listed on the left, while their Monte Carlo non-Gaussian counterparts are listed on the right. The focus of this thesis is on the Monte Carlo filters.

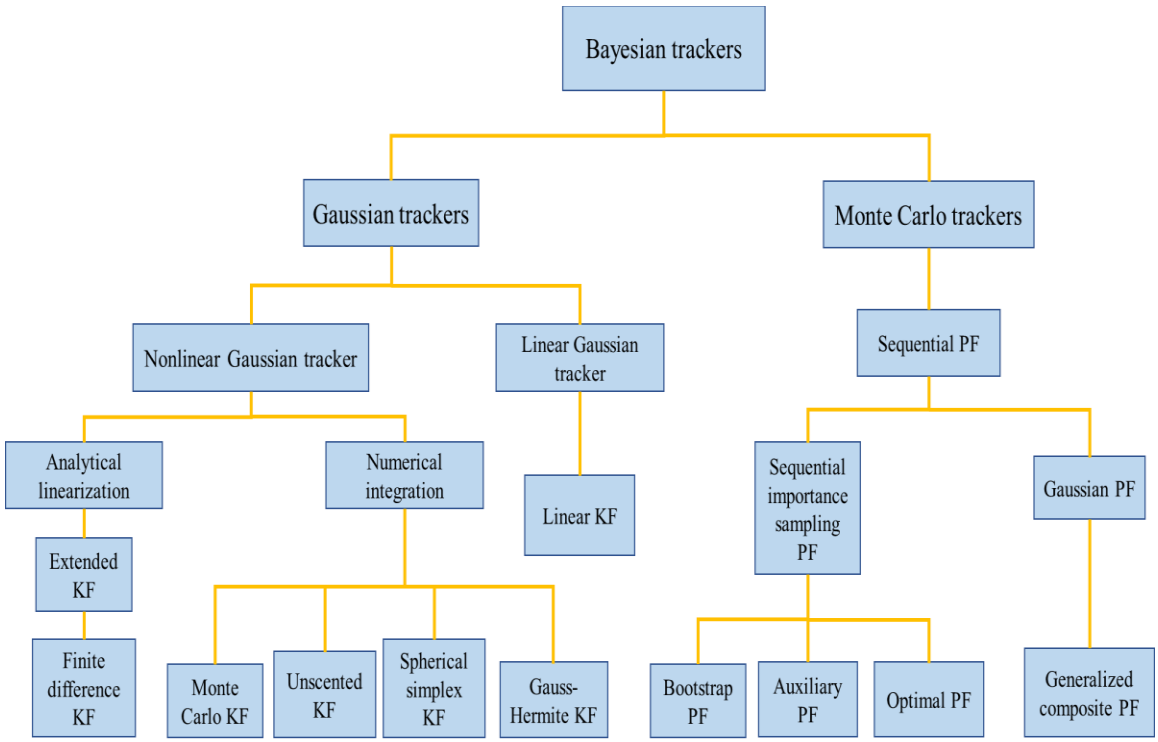

Figure 3. 2 Classification of Bayesian Filters.

3.3.2 Bayesian Estimation

The Bayesian estimation aims to determine the consecutive values of a parameter vector x given an observation vector z [134]. This is the purpose of the Bayesian estimation. As mentioned before, it is common to practise considering both x and z to be random vectors. For the parameter vector, the assumption of randomness is built into the equations that describe how the parameter changes over time. Unmodeled effects are added as random noise. 'Unmodeled effects' refer to the variations or changes in the observed data that are not accounted for by the existing model. These effects could stem from a multitude of sources such as unconsidered variables, complex interactions between factors, errors in data measurement or collection, or other random and unpredictable influences that the current model doesn't include [134]. One can explain the stochastic nature for the observation vector by supposing that there is always a certain random measurement noise [135]. The random vector x is assumed to have a known prior density function $p(x)$. Before any observational data are

available, the whole set of known and unknown values for the parameter vector is included in this prior distribution [136]. If the correct value for the parameters x were known. In that case, the conditional density or likelihood function $p(z|x)$ could be used to calculate the probability density of z, and the whole statistical features of z could be determined from this information.

Bayes' law can be used to find the posterior conditional density of x once an experiment has been done and a realisation of the random variable z is known [137-139]:

$$p(x|z) = \frac{p(z|x)p(x)}{p(z)} \tag{3.1}$$

In light of this, the posterior density x is a part of the Bayesian framework that incorporates all of the information there is to know about x. This is achieved by taking into consideration the results of an experiment. Given that the experimental outcome, z, is now accessible, the denominator of the equation (3.1) is just a scalar normalising constant that can be derived as follow [140]:

$$p(z) = \int p(z|x)p(x)dx \tag{3.2}$$

For the full Bayesian estimation problem, the statistical model for estimation is the likelihood and the posterior, or their joint density. The combined density of the parameter and observational trajectories is described by [141]:

$$p(x, z) = p(x|z)p(z) \tag{3.3}$$

For the estimation issue, the posterior distribution contains the answer (3.1). Therefore, if desired point estimates of x exist, they can be generated from the posterior distribution. Considering that the density function can frequently be used to quantify x, the posterior density should be regarded as the most generic answer to the estimation issue.

3.3.3 Recursive Bayesian Filtering of Probability Density Functions

A discrete dynamic process refers to a system where the current state is determined by a finite number of previous status, often represented by a sequence of discrete time steps [142].

On the other hand, in a continuous process, the current state of the system is determined by an infinite number of previous states, represented by a continuous function modelled by a differential equation [143]. When observations occur at discrete times, it is not possible to estimate the state of the system between those observations. Therefore, the differential equation that describes the continuous process must be replaced by a difference equation, which relates the state of the system at a specific observation time to the states at previous observation times. This is known as a finite difference equation [144].

The current state of a first-order Markov process depends only on the previous state. So, we can characterise a discrete random Markov dynamic process as [145, 146]:

$$x_n = f_{n-1}(x_{n-1}, u_n, \eta_{n-1}) = f_{n-1}(x_{n-1}) + u_n + v_{n-1}) \tag{3.4}$$

where x_n is the state of the system (state vector) at the time t_n, f_{n-1} is a deterministic transition function (matrix) that moves the state x from tim subscript to time t_n and u_n It is a known (usually deterministic) control that constitutes some external input that drives the system dynamics. Although the white noise η (not necessarily Gaussian) can start at the input and be transformed by the transition function, it is usually assumed that the noise is additive and represents those parts of the true transition function that are not modelled.

Given the set of all experimental observation vectors, the problem of interest is to estimate the unobservable state vector. x_n based on the information provided by the observation vectors. It will be assumed that there is an analytical relationship between the observable vector at the time. t_n and the state vector at the time t_n, which is denoted by [147]:

$$z_n = h_n(x_n, \mu_n) = h_n(x_n) + w_n \tag{3.5}$$

Here, z_n is designated as the observation vector and h_n is a deterministic observation function that links the state vector with the observation. Once again, the white noise μ_n (not necessarily Gaussian) can be transformed by the transition function, but it is usually assumed that the observation noise is additive.

Consider that we have previous knowledge of the state and observation equations, i.e., $x_{k+1} = f_x(x_k, v_k)$, which may also consider to be sampled from $x_{k+1} \sim p(x_{k+1}, x_k)$ due to random noise. Likewise, the observation equation for this hidden process is $z_k = h(x_k, v_k)$. Which is considered to have been sampled from $p(y_k|x_k)$ The values created by the state equation are hidden, and only the observation values are visible. Suppose the proposal distribution $q(x_k|z_{1:k})$ can be factorised into [148]:

$$q(x_{0:k}|z_{1:k}) = q(x_{0:k-1}|z_{1:k-1})q(x_k|x_{0:k-1}, z_{1:k}) \tag{3.6}$$

The recursive form of the posterior probability density function can be expressed as [149]:

$$p(x_{0:k}|z_{1:k}) = \frac{p(z_{1:k}|x_{0:k}, z_{1:k-1})p(x_{0:k}|z_{1,k-1})}{p(z_{1:k}|z_{1:k-1})}$$

$$= \frac{p(z_{1:k}|x_{0:k}, z_{1:k-1})p(x_k|x_{0:k-1}, z_{1:k-1})p(x_{0:k-1}|z_{1:k-1})}{p(z_{1:k}|z_{1:k-1})}$$

$$= \frac{p(z_{1:k}|x_k)p(x_k|x_{k-1})p(x_{0:k-1}|z_{1:k-1})}{p(z_{1:k}|z_{1:k-1})}$$

$$\propto p(z_{1:k}|x_k)p(x_k|x_{k-1})p(x_{0:k-1}|z_{1:k-1}) \tag{3.7}$$

Finally, the conditional probability density function equations need to be written in a fully recursive manner. The prior density is related to the prior posterior density through the Chapman-Kolmogorov equation [150]:

$$p(x_k|z_{1:k-1}) = \int p(x_k|x_{k-1})\, p(x_{k-1}|z_{1:k-1})dx_{k-1} \tag{3.8}$$

Figure 3.1 depicts one iteration of this Bayesian recursive process for generating consecutive posterior densities. The recursive procedure is initiated by $p(x_0)$, the pdf associated with x prior to any observations. In this procedure, the prior probability distribution is updated with each iteration by incorporating new data and recalculating the likelihood and evidence. The

updated posterior probability distribution becomes the new prior for the next iteration. This process continues until a desired level of convergence is reached [151].

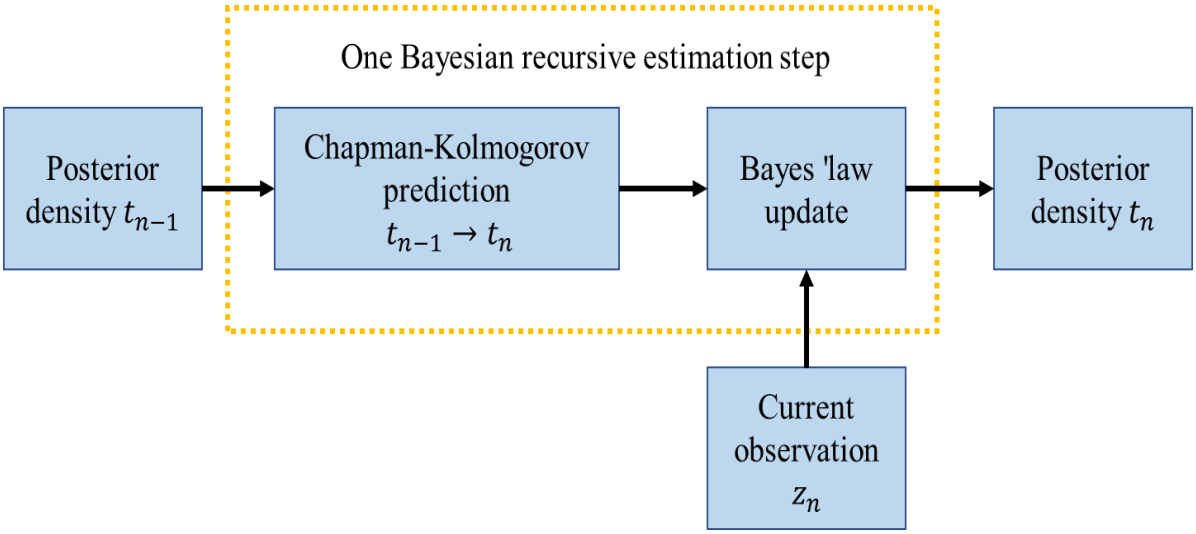

Figure 3. 3 Depiction of one step in the recursive Bayesian posterior density estimation procedure.

3.3.4 PF Algorithm

The PF algorithm combines two techniques: recursive Bayesian and sequential importance sampling (SIS) [120, 152, 153]. It also contains two important elements, which are the initialisation of parameters and the state model equation. The state-spatial dynamic model can be represented by the state transformation model and the measuring model, using (3.9) and (3.10) [154].

$$x_k = f(x_{k-1}) + \omega_{k-1} \leftrightarrow p(x_k|x_{k-1}) \tag{3.9}$$

$$z_k = h(x_k) + v_k \leftrightarrow p(z_k|x_k) \tag{3.10}$$

Where, $f(x_{k-1})$ and $h(x_k)$ refer to the hidden state of the transition function and measurement function, respectively; x_k denotes the system's state variables at the k^{th} time, y_k represents the observed system value of x_k at the k^{th} time, and x_k represents the hidden state variables at the k^{th} time, z_k represents the measurement system at the k^{th} time, ω_k is the noise process, and v_k is the noise measurement.

The main idea of the PF algorithm is to draw many random sample particles from a proposal distribution $q(x_{0:k}|z_{1:k})$ and to allocate each with an importance weight representing the posterior probability density (PDF) [155, 156]. In this way, PDF $p(x_k|z_{1:k})$ can be ascertained as below:

$$p(x_{0:k}|z_{1:k}) \approx \sum_{i=1}^{N} w_k^i \delta(x_{0:k} - x_{0:k}^i) \tag{3.11}$$

Where N is the number of particles, $\delta(\cdot)$ represent the Dirac delta function. The particles generated by the distribution $p(x_k|z_{1:k})$ represent the sample perfectly. However, from the accurate PDF posterior density, it is still difficult to take a precise sample, and so an alternative way of sampling needs to be found to sample proposal distribution $q(x_k|z_{1:k})$ [157]. The weighting of the filter may be improved by using the SIS and taking another sample in the stages of the SMC algorithm. The associate weight of random particle drawn from $q(x_k|z_{1:k})$ is represented as:

$$w_k^i \propto \frac{p(x_k^i|z_{1:k})}{q(x_k^i|z_{1:k})} \tag{3.12}$$

$$w_k^i \propto \frac{p(z_k|x_k^i)p(x_k^i|x_{k-1}^i)p(x_{0:k}^i|z_{1:k-1})}{q(x_k^i|x_{0:k-1}^i, z_{1:k})q(x_{0:k-1}^i|z_{1:k-1})}$$

$$= w_{k-1}^i \frac{p(z_k|x_k^i)p(x_k^i|x_{k-1}^i)}{q(x_k^i|x_{0:k-1}^i, z_{1:k})} \tag{3.13}$$

As long as $q(x_k^i|x_{0:k-1}^i, z_{1:k}) = q(x_k^i|x_{k-1}^i, z_k)$ is satisfied, the modified weight calculation (3.13) can be transformed into:

$$w_k^i \propto w_{k-1}^i \frac{p(z_{1:k}|x_k^i)p(x_k^i|x_{k-1}^i)}{q(x_k^i|x_{k-1}^i, z_{:k})} \tag{3.14}$$

Table 3.1 depicts a detailed illustration of the PF algorithm [158]. In the first step, a random set of starting particles $\left\{x_k^{(i)}\right\}_{i=1}^{N}$ is produced using the system's prior probability distribution, and a specific weight is assigned to each particle. The second step is to update the particles using equations (3.9) and (3.10), and the importance density function $q\left(x_k^i|x_{k-1}^i, y_{1:k}\right)$ is chosen as $p\left(x_k^i|x_{k-1}^i\right)$, such that weights may be determined at time k by:

$$w_k^i = w_{k-1}^i p\left(y_k|x_k^i\right) \tag{3.16}$$

Then, the weight is normalised as:

$$w_k^i = \frac{w_{k-1}^i}{\sum_{j=1}^{N} w_k^i} \tag{3.17}$$

In the third step, the particles are resampled, where new samples are formed by copying the current particles with large weights [159]. Then, the weights are assigned to w_k^i. In the last step, the new state can be updated based on the new particles and weights obtained by:

$$\hat{x}_k = \sum_{i=1}^{N} \tilde{w}_k^i \tilde{x}_k^i \tag{3.18}$$

The state transition model (3.9) and the system observation model (3.10) are represented by the state transition PDF $p\left(x_k^i|x_{k-1}^i\right)$ and the observation PDF$p\left(y_k|x_k^i\right)$, respectively.

Table 3. 1 Procedures of the PF algorithm.

Step1	Initialisation: produce N particles randomly for $\boldsymbol{k = 0}$, randomly generate N particles from the prior Gaussian distribution with corresponding particle weight $\left\{\boldsymbol{w_k^{(i)}}\right\}_{\boldsymbol{i=1}}^{\boldsymbol{N}}$
Step 2	Calculation of importance weight and importance sample for $\boldsymbol{i = 1, 2, \ldots, N}$ draw $\boldsymbol{x_k^i \sim q\left(x_k^i|x_{0:k-1}^i, z_{0:k}\right)}$.In standard SMC, define $\boldsymbol{q\left(x_k^i|x_{0:k-1}^i, z_{0:k}\right) = p\left(x_k^i|x_{k-1}^i\right)}$. Assign the weight of the particle according to:

$$w_k^i = w_{k-1}^i \frac{p(z_k|x_k^i)p(x_k^i|x_{k-1}^i)}{q(x_k^i|x_{k-1}^i, z_k)}$$

Normalise the weight:

$$w_k^i = {w_k^i}/{\sum_i^N w_k^i}$$

Step 3 Re-sampling the effective sample size N_{eff}

$$N_{eff} \approx {1}/{\sum_{i-1}^{N} (w_k^i)^2}$$

Draw N particles $\tilde{x}_k^i$ from the current set x_k^i and replace the present array with a new array:

$$\tilde{w}_k^i = {1}/{N}$$

Step 4 State estimation:

$$\hat{x}_k = \sum_{i-1}^{N} \tilde{w}_k^i \tilde{x}_k^i$$

3.3.5 Common Issues in Particle Filters

One of the most common issues with PF is the problem of ensemble collapse or sample impoverishment [160, 161]. This occurs when the particles become highly concentrated in a small region of the state space, resulting in a lack of diversity among the particles (see Figure 3.4). This can lead to poor estimation of the posterior distribution, and the filter can become stuck in a local maximum. This issue is often caused by poor initialisation, poor choice of proposal distribution, or poor choice of resampling technique. To mitigate this issue, resampling techniques such as systematic or stratified resampling can be used to ensure that the particles remain diverse, and importance sampling can be used to reduce the risk of ensemble collapse [162].

Another common issue with PF is the problem of particle depletion, which occurs when the number of particles that are used to represent the posterior distribution becomes too small, resulting in a poor estimation of the posterior distribution [163]. This can be caused by several factors, such as the choice of resampling technique, the dynamic model used to propagate the particles forward in time, and the choice of proposal distribution. One way to mitigate this issue is to use larger numbers of particles or to use more sophisticated resampling techniques, such as resampling with replacement or resampling with importance weighting [164].

Finally, the PF algorithm is sensitive to the choice of the proposal distribution $q(x_k^i|x_{k-1}^i, z_k)$ [165]. The proposal distribution is used to generate new particles from the current particles, which is used to approximate the posterior distribution. If the proposal distribution is not well chosen, the filter can converge to a suboptimal solution [166]. This can be mitigated by using more sophisticated proposal distributions, such as adaptive proposal distributions or by using more sophisticated resampling techniques [167].

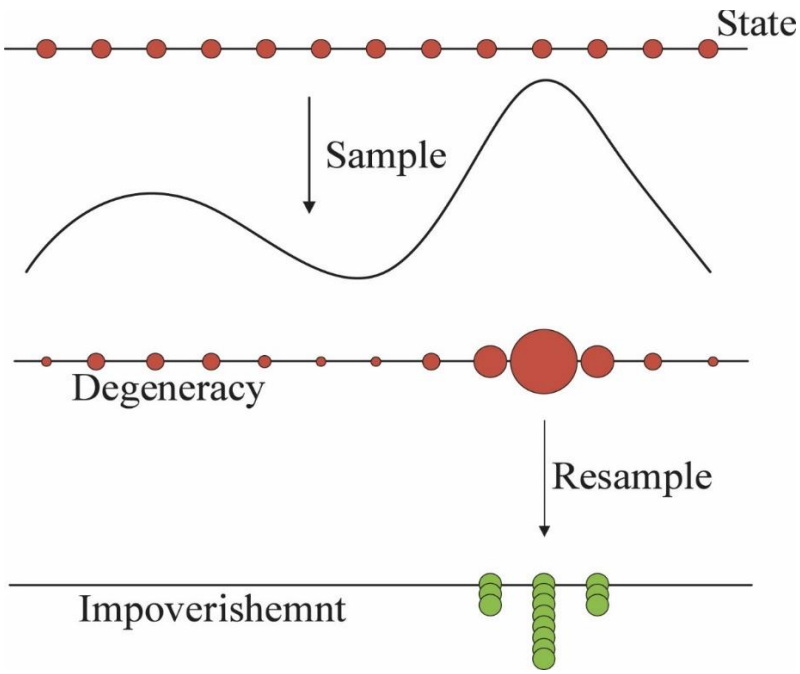

Figure 3. 4 Schematic diagram of weight degeneracy and particle impoverishment for classic PF [162].

3.3.6 The Proposed SPF Algorithm

When using the PF algorithm to estimate maximum probability (likelihood) parameters in the non-linear state-space model, the PF removes the light weights and copies the heavy weights in a resample phase, which results in a loss of diversity in the particle distribution [168]. The main challenge is that likelihood distribution estimation, and its derivatives are fundamentally noisy. The main idea of the SPF method [101] is to choose the proposal distribution $q\left(x_k^i | x_{k-1}^i, z_k\right)$ and the resampling weights w_k^n, such that it is entirely independent of parameters θ. Based on this choice, we note that all the randomly extracted elements, such as particles $x_{0:T}^n$ and ancestor indices $a_{1:T}^n$ in the PF algorithm, became independent of θ; this is critical in the analysis and estimation of battery degradation as the true values of the degradation model parameters are unknown and highly influenced by uncertainty [169]. Now, if we apply the certain condition to the realisation of $\{x_{0:T}^n, a_{1:T}^n\}$, the $\hat{z}_\theta$ estimation will convert into a deterministic function within θ, and any standard optimisation routine can then be implemented to solve (3.19) and find the maximum likelihood estimate of θ [101].

$$p_\theta(z_{1:T}) = \int p(x_0) \prod_{t=1}^{T} f_\theta(x_t|x_{t-1}) h_\theta(z_t|x_t) dx_{0:T} \tag{3.19}$$

$$\hat{\theta} = \arg max_\theta p_\theta(z_{1:T}) \tag{3.20}$$

Where $p_\theta(z_{1:T})$ refers to the likelihood function when considered a function of θ. This follows from (3.1) and the initial state density $p(x_0)$. However, the strength of the PF method is the ability to construct samples sequentially over high-space dimensions X^{T+1}, where the resampling phase provides valuable feedback information to discover which parts of the state space should be explored further. Based on the arbitrary decision, the weights of θ-independent resampling w_k^n will be lost, and thus missing this feature may lead to a discrepancy in the estimate obtained. The deterministic function can be ascertained in θ-independent re-sampling by allowing the algorithm to let the resampling weights w_k^n and $q(x_t|x_{k-1}, z_k)$ rely on certain current parameter predictions, θ_{k-1}, as [101],

$$q(x_t|x_{t-1}, z_t) = f_{\theta_{k-1}}(x_t|z_t) \tag{3.21}$$

$$w_k^n = h_{\theta_{k-1}}(z_t|x_t^n) \tag{3.22}$$

The SPF choice was θ_{k-1} instead of θ. If the θ value is somewhat close to the value of θ_{k-1}, the variance of the estimate of the maximum likelihood state of the particle distribution, referred to as $\hat{z}_{\theta_{k-1}}(\theta)$, may not be prohibitively large. On the other hand, if the current value of θ_{k-1} is far from the current value of $\hat{\theta}$, then the estimate $\hat{z}_{\theta_{k-1}}(\theta)$ will not be particularly good at the $\hat{\theta}$. For this reason, we must repeat the parameter values over k until we roughly arrive at values close to $\hat{\theta}$. By inserting (3.21) and (3.22) into the particle filter algorithm and combining with an external optimisation loop, we reached the novel proposed method, presented in Figure 3.5 [101].

Computationally, the SPF method estimates a final parameter by iterating a four-step process, as shown in Figure 3.5. The first step, an initial guess for each model parameter, is used to create a first-order Taylor series, then used to solve this nonlinear state-space model. The second step is the main step of the proposed method; we run a conventional PF to plot particle distribution based on the prime distribution function in the first line (assuming it is independent of θ) and set the significance weight as $\boldsymbol{w_k^i} = 1$. Then, we utilised the results of the PF run to recalculate the likelihood function approximation for subsequent parameter values. Moreover, in step 2-line 10, $a_{1:T}^n$ is drawn concerning the reconfiguration of weights w_{t-1}^j. Proposal distribution $q\left(x_k^i \middle| x_{k-1}^i, z_{:k}\right)$ is used to generate the new particles in step 2-line 11. In the third step, new particle samples are obtained from $\left\{x_0^i\right\}_{i=1}^N$ by re-balancing the heavy weights and assigning corresponding weights $\frac{1}{N}\sum_{n=1}^N log w_t^n$.

3.3.6.1 Solving the problem of maximisation

As shown in Figure 3.5 (Step 2), the optimisation step related to solving $\arg max_\theta \hat{z}_{\theta_{k-1}}(\theta)$ has been established. Crucially, this issue is now deterministic, and any usual numerical optimisation tool can be implemented, and the experiments will show this using the general-purpose optimisation tool fminunc in MATLAB. The structure of $\hat{z}_{\theta_{k-1}}(\theta)$, which is implicitly defined in the function likelihood of the proposed algorithm, might still be utilised by a more suitable optimisation scheme. Its structure can be shown as [101],

$$\hat{z}_{\theta_{k-1}}(\theta) = \frac{1}{N}\prod_{k=1}^{T}\sum_{n=1}^{N} c_k^N w_k^N(\theta) f_\theta\left(x_k \middle| x_{k-1}^{a_k^N}\right) h_\theta(z_k|x_k^N) \tag{3.23}$$

Where, c_k^N is a constant that is independent of θ; $w_k^N(\theta)$ depends on θ but always fulfils $\sum_{n=1}^N w_k^N(\theta) = 1$, and f_θ and h_θ relies on the degradation model.

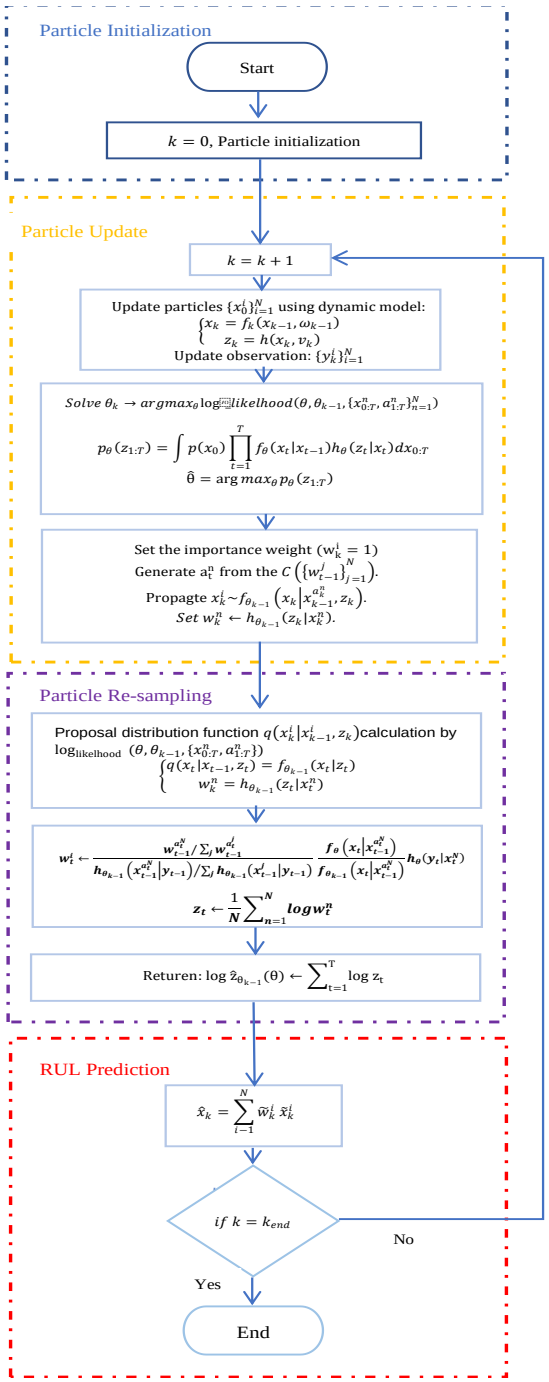

Figure 3. 5 Flowchart of the proposed SPF algorithm.

3.4 Capacity Degradation Modelling

3.4.1 Battery Dataset

The Prognostics Centre of Excellence (PCoE) at NASA Ames Research Centre has made available a widely used battery dataset, which includes data from experiments on LiBs [170]. The dataset includes a variety of sensor measurements, such as voltage, temperature, and current, collected over time during different discharge and charge cycles. The dataset is used for research in the field of prognostics and health management, which aims to predict the RUL of batteries.

In this thesis, four cells were selected (B05, B06, B07 and B18), and their experimental data published by (PCoE), was used to investigate the performance and accuracy of the proposed algorithm [170]. As shown in Figure 3.6, the dataset consists of four cells using commercial lithium cobalt oxide batteries. The stated capacity of the cells is 2 Ah, and their nominal voltage is 3.3 V. The cells are iterated through the cycle until they fail at a room temperature of 24 ℃. Below is a description of the test procedure and data collection conditions [170]:

1. In the charge step, Constant-Current, Current-Voltage protocol (CC-CV) is used. A Constant-Current (CC) of 1.5 Ah was applied until the cell voltage reached the maximum limit (4.2 V), and then the Current-Voltage (CV) continued until the current dropped to 20 mAh.
2. In the discharge step, a CC 2 A is applied until the voltage of the battery dropped to 2.7 V, 2.5 V, 2.2 V and 2.5 V for batteries B05, B06, B07 and B18, respectively. In the testing protocol, the discharge cut-off voltages for the battery cells B05, B06, B07, and B18 have been purposefully set at differing levels. This methodological choice is designed to emulate the varied operating conditions under which these batteries might be deployed in real-world applications [170]. Through this approach, the researchers aim to gain a comprehensive understanding of the impact of distinct discharge levels on the performance and longevity of each battery, thereby enriching

the accuracy and reliability of RUL prediction. The cells were cycled at a depth of discharge (DOD) 20–80%.

3. Repeated previous steps until the batteries reach the point of failure, here it is 30% of the nominal capacity, and so the battery's EoS is placed at a capacity threshold of $U = 1.4$ Ah.

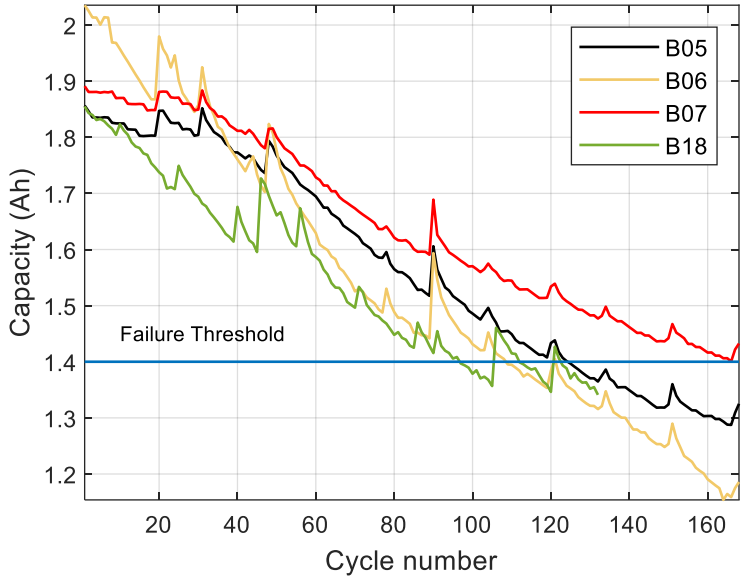

Figure 3. 6 The capacity degradation curve.

3.4.2 Empirical degradation model

During the degradation process, a LiB continues to decrease in capacity. As shown in Figure 3.6, battery capacity decreases dramatically with an increase in the number of cycles used. Thus, the degradation curves are well-fitted using an exponential growth model, as presented in (3.19).

$$Q = a \cdot exp(b \cdot k) + c \cdot exp(d \cdot k) \tag{3.24}$$

Here, Q represent the capacity of the battery, a, b, c and d are the model parameters, and k is the number of cycles. A curve-fitting toolbox was used to obtain an accurate exponential degradation model. Figures (3.7−3.10) shows the fitting results. The findings show that the degradation model is effective and can be used to predict the RUL battery. The modelled

parameters of the four batteries in the study were produced at the fitting stage to attain the starting parameters for the training data. These were used in the prediction step, as shown in Table 3.2.

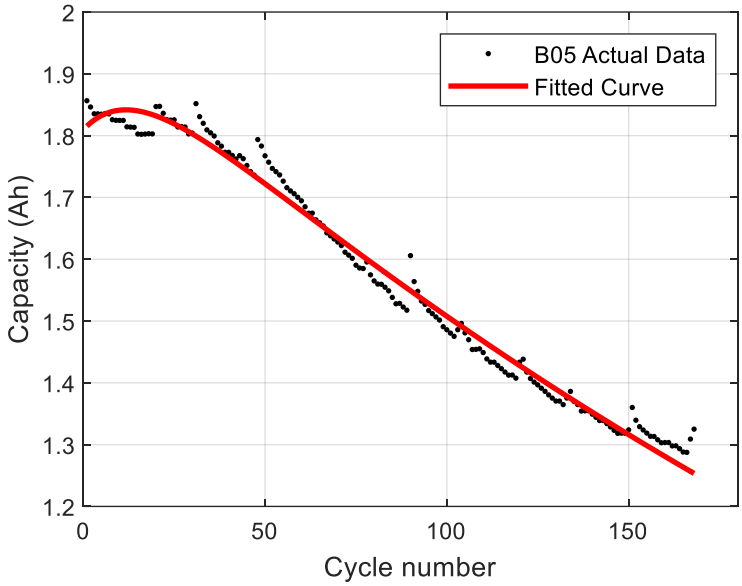

Figure 3. 7 Degradation data and fitted curve of B05.

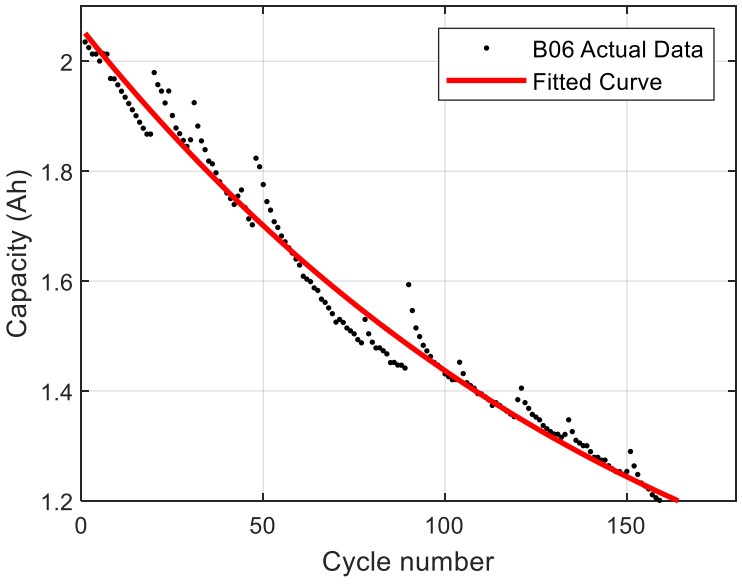

Figure 3. 8 Degradation data and fitted curve of B06.

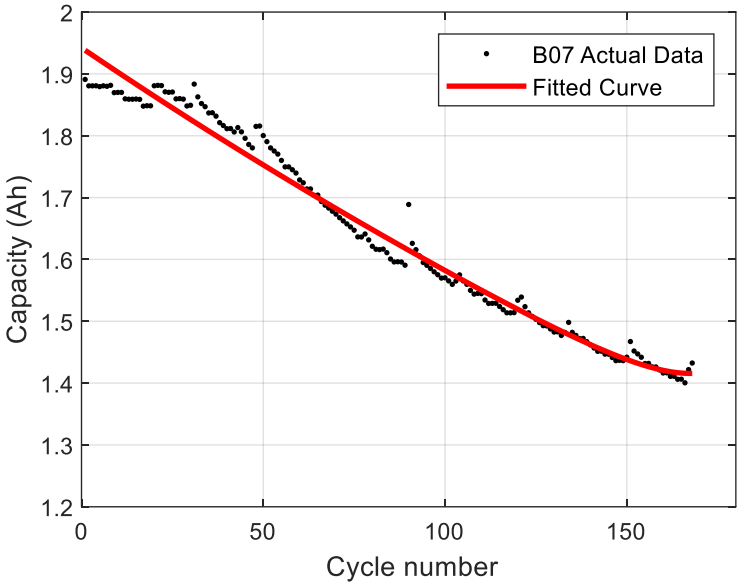

Figure 3. 9 Degradation data and fitted curve of B07.

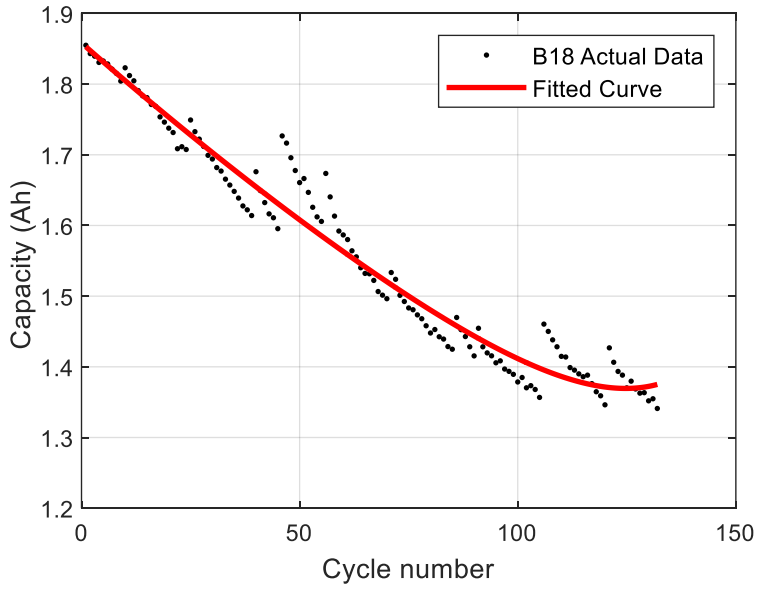

Figure 3. 10 Degradation data and fitted curve of B18.

Table 3. 2 Initial model parameters.

Cell ID	*a*	*b*	*c*	*d*
B05	1.974	-0.00027	-0.158	-0.06942
B06	1.562	-0.00557	0.4895	0.0009
B07	1.938	-0.00205	1.e-07	0.074
B18	1.853	-0.00291	0.0002	0.0428

3.5 Experimental Validation

3.5.1 Prognostic Performance Evaluation Metrics

To demonstration the effectiveness of the proposed solution, the SPF and PF algorithms in Table 3.1 and Figure 3.5 have been implemented. Now, to test the accuracy of the prediction of the PF and proposed SPF algorithm, different cycle 'starting points' were applied, such as $20, 50$ and 80 cycles. Again, the two algorithms were used here for online estimation of the parameters in (3.24). A second-order degradation model has been developed based on the fitting results explained earlier in Section 3.5.2. The performance of the prediction has been evaluated using the Absolute Error (AE) of the RUL and the Relative Error (RE) of the RUL. As given in (3.25), AE is defined as the difference between the number of remaining true (RUL_T) cycles and the number of predicted (RUL_P) cycles. While the RE is defined as presented in (3.26).

$$AE = |RUL_T - RUL_P| \tag{3.25}$$

$$RE = {}^{AE}/_{RUL_T} \tag{3.26}$$

3.5.2 RUL Prediction

According to the capacity degradation model, the state transition of the battery system can be defined as follows:

$$x_k = [a_k; b_k; c_k; d_k] \tag{3.27}$$

Where,

$$\begin{cases} a_k = a_{k-1} + \omega_a & \omega_a \sim N(0, \sigma_a) \\ b_k = b_{k-1} + \omega_b & \omega_c \sim N(0, \sigma_b) \\ c_k = c_{k-1} + \omega_c & \omega_c \sim N(0, \sigma_c) \\ d_k = d_{k-1} + \omega_d & \omega_d \sim N(0, \sigma_d) \end{cases} \tag{3.28}$$

Now equation (3.24) can be written as

$$Q_k = a_k\, exp(b_k k) + c_k\, exp(d_k k) + v_k \quad v_k \sim N(0, \sigma_V) \tag{3.29}$$

Here, Q_k is the measurement of the capacity cell at cycle k, and $N(0, \sigma)$ is the Gaussian noise with zero mean, and σ is the standard deviation. Then, the measurement of the capacity cell can be estimated by:

$$Q_k = \sum_{i=1}^{N} Q_k^i = \sum_{i=1}^{N} [a_k^i . \exp(b_k^i \cdot k) + c_k^i . \exp(d_k^i \cdot k)] \tag{3.30}$$

At cycle k, the prediction step (p-th) can be calculated by

$$Q_{k+P} = \sum_{i=1}^{N} [a_k^i . \exp\left(b_k^i \cdot (k+p)\right) + c_k^i . \exp\left(d_k^i \cdot (k+p)\right)] \tag{3.31}$$

The posterior PDF can be estimated with weights on each trajectory:

$$P(Q_{k+p} | Q_{O:k}) \approx \sum_{i=1}^{N} w_k^i \delta(Q_{k+p} - Q_{k+p}^i) \tag{3.32}$$

In this analysis, the value of the failure threshold is 70% of the nominal capacity value. Then, at cycle k the RUL distribution can be predicted by

$$0.7Q_{nominal} = a_k^i.exp\left(b_k^i \cdot L_k^i\right) + c_k^i.exp\left(d_k^i \cdot L_k^i\right) \tag{3.33}$$

Then,

$$P(L_k|Q_{0:k}) \approx \sum_{i=1}^{N} w_k^i\left(L_k - L_k^i\right) \tag{3.34}$$

Here, L_k^i is the RUL at cycle k.

3.6 Results and Discussion

3.6.1 RUL prediction Using B05 Cell

In this work, the $B05$ battery cell was used for RUL prediction. The initial values of the PF and proposed SPF parameters were selected as number of particles $N = 200$, and battery failure threshold 1.4 Ah. The initial parameters for the degradation model for all battery cells are shown in Table 3.2.

Figure 3.11 shows the prediction results with PF and the proposed SPF algorithm for battery cell $B05$. It is important to mention that the first 80 cycles from the data are used as training data to update the prediction process. There are two curves of prediction, and the respective PDFs of the RUL were obtained to compare between the PF and the proposed SPF, as shown in Figure 3.11 and Figure 3.12, respectively. As seen in Figure 3.9, at $T_s = 80$ cycles, the final life cycle was 125 cycles, while the average predicted life cycle using the PF was 108 cycles. Thus, the AE for the PF algorithm is around 16, and the RE error was approximately 0.136. While for the proposed algorithm (see Figure 3.12), the average number of life cycles predicted was around 127 cycles, the prediction AE was approximately 2 cycles, and the prediction RE was around 0.024. From the prediction results, it observed that the prediction

curve obtained from the proposed SPF method is closer to the actual capacity degradation curve than the PF prediction curve, and its PDF of RUL, based on the proposed SPF algorithm, is more concentrated. Figure 3.12 show that the prediction jumps from the actual value at the starting point prediction (Ts=80 cycles). This is because the prediction framework used to estimate the remaining useful life of batteries relies on continuous updates of degradation parameters, which are based on historical data available before the start of the prediction [90]. The degradation model's parameters have non-linear characteristics that describe how battery capacity degrades over time [171]. When the prediction starts, the framework relies on the latest update of the degradation parameters, which takes into account the available historical data. However, any data that exists beyond the prediction start point is not used in the model since it is considered hidden [172]. As a result, this leads to a sudden change or "jump" in the prediction. This is because the model can only use the information available up to the prediction start point, which is typically based on the number of cycles completed by the battery at that point in time. Therefore, the model cannot take into account any changes in usage patterns or other factors that may affect the battery's remaining life beyond that point. Figure 3.13 show the two prediction curves at the same time to check the PF algorithm and proposed SPF algorithm performance results during the entire lifecycle, which clearly reveals the effectiveness of the proposed algorithm. Figure 3.14 - Figure 3.16 likewise shows the process of predicting the RUL by relying on the above-mentioned two methods. Here, the first 50 cycles were used to update the prediction process. As shown in Figure 3.14 - Figure 3.16, an identical conclusion as that above can be deduced from Figure 3.11 - Figure 3.13, which shows the robustness and strong accuracy of the proposed SPF algorithm.

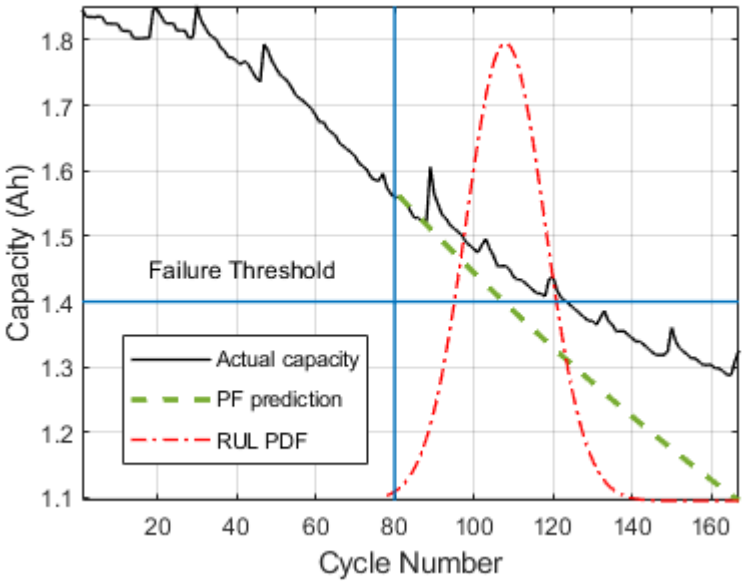

Figure 3. 11 Prediction RUL results of PF at 80 cycles for B05.

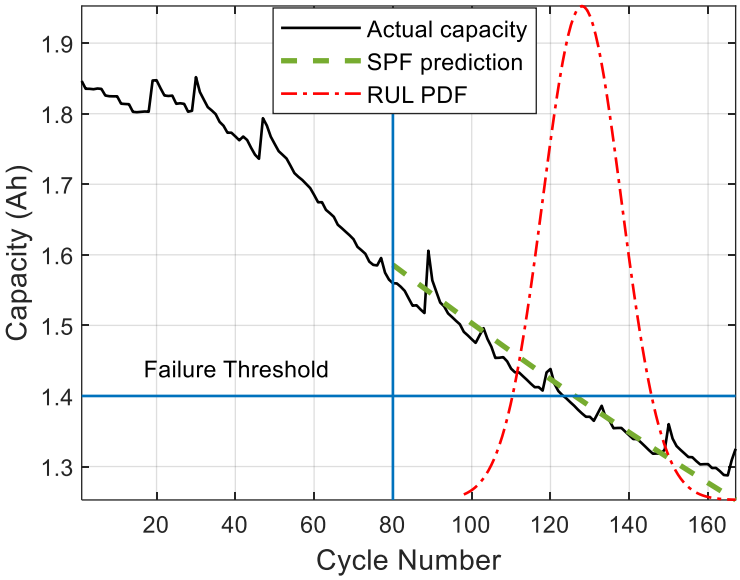

Figure 3. 12 Prediction RUL results of SPF at 80 cycles for B05.

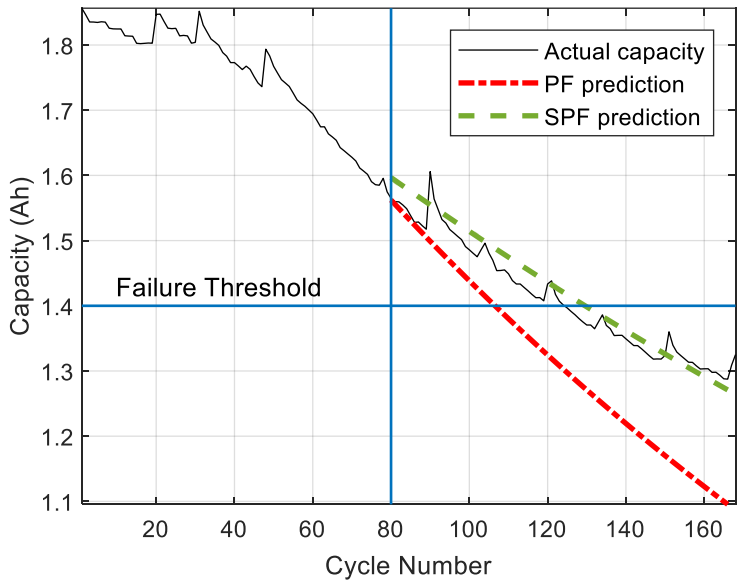

Figure 3. 13 comparison results at 80 cycles for B05.

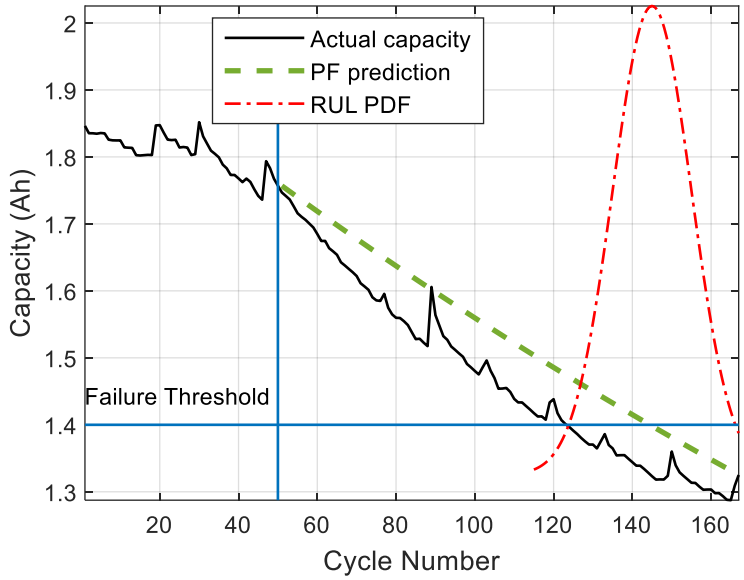

Figure 3. 14 Prediction RUL results of PF at 50 cycles for B05.

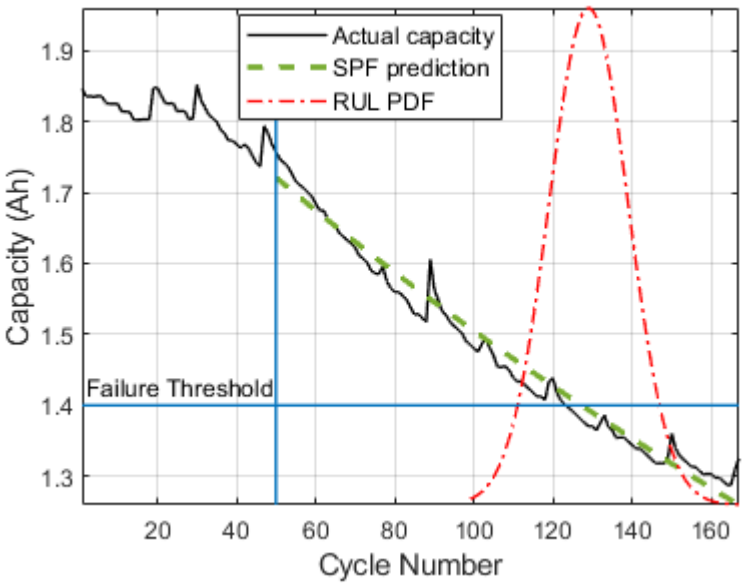

Figure 3. 15 Prediction RUL results of SPF at 50 cycles for B05.

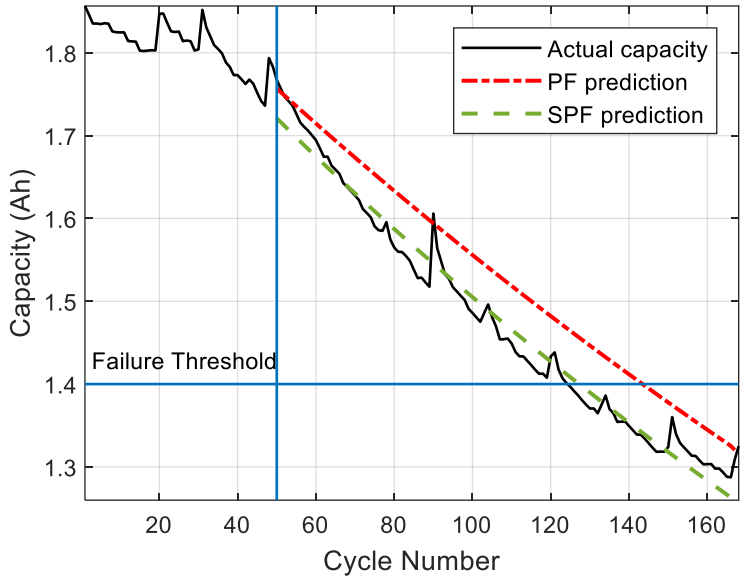

Figure 3. 16 comparison results at 50 cycles for B05.

Figures 3.17 and 3.18 show the prediction RE of the RUL using the PF method and the proposed SPF method; in the prediction update phase, the first 50 and 80 cycles are used, respectively. The RE of the SPF method is less than the relative error of the PF method.

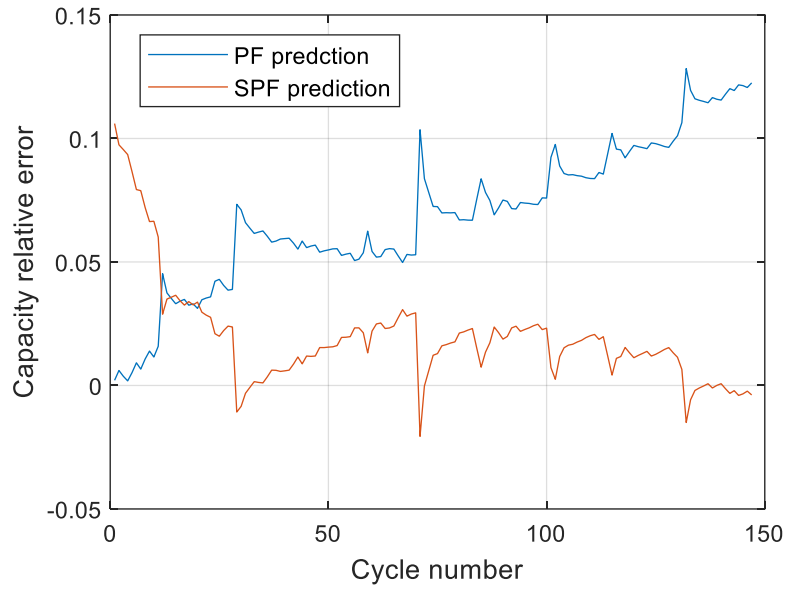

Figure 3. 17 Prediction RUL results of PF at 50 cycles for B05.

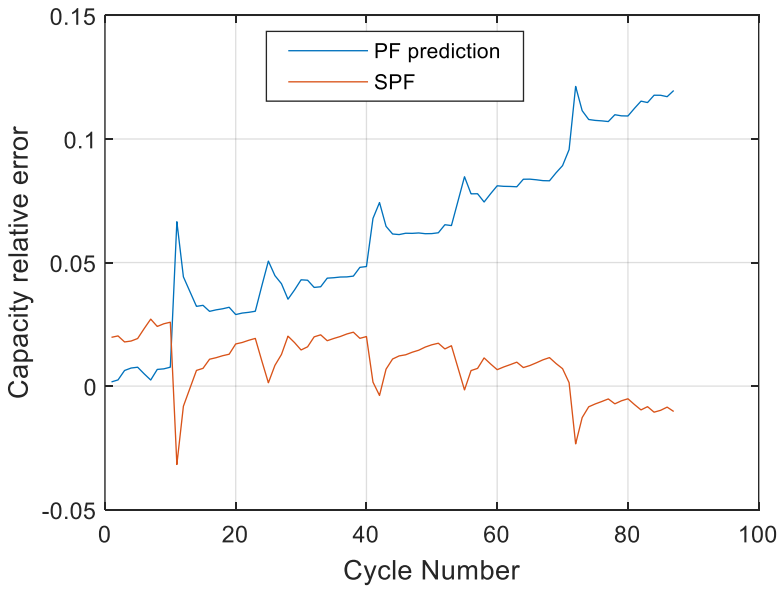

Figure 3. 18 Prediction RUL results of SPF at 50 cycles for B05.

Table 3.3 shows the error rates for the prediction RUL of the battery B05 obtained by the PF and proposed SPF methods with different starting points. The AE, RE and RMSE of the proposed SPF algorithm are significantly smaller than of the PF algorithm. In addition, the

findings clearly show (Figures 3.11–3.16) that the start point is continuously regressed, and so the prediction error becomes nearer to zero; this is in line with the real-time application. The findings also show that the algorithm converges with the predicted start point, and thus much more training data can be employed for learning, and better degradation knowledge and characteristics can be revealed. It was also seen that the prediction error is lower in the reverse direction, indicating that the particles are more compacted as more capacity data are accessible.

3.6.2 RUL Prediction Using ($B06, B07$ & $B18$) Batteries

To verify the result obtained previously, capacity degradation data was used for $B06$ and $B18$ batteries to check the accuracy of the proposed method for RUL prediction. Battery $B07$ was dispensed for the investigation because it did not possess degradation data below the failure threshold (see Figure 3.6). Figures.3.19-3.25 show the RUL result for the battery $B06$ and $B18$ data using the PF and proposed SPF algorithms at starting point 50 cycles. Similar to $B05$ dataset, the accuracy of the estimation findings and the RUL PDF gained by the suggested SPF approach is just greater than that provided by the PF. That is, the prediction error of the suggested approach is four cycles lower than the PF using 50 cycles, and the value of the RE and AE are also reduced.

Table 3. 3 RUL prediction result of B05.

Method	T_S	RUL_{True}	RUL_{Pred}	AE	RA
PF	20	125	94	31	0.2480
	50	125	144	19	0.16
	80	125	108	16	0.1360
SPF	20	125	134	9	0.072
	50	125	129	4	0.032
	80	125	127	2	0.024

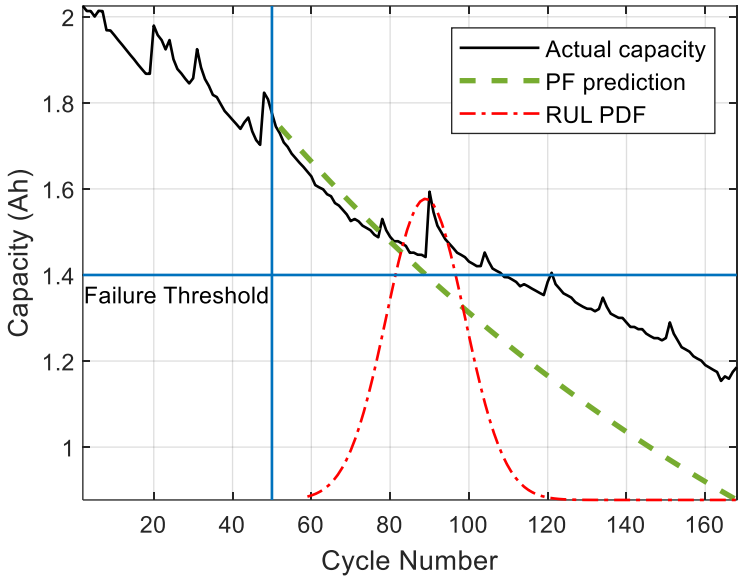

Figure 3. 19 Prediction RUL results of PF at 50 cycles for B06.

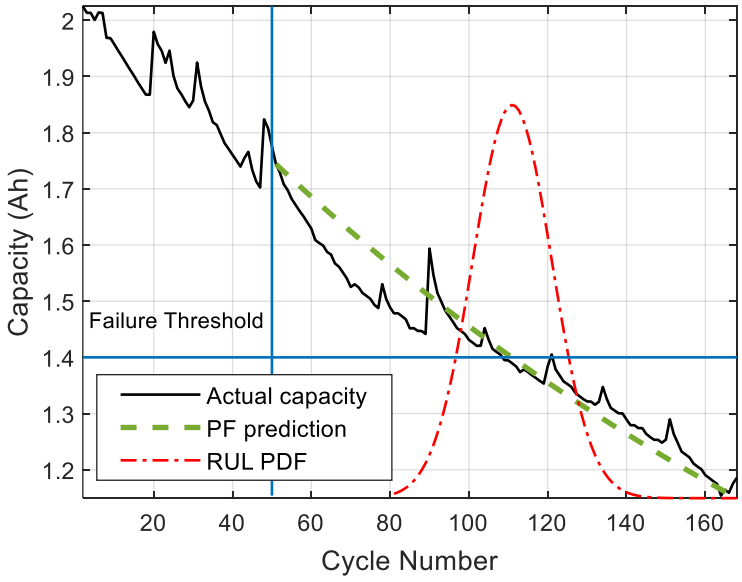

Figure 3. 20 Prediction RUL results of SPF at 50 cycles for B06.

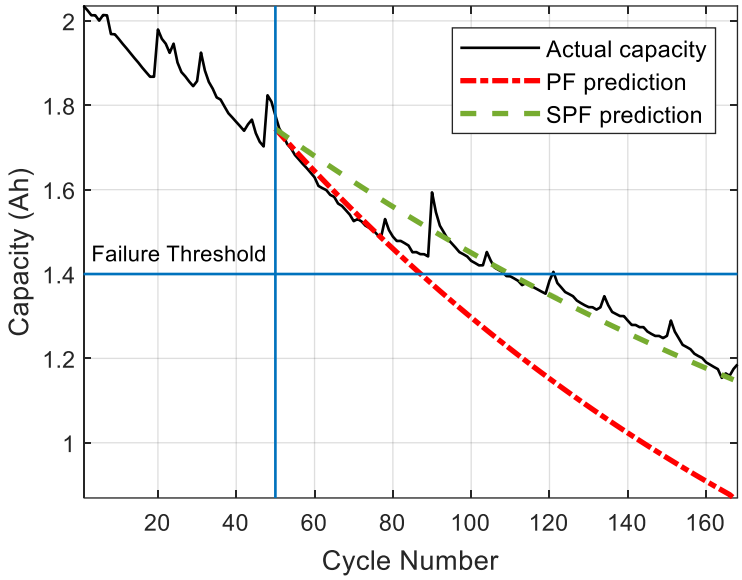

Figure 3. 21 comparison results at 50 cycles for B06.

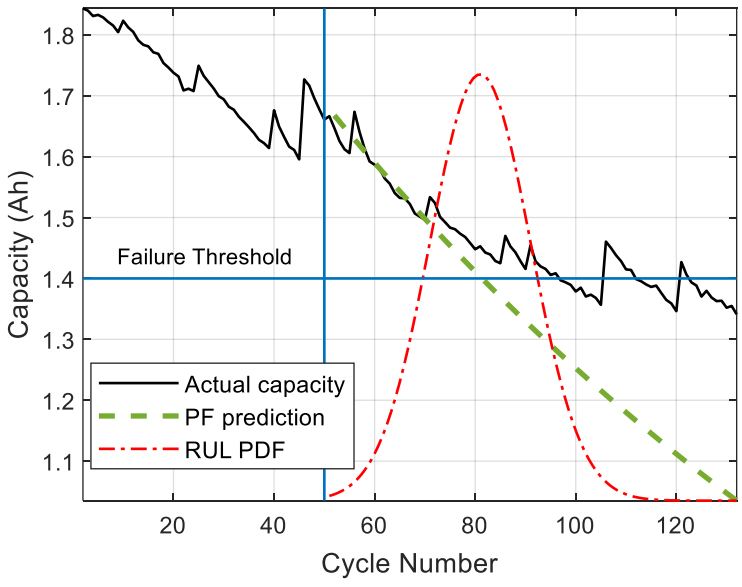

Figure 3. 22 Prediction RUL results of PF at 50 cycles for B18.

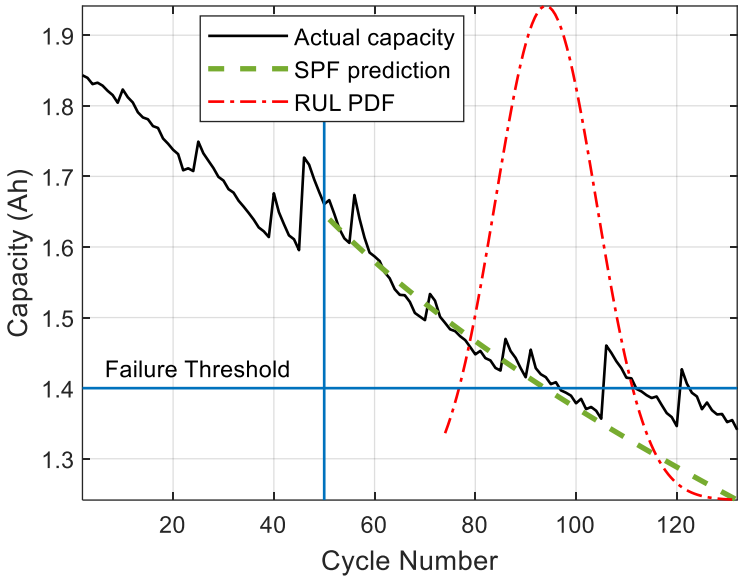

Figure 3. 23 Prediction RUL results of SPF at 50 cycles for B18.

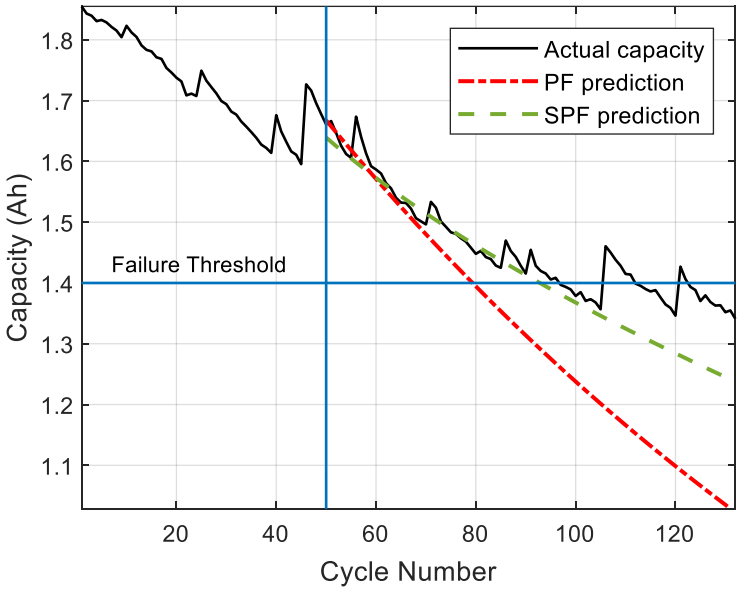

Figure 3. 24 comparison results at 50 cycles for B18.

As shown in Table 3.4, the prediction relative error and absolute error under various prediction starting points (T_s) of the proposed SPF algorithm for $B06$ and $B18$ are both smaller

than that of the PF algorithm, which indicates that the stability of the proposed SPF algorithm is higher than the PF algorithm. For example, at $T_s = 50$ cycles, the B06 battery's AE prediction of SPF was approximately 2 cycles, the maximum RE was about 0.0183 and that AE of the PF algorithm was around 20 cycles, and the RE was approximately 0.1835, which can lead to the same conclusions as discussed for B05.

Table 3. 4 RUL prediction results of B06 and B18.

Cell ID	Method	T_S	RUL_T	RUL_p	AE	RA
B06	PF	20	109	133	24	0.2202
		50	109	89	20	0.1835
		80	109	98	11	0.1009
	SPF	20	109	113	4	0.0367
		50	109	111	2	0.0183
		80	109	108	1	0.014
B18	PF	20	98	74	24	0.2474
		50	98	81	17	0.1694
		80	98	89	8	0.0825
	SPF	20	98	106	9	0.0928
		50	98	93	5	0.0309
		80	98	100	2	0.0206

3.7 Summary

In the area of RUL prediction, Bayesian filter methods, like the classic PF algorithm, provide promising results in terms of fast convergence rates and small prediction errors when used for

RUL prediction. This is because Bayesian filter methods can effectively handle the uncertainty and noise inherent in real-world data and provide probabilistic estimates of the remaining useful life, which is crucial for reliable and safe systems operation. However, the PF algorithm needs to improve on two main problems: particle degeneracy and particle impoverishment. Therefore, this chapter has proposed a novel approach to predict the RUL of batteries. The proposed method combines the SPF algorithm with a likelihood approximation technique to estimate the probability distribution of the RUL of the battery. In this algorithm, the system's state is represented by a set of particles, and each particle is propagated over time according to a degradation model. The degradation model used in the SPF algorithm is a second-order exponential model, which has been found to represent LiB's degradation behaviour accurately. The SPF algorithm has demonstrated its effectiveness as a robust and reliable method for predicting the RUL of LiBs. This is due to its ability to handle noisy measurements and adapt to various battery degradation models. Results show that the proposed prediction approach has an improved prediction accuracy and convergence rate in comparison with PF and other methods such as UPF. Since the maximum error of the SPF predicting approach is relatively small, RUL prediction in the best case at the prediction starting point of 80 cycles is 127 cycles. The prediction relative error was approximately 0.024, and the absolute error of the proposed algorithm is around 2 cycles, lower than the PF (around 16 cycles). RUL prediction is nearby 108 cycles, and the relative error is around 0.136, while the absolute error prediction is approximately 16. Moreover, the results showed that the SPF algorithm improved the prediction accuracy compared to the classical PF algorithm, with lower average RUL errors and PDF width. Testing with various predicted starting points revealed that the amount of data affected the accuracy of the prediction, with higher starting points resulting in lower prediction error rates. Ongoing research is planned to focus on developing robust degradation models, such as the Multiphysics model, to improve RUL prediction accuracy and convergence rate.

Chapter 4 Physics-Based Modelling for Monitoring Battery Lifetime

'In Chapter 3, an innovative approach was devised for RUL prediction for LiBs using an advanced method known as SPF to approximate likelihood. The proposed SPF algorithm demonstrates the capability to accurately foresee unknown degradation model parameters and compute the degradation state by solving an optimization problem in each cycle. This method surpasses a mere gradient step, facilitating faster convergence, stability, and improved prediction precision. A critical discovery in Chapter 3 was that this approach significantly improved the RUL prediction accuracy and speed of convergence when contrasted with the classic PF and other sophisticated PF algorithms, such as the UPF algorithm. Despite these promising results, the proposed approach does exhibit certain operational constraints. Firstly, a sizable amount of data is required to extend predictions to typical operating scenarios. Secondly, the algorithm needs help to readily illustrate variations from one battery cell to another due to disparities in manufacturing or the heterogeneity of temperatures within a single battery pack or current distribution. Lastly, using an empirical aging model presents limitations, as it doesn't account for physical degradation mechanisms, which hinders the capturing of knee points - significant shifts in degradation on the capacity fade curve. Degradation rates may be attributable to modifications in the fundamental mechanism, such as an increase in the SEI layer, which prompts lithium plating [37–39]. These elements are challenging to evaluate, especially when dealing with rudimentary empirical degradation models.'

4.1 Introduction

The RUL is critically important for the PHM of LiBs to provide early warning to ensure the reliability and safety of host devices. Recently developed methods in the literature for RUL prediction face two challenges. First, most approaches are mainly developed based on traditional empirical degradation models without considering degradation mechanisms. Second, the stability of the standard PF method is strongly constrained by the issue of a lack of particles and the uncertainty in the degradation model parameters, which are constrained by the availability of sufficient and reliable data. Consequently, this can lead to inaccurate RUL prediction. To address these challenges, this chapter proposes a novel approach that integrates a physics-based model with an SPF for RUL prediction. The physics-based model considers three main degradation mechanisms [103, 107, 173]: LAM in positive and negative electrodes and LLI. By incorporating these mechanisms directly correlated with the RUL of LiB, the model provides a more accurate representation of the degradation process. The SPF, on the other hand, is an improvement over the classical PF method, which suffers from particle degradation and diversity deficiency issues. The proposed algorithm uses a likelihood approximation scheme to smooth the PF, enhancing its stability and overcoming the limitations associated with particle decomposition. Compared with the conventional capacity-based methods, such as the SPM-based particle filter (SPM-PF), the proposed physics-based method produces a more accurate RUL prediction. The results demonstrate that the proposed framework predicting is relatively small. At the prediction starting point of 2000 cycles, the best-case RUL prediction is 2402 cycles. Additionally, the minimum relative error is found to be around 0.089%, and the relative error of the traditional framework is approximately 0.8%. Furthermore, LiBs data, including Gaussian white noise and dynamic discharging profiles, have been utilised to demonstrate the dependability and robustness of the proposed framework.

The chapter starts in section 4.2, explaining the proposed physics-based model. Then the incorporation of three main degradation mechanisms: LAM in positive and negative electrodes, and LLI are mathematically formulated in sections 4.3. to 4.4. Root-mean-square error and mean absolute percentage error comparison are presented in section 4.5. Sections 4.6 and 4.7

presents the RUL prediction by integrating the SPM into the SPF framework. The results are reported and discussed in sections 4.8. to 4.11

4.2 Single Particle Model for Lithium-ion Batteries

The foundation of this study is based on the enhanced single particle model presented in [173] and which has been widely employed for simulating battery packs, SOC, and SOH for various Li-ion chemistries. The electrochemical SPM of LiBs has been simplified for a more complex Li-ion P2D model in [174-176]. In SPM, the active porous materials are expressed at the anode and the cathode electrode by one spherical particle of the active material, as shown in Figure 4.1 [176]. The load current, material qualities, geometric design parameters, and operating temperature are all inputs to the model. The main output of this model is the cell voltage and SOC [177].

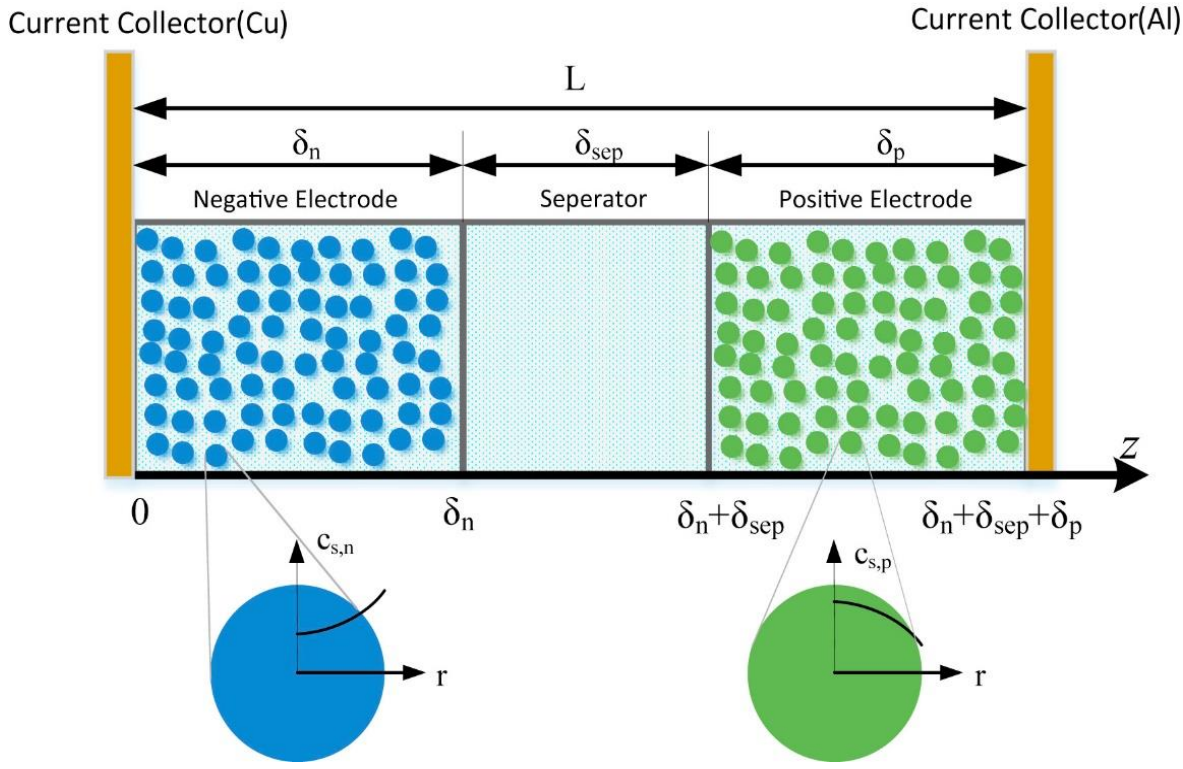

Figure 4. 1 Physics-based model for LiB [175].

4.2.1 Governing equations

One of the most critical assumptions in the SPM is that current distribution in the porous electrode is assumed to be uniform and therefore represents a single intercalation particle, the complete porous electrode (positive and negative). The second law of Fick in a spherical coordinate system describes the balance of mass material for lithium-ion inside each electrode's active material (cathode/anode) as:

$$\frac{\partial c_{s,j}}{\partial t} = \frac{1}{r^2}\frac{\partial}{\partial r}\left(D_{s,j} r^2 \frac{\partial c_{s,j}}{\partial r}\right) \tag{4.1}$$

With initial boundary conditions ($r = 0$), the molar flux of lithium-ions is zero, indicating no diffusion in the centre of the particle. At ($r = R_j$), the molar flux of lithium-ions is equal to J_j, meaning that the transfer of charges occurs at the outer boundary of the particle. These initial boundary conditions can be expressed as follows:

$$D_{s,j}\frac{\partial c_{s,j}}{\partial r}\bigg|_{r=0} = 0 \tag{4.2}$$

$$D_{s,j}\frac{\partial c_{s,j}}{\partial r}\bigg|_{r=R} = J_j \tag{4.3}$$

Where, $c_{s.j}$ represents the solid-state concentration, t is time, $D_{s,j}$ represents the solid phase diffusion coefficient, r refers to the radius direction coordinate, R_j is the solid particle radius, and $j = p, n$ corresponds to the positive and negative electrodes, respectively; J_j is the molar flux of lithium ions at the surface and can be defined as [175]:

$$\begin{cases} J_P = \dfrac{1}{FS_p} \\ J_n = \dfrac{-1}{FS_n} \end{cases} \tag{4.4}$$

Where, I refers to the total input current, defined as positive for the charging and negative for the discharging processes; S_j is the total electroactive surface area of each electrode and can be expressed as:

$$S_j = \frac{3\varepsilon_j V_j}{R_j} \tag{4.5}$$

Where, $\varepsilon_j$is the active volume fraction of the material in electrode j, and V_j represents the total volume of the electrode j. The SOC variable for the solid electrode particles is defined as follows:

$$SOC_j = \frac{C_{s,j}^{surf}}{C_{s,j}^{max}} \tag{4.6}$$

Where, $C_{s,j}^{surf}$ and $C_{s,j}^{max}$ are the surface and maximum concentration of lithium into electrode particles, respectively. The Butler-Volmer rate in (4.7) is used to calculate the rate of local electrochemical reactions in terms of concentration and potential. Where, i_o represents the exchange current density, T is the temperature, and R refers to the universal gas constant.

$$i_n = i_o\left[exp\left(\frac{0.5F\eta}{RT}\right) - exp\left(\frac{-0.5F\eta}{RT}\right)\right] \tag{4.7}$$

The overpotential (η) is defined as the thermodynamics potential drop between the solid and the solution at the existing surface concentrations.

$$\eta = \phi_s - \phi_l - E_{eq} \tag{4.8}$$

Where, ϕ_s is the solid potential, ϕ_l is the liquid potential, and E_{eq} represents the open-circuit potential of the solid material evaluated at the surface concentration. By applying an inverse hyperbolic form of Butler-Volmer expression as in (4.8), solid-phase potential can be defined as:

$$\phi_s = E_{eq} + \phi_l + \frac{\eta RT}{0.5F} \sinh^{-1}\left(\frac{i_{loc}}{2i_o}\right) \tag{4.9}$$

The potential difference between the positive and negative electrodes in the solution phase can be calculated as [176]:

$$\phi_{l,positive} - \phi_{l,negative} = IR_{solution} \tag{4.10}$$

Where, $R_{solution}$ denotes the solution phase resistance, determined by a combination of mass and charge transfer processes. After solving the above equations, the cell voltage is determined by the difference between the potentials of the positive and negative electrodes:

$$E_{cell} = \phi_{s,positive} - \phi_{s,negative} \tag{4.11}$$

The values of the model's parameters used in this study are given in Table 4.1 [173] .

Table 4. 1 Single particle Dimensional Battery Model Parameters.

Parameter	Value	Description
L_n	168×10^{-6} (m)	Thickness of the negative electrode
L_s	19×10^{-6} (m)	Thickness of the separator
L_p	124×10^{-6} (m)	Positive electrode thickness
ε_n	0.5	Negative electrode porosity
ε_s	1	The Separator porosity

ε_p	0.5	positive electrode porosity
D_e	7.5×10^{-11} $(m^2 s^{-1})$	Coefficient of diffusion in electrolyte.
k_j	2 $\times 10^{-6}$ $(m^{2.5} mol^{0.5} s^{-1})$	Reaction rate constate
F	96487 $(C\ mol^{-1})$	Faraday's constant
i_{app}	$2.7 \times C - rate$ $(A\ m^{-2})$	the density of discharge current equal to C rate multiplied by 1C
c_o	2000 $(mol\ m^{-3})$	Initial concentration
$D_{s,n}$	8×10^{-14} $(m^2 s^{-1})$	Diffusion of Lithium in a Solid, at a negative electrode
$D_{s,p}$	7×10^{-13} $(m^2 s^{-1})$	Diffusion of Lithium in a Solid, at a positive electrode
r_n	12.5×10^{-6} (m)	Radius of a particle at a negative electrode
r_p	8.5×10^{-6} (m)	Radius of a particle at a positive electrode
R_g	8.314 $(J\ mol^{-1}\ K^{-1})$	Universal gas constant
T	298.15 K	Temperature of ambient
E_s	10 GPa	LMO modulus of Young
E_n	60 GPa	LiC_6 modulus of Young
v_s	0.3	LMO ratio of Poisson
v_n	0.25	LiC_6 ratio of Poisson
$C_{max,Pos}$	51385 $(mol\ m^{-3})$	Positive maximum concentration
$C_{max,Neg}$	30555 $(mol\ m^{-3})$	Negative maximum concentration

4.3 SPM Coupled with Capacity Degradation Model

In the literature, there are several degradation mechanisms reported for LiBs. Different models can describe these mechanisms, with multiple models often used to describe a single mechanism [173]. The four main degradation mechanisms included in this model are SEI layer growth at the anode particle surface, surface cracking, LAM due to mechanical stress, and

lithium plating. The degradation model is dependent on the previously described SPM and is used to mathematically describe the impact of these degradation mechanisms on the performance and safety of the LiBs [178].

4.3.1 SEI layer growth

Many researchers have argued that the growth of the SEI layer on the graphite electrode is considered the most critical degradation mechanism in LiBs [118, 179]. The SEI layer forms due to the reduction of components of the electrolyte solvent in a reaction with lithium ions and electrons from the graphite electrode. The reaction products deposit on the graphite surface and form the SEI layer [31, 32]. Various reactions between the electrolyte components and lithium ions have been proposed, depending on the local voltage. However, the reaction most commonly modelled by researchers is the one between ethylene carbonate and lithium ions [180, 181].

$$2C_3H_4O_3\,(l) + 2e^- + 2Li^+ \leftrightharpoons (CH_2OCO_2Li)_2\,(s) + C_2H_4\,(g) \tag{4.12}$$

By integrating the side reaction current (i_{SEI}), the capacity loss rate due to SEI layer expansion (Q_{SEI}) can be calculated as in (4.13)

$$Q_{sei} = \int_0^t i_{sei}\, A\, dt \tag{4.13}$$

The side-reaction current (i sei) can be estimated to (4.13) by assuming that the diffusion of the solvent components is the significant contributing factor in the side reaction of (4.14) [182]:

$$i_{sei} = -nF k_s c_s(0,t) \exp\left(-\frac{\alpha_c nF}{R_g T}\eta_s\right) \tag{4.14}$$

Where $(-nF)$ is the total charge of electrons, (k_s) is the side-reaction constant, $(c_s(0,t))$ is the concentration of the reaction and reduction product at $x = 0$, and (η_s) is the side-reaction overpotential given in (4.15).

$$\eta_{sei} = V_{neg} + \eta_{neg} - V_{sei} + r_{sei}\delta I \tag{4.15}$$

Where the overpotential for the SEI side reaction ηsei is a function of the anode potential V_{neg}, the anode overpotential η_{neg}, the equilibrium potential of the SEI growth reaction V_{sei}, and the resistive voltage drop across the existing SEI layer of thickness δ and specific resistance r_{sei} .

As the SEI layer grows, it can have serval impacts on the battery performance. The growth rate of the SEI layer and its corresponding passivation layer is directly proportional to the SEI side reaction current density [181]:

$$\frac{d\delta}{dt} = \frac{i_{sei}M}{\rho nF} \tag{4.16}$$

Where M is the molecular weight of the SEI layer, and ρ is its density. The side reaction of the SEI layer can also lead to a LLI, where the lithium ions that are consumed in the side reaction can no longer participate in the main reaction. This loss of lithium ions affects the boundary condition for lithium diffusion at the surface of the graphite electrode [118]. The lithium concentration gradient at the negative particle surface becomes a function of both the main current density on the negative electrode (i_{neg}) and the SEI side reaction current density (i_{sei}). This means that the boundary condition for lithium diffusion must be revised to account for the SEI side reaction and its impact on the lithium concentration gradient. The new boundary condition can be represented by an equation that considers both the main current density and the SEI side reaction current density:

$$D_{neg}\frac{dc_{neg}(r,t)}{dr}\bigg|_{r=R} = -\frac{i_{neg}}{nF} - \frac{i_{sei}}{nF} \tag{4.17}$$

Surface cracking

The volume expansion and contraction of LiBs during intercalation and deintercalation can cause stress and fatigue in the electrodes, leading to crack propagation. The formation of cracks

increases the surface area for the growth of the SEI layer, resulting in a greater loss of cyclable lithium [183].

To model this, several researchers [183-185] have developed a model to study the relationship between stress and the growth of the SEI layer in Li-ion batteries. The model started with a physical description of the stress and strain in spherical graphite particles and the SEI layer but was eventually simplified to a correlation between surface concentration and stress. They then utilised Wöhler curves with a slope m_1 to link the number of cycles to failure with the stress variation $(\sigma_{max} - \sigma_{min})$ in Li-ion batteries relative to the maximum yield strength σ_{yield}. The Wöhler curves are based on a statistical analysis of metal fatigue, and the value of m_1 was obtained by fitting the simulation results to experimental data [186]. Due to a lack of experimental data, the yield strength of a material is often viewed as a fitting parameter instead of a material property. Thus, the authors in [183] modelled the relationship between the lost charge capacity (Q_{lost}) and the mean stress by assuming linear damage accumulation. They related Q_{lost} per cycle N to the mean stress using a fitting parameter β_2, according to:

$$\frac{Q_{lost}}{N} = \beta_2 \left(\frac{\sigma_{max} - \sigma_{min}}{\sigma_{yield}} \right)^{\frac{1}{m_1}} \tag{4.18}$$

4.3.2 Loss of active material

The above section discussed how fractures could start and spread from electrode surfaces. Electrode cracking can also be caused by the same underlying physical events (such as alternating stresses). This may reduce the amount of active material available for utilisation and lead to a loss of electrical contact.

Several researchers [26, 184, 187-189] have developed mathematical expressions used in mechanical stress models for spherical particles (R_0) in battery electrodes. These models use physical properties such as the partial molar volume (Ω), Young's modulus (E), Poisson's ratio (v), and Li-concentration (c) to calculate the radial stress (σ_r) and tangential stress (σ_r) at different points within the particle. The dummy integration variable (ζ) is used to

perform numerical integrations in the model. These models are useful in understanding the behaviour of spherical particles under mechanical stress and improving the performance and reliability of batteries. The equations for radial and tangential stress, respectively, are

$$\sigma_r(r) = \frac{2\Omega E}{3(1-v)}\left(\frac{1}{R_0^3}\int_0^{R_0} c(r)r^2 dr - \frac{1}{r^3}\int_0^r c(\zeta)\zeta^2 d\zeta\right) \tag{4.19}$$

$$\sigma_t(r) = \frac{\Omega E}{3(1-v)}\left(\frac{2}{R_0^3}\int_0^{R_0} c(r)r^2 dr - \frac{1}{r^3}\int_0^r c(\zeta)\zeta^2 d\zeta - c\right) \tag{4.20}$$

The radial and tangential stress can be combined into the hydrostatic stress σ_h, given by:

$$\sigma_h(r) = \frac{\sigma_r(r) + 2\sigma_t(r)}{3} \tag{4.21}$$

4.3.3 Lithium plating

The formation of metallic lithium, also known as lithium plating, can occur in lithium-ion batteries when the battery is overcharged. This process can be described by the Butler-Volmer or Tafel kinetics models, which are commonly used to model electrochemical reactions in batteries [190-193].

The degradation caused by the plating side reaction current in a lithium-ion battery has similar consequences as the growth of the SEI layer, leading to the clogging of anode pores and loss of capacity. The authors in the study [44] have shown partial recovery of lost capacity through re-insertion of plated lithium; however, this mechanism is not included in the current model being considered. The equations used to describe lithium plating are very similar to the kinetically limited SEI growth model, namely:

$$\mathrm{i_{pl}} = \mathrm{i_{0,pl}}\exp\left(\frac{\alpha \mathrm{nF}}{\mathrm{RT}}\eta_{\mathrm{pl}}\right) \tag{4.22}$$

$$\eta_{\mathrm{pl}} = \mathrm{V_{neg}} + \eta_{\mathrm{neg}} - \mathrm{V_{pl}} + \mathrm{r_{sei}}\delta I \tag{4.23}$$

4.4 Parameters of Degradation Model

Various studies have successfully applied a physics-based model for LiBs in the quantification of the three degradations mechanisms of LiBs: LAM_{PE}, LAM_{NE} and LLI. In total, active mass loss is the amount of the loss of active mass in both lithiated and delithiated status [103]. However, estimating the loss of lithified active material is difficult since the degree of lithification of the lost mass is frequently unclear. Consequently, the loss of active mass, or LAM, is typically considered to be the loss in a delithiated condition. In this study, LLI is also considered the loss when the active mass is in a lithiated state [174]. A degradation parameter can correspond to each degradation mechanism. Moreover, tracking m_p (positive) and m_n (negative) active masses can help estimate LAM_{PE} and LAM_{NE}. To predict the LLI, the LII (lithium inventory indicator) is defined as related to both x_{offset} and m_p [103]:

$$LLI = Q_p - x_{offset} \tag{4.24}$$

Where, Q_p represents the capacity of the positive electrode in SPM. In a lithium-ion cell, ions transfer from the negative to the positive electrode during the discharging state and from the positive to the negative electrode during the charging state (see Figure 4.2). After the negative electrode has been completely delithiated, the battery cell cannot physically discharge since no lithium is left in the negative electrode to be transferred to the positive electrode [107]. Similarly, the battery cell will not charge if the positive electrode has been "completely delithiated" to the point that the material's structural integrity has been compromised. As a result, the *LII* in Figure 4.3 is the maximum lithium inventory for the battery cell that spans from the left end of the negative electrode SPM curve (i.e., NE is completely delithiated for the drained cell) to the right end of the positive electrode SPM curve (i.e., PE is fully delithiated for the charged cell). According to (12), *LLI* in the battery cell grows faster than LAM_{PE} when an offset (x_{offset}) becomes progressively negative (i.e., moves to the left or right in the positive electrode or negative electrode curves) [103, 107]. In contrast, as x_{offset} becomes more positive, either the positive electrode curve moves to the right, or the negative electrode curve moves to the left. Thus, the rate of LAM_{PE} in the battery cell rises faster than the rate of *LLI* in the battery cell. Practically, a rise in *LLI* is

caused by a battery cell's lithium inventory being depleted by parasitic processes (such as the formation of SEI and delamination of lithiated electrode material). Upon estimation of the degradation parameters mp, mn, and LII in the battery cell, the most suitable mathematical models must be employed to reveal the parameter trends and thus achieve physics-based prognostics [103].

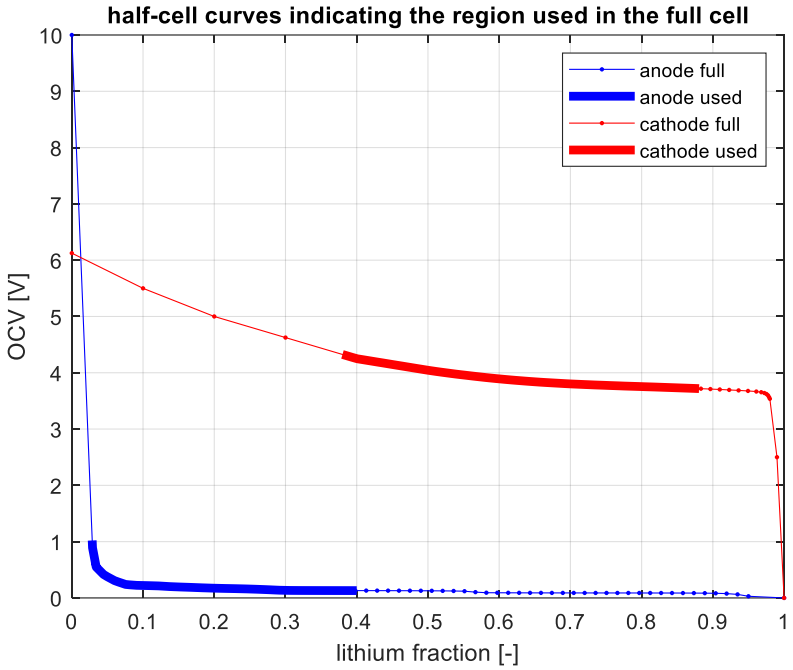

Figure 4. 2 Schematic of the shift in stoichiometric range of each electrode due to loss of cyclable lithium.

4.5 Experimental Validation and Analysis

For the purposes of comparison, the prediction performance of the proposed SPM-SPF prognostic framework and the traditional capacity prognostic framework were employed. This comparison was made to verify both the accuracy of the conventional framework and the proposed SPM-SPF framework's predictions using alternative cycle "beginning points," such as 1,000 or 2,000 cycles. The prediction accuracy was assessed by comparing the RUL's AE, RMSE. As shown in (3.24), AE is the difference between how many actual (RUL_A) cycles are left and how many predicted (RUL_P) cycles there are in total. The RMSE and mean absolute percentage error (MAPE) are defined in this manner in (4.25, 4.26), respectively, as

shown in (4.25), Q_k represents the actual capacity value, and $\hat{Q}_k$ detonates the estimated capacity value. MAPE measures the average absolute percentage deviation between the actual values and the predicted values, as shown in (4.26). Where M represents the mean absolute percentage error, and n is the number of times the summation iteration happens.

$$RMSE = \sqrt{\frac{1}{k_p}\sum_{k=T_s}^{C}(Q_k - \hat{Q}_k)} \tag{4.25}$$

$$M = \frac{1}{n}\sum_{t=1}^{n}\left|\frac{Q_k - \hat{Q}_k}{Q_k}\right| \tag{4.26}$$

4.6 Prediction of Physically Based Capacity and RUL

For physics-based prognostic approaches, accurate tracking of the three degradation trends (m_p, m_n, and LLI) required to obtain robust predictions by tuning the parameters of the empirical degradation model (Section 4.4). To achieve this, the least-squares approach is used to find the coefficients of the degradation models that best fit the empirical models and the estimated degradation parameters, assuming adequate measurements are presented. Due to this restriction, the RUL prediction is usually based on a set of measurements from a cell which has been assessed. Consequently, the estimated parameters of the model might be inaccurate [194]. According to [103], the model coefficients can be constrained by additional information in a training group of cells, differently from the assessed cell. The characterisation of the characterisations indicates that it can be used as training data to estimate cell degradation parameters. As shown in Figure 4.3, firstly, the future test cell degradation coefficients ($tests\ k + I, i = 1,\ldots$) are extracted using model configurations. Moreover, all three degradation parameters are computed based on model parameter estimation up to time k. In the second stage, the physical model stimulates cell capacity degradation based on the predicted degradation parameters. However, voltage cut-off points must be chosen when simulating the capacity of a full-cell curve. During the cycle ageing test, the battery cells are cut off at 3.4 V. The predicted capacity from the half-cell model is calculated with a lower cut-off voltage of 3.45 V to account for the polarisation impact at the

start of charging. In the third stage, the proposed SPF method is constructed and initialised (see Section 3.3.6). Finally, when the estimated capacity falls below the end-of-life threshold, the RUL is determined by subtracting the present time (or test number) from the end-of-life.

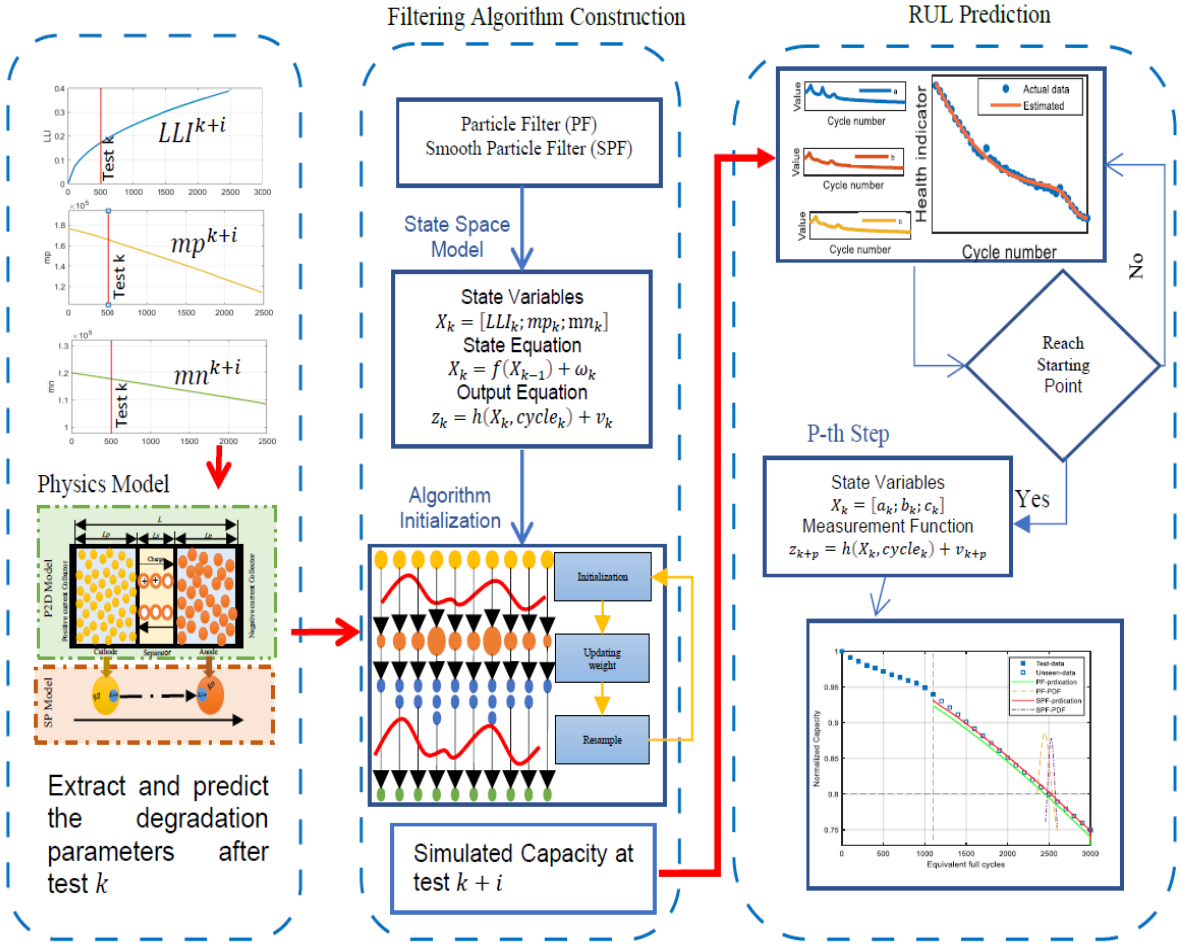

Figure 4. 3 Block diagram of physics-based capacity and RUL prediction.

In this study, we have demonstrated a physics-based model approach to tracing the three degradation parameters to allow a physical explanation of the significant degradation mechanisms that lead to battery cell degradation. This feature distinguishes the proposed framework from current traditional capacity prognostic approaches that only measure cell capacity. The proposed SPF and PF methods are used to fit mathematical degradation models

to degradation parameter estimation, each of which captures the evolution of a single parameter. Degradation model coefficients are estimated from a training data group. When fitting the model to the test data, these estimated coefficients provide boundaries for restricting the model coefficients.

In this work, the battery cell is used for RUL prediction, and the end of service is defined as the total number of cycles when the battery's capacity falls below the 80% threshold for safe operation. The dataset of capacity is divided into training data and testing data. The proposed SPM-based and traditional capacity-based approaches are used with different operating conditions when the starting point of the prediction (T_p) is the 1,000th and 2,000th cycle. The initial setting values of the PF and proposed SPF parameters were selected as the number of particles is 200, and residual resampling was used. The process noise was $\omega_k = [1 \times 10^{-6}, 1 \times 10^{-6}, 1 \times 10^{-6}, 1 \times 10^{-6}]^T$, while the observation noise was $v_k = 1 \times 10^{-4}$, which is more in the traditional capacity-based approach. Unlike the conventional capacity-based system, the process noise was $\omega_k = [1 \times 10^{-6}, 1 \times 10^{-3}, 1 \times 10^{3}, 1 \times 10^{-6}]$, while the observation noise was $v_k = 1 \times 10^{-1}$ in the SPM-based system.

4.7 RUL Prediction

Empirical, basic mathematical models can be used to track nonlinear degradation trends in cell capacity and degradation parameters.

$$Q(t) = 1 - \alpha t^{\beta} \tag{4.27}$$

Where $Q(t)$ represents the model output, which can either indicate the battery capacity or a degradation parameter, t is the amount of time passed during the test, and α and β refer to the model parameters estimated from measurements data. The empirical model is similar to the well-known square root of the t degradation model (also known as the standard capacity fade model) [195], which captures the increase in SEI when = 0.5. The battery system state change may be described as follows using the capacity degradation model:

$$x_k = [\alpha_k; \beta_k] \tag{4.28}$$

Where,

$$\begin{cases} \alpha_k = \alpha_{k-1} + \omega_\alpha \rightarrow \omega_\alpha \sim N(0, \sigma_\alpha) \\ \beta_k = \beta_{k-1} + \omega_\beta \rightarrow \omega_\beta \sim N(0, \sigma_\beta) \end{cases} \tag{4.29}$$

Now the measurement in (4.27) is given by:

$$Q(t)_k = 1 - \alpha_k t^{\beta_k} + v_k \rightarrow v_k \sim N(0, \sigma_v) \tag{4.30}$$

A measurement of the capacity cell at cycle k is represented by $M(t)_k$, whereas $N(0, \sigma_V)$ represents the zero-mean Gaussian noise and represents the standard deviation. Then, the capacity of the cell can be estimated as:

$$Q(t)_k = \sum_{i=1}^{N} Q(t)_k^i = \sum_{i=1}^{N} \left[1 - \alpha_k^i t^{\beta_k^i}\right] \tag{4.31}$$

The prediction step (p-th) may be determined using the following formula at cycle k:

$$Q(t)_{k+p} = \sum_{i=1}^{N} Q(t)_k^i = \sum_{i=1}^{N} \left[1 - \alpha_k^i t(k+p)^{\beta_k^i}\right] \tag{4.32}$$

As a result, an estimate of the RUL for each particle can be calculated by:

$$RUL_k^i = argmin_j \left[\left(1 - \alpha^i t(k+p)^{\beta^i} - EOL\right)^2\right] \tag{4.33}$$

Using the weights on each trajectory, the posterior PDF can be estimated:

$$P\left(Q(t)_{k+p} | Q(t)_{0:k}\right) \approx \sum_{i=1}^{N} w_k^i \delta\left(Q(t)_{k+p} - Q(t)_{k+p}^i\right) \tag{4.34}$$

Finally, the RUL predict is determined by taking the expected value of the RUL:

$$P(L_k | Q(t)_{0:k}) \approx \sum_{i=1}^{N} w_k^i \left(RUL_k - RUL_k^i\right) \tag{4.35}$$

4.8 Results

This section contains the RUL prediction results using the proposed predictive physics approaches compared to conventional predictive capacity-based approaches. The SP model in [173] was deployed to estimate the trends of the degradation parameters when the number of available measurement data points exceeds the number of coefficients in the empirical model. A RUL prediction can be performed at any point, called the checkpoint or starting point, in the battery cell's lifecycle. Figure 4.4 depicts four curves simultaneously representing the prediction result obtained by applying four methods for the battery cell at a constant current $1C - rate$ and temperature of 25℃ to evaluate the performance of the proposed approach for prognostic LiB lifetime. The solid red line shows tracking degradation trends to predict RUL using the proposed physical SP model based on the SPF approach, while the dashed green line shows the prediction with the physical SP model with PF (SPM-PF) approach. The prediction results obtained from the conventional empirical model with the SPF and PF (EM-SPF and EM-PF) approaches are illustrated in the curves (yellow dotted and violet, respectively).

As shown in Figure 4.4, the LiB test data are comprised of the previous and present measurements of cell capacity used to determine the coefficients of an empirical model (EM). The unseen data are included in the plots prior to checking the prediction quality under different approaches. The first 1,000 cycles were used as training data to keep the prediction process updated. More precisely, a data set estimates that the battery should reach the actual end-of-life threshold in 2,400 cycles. LiB mean lifecycle predicted using the proposed SPM-SPF method is about 2,408 cycles. As a result, RUL prediction differs from the actual end-of-life by about eight cycles, the maximum RMSE error was approximately 0.003, and the RE error was approximately 0.0035. At the same time, the SPM-based PF algorithm predicts that the battery's cycle life is 2,413 cycles. There is a 13-cycle discrepancy between the expected and actual value. While the expected capacity of the SPM-PF method decreased below the threshold at 2,413 cycles, indicating that the AE of the predict RUL was 13 cycles, the maximum RA was about 0.0054, and the RMSE error was approximately 0.0056. A comparison of the two prediction curves found that the proposed SPM based on the SPF

framework prediction curve is more accurate in predicting an actual capacity loss than the SPM based on the PF prediction curve. To assess the accuracy of the proposed approach's prediction, it is necessary to compare the outcomes with the traditional capacity prognostic method that only depends on capacity degradation data. Figure 4.4 shows that the curves resulting from the two methods (EM-SPF and EM-PF) diverged more from the actual capacity curve than the physical model's prediction curves. The values of RUL predicted by EM-SPF and EM-PF are, respectively, 55 and 154 cycles, much higher than the value estimated by the proposed SPM-SPF methods. More details of the comparison are listed in Table 4.1. Figure 4.5 shows the prediction error of the RUL using the four prognostic capacity approaches; in the prediction update phase, the first 1,000 cycles are used. The capacity RMSE error estimated from the proposed SPM-SPF method with the cycle passage was reduced more than the capacity error extracted from the other approaches, indicating that the proposed method is more reliable. Moreover, the PDF of EoL obtained by the proposed method is higher and narrower, as shown in Figure 4.6. This indicates that the proposed SPM-SPF can achieve better prediction performance than the other methods.

Figure 4.7 depicts how the RUL may be predicted using the four approaches. Here, the first 2,000 cycles were utilised as training data for the forecast. The prediction performance of the proposed SPM-based SPF approach can be seen to have significantly improved with the increase in training data. The battery's cycle life predicted by the SEM-based PF algorithm is 2,402 cycles. The difference between the predicted value and the actual value is two cycles. Compared to Figure 4.4, as the quantity of training data grows, so does the RUL prediction performance. With more training data, more ageing data can be employed, leading to improved predicted performance across all four approaches under the assumption of addressing the battery mechanism.

Figure 4.8 demonstrates RUL prediction error utilising four prognostic capacity approaches; the first 2,000 cycles are considered in the prediction update phase. The suggested SPM-SPF technique with cycle passing lowered capacity RMSE error more than previous alternatives, showing that it is more reliable. Moreover, Figure 4.9 shows that the width of the PDF of RUL

of all approaches is more concentrated compared with the width in Figure 4.6. Table 4.1 shows the error rates for the prediction RUL of the LiBs obtained by the proposed SPM-SPF approach compared with the previously mentioned approaches under different starting points. The RE and RMSE of the proposed SPM-based SPF algorithm are significantly smaller than those of the SPM-based PF algorithm.

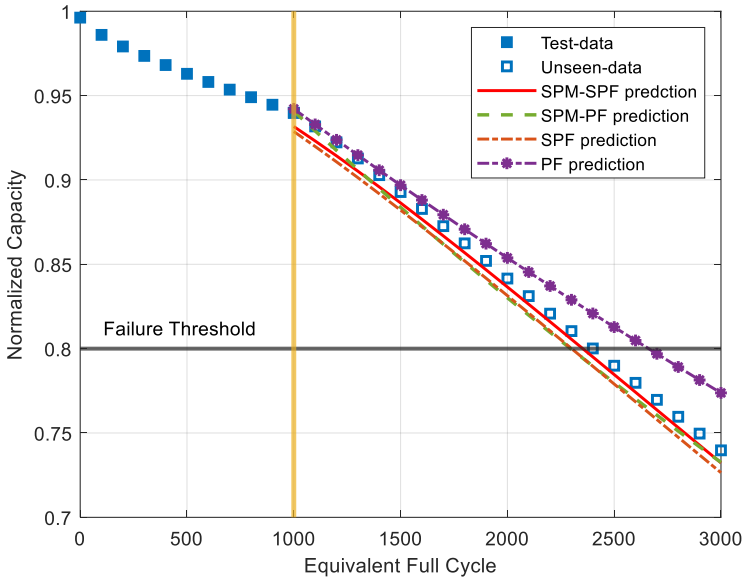

Figure 4. 4 Prediction RUL results at $T_s = 1000$ cycles for LiBs.

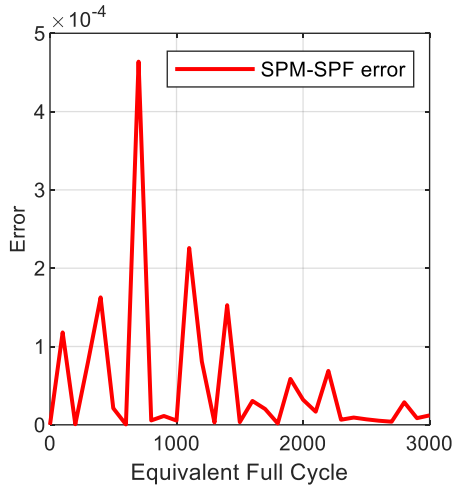

(a) Error of SPM-SPF.

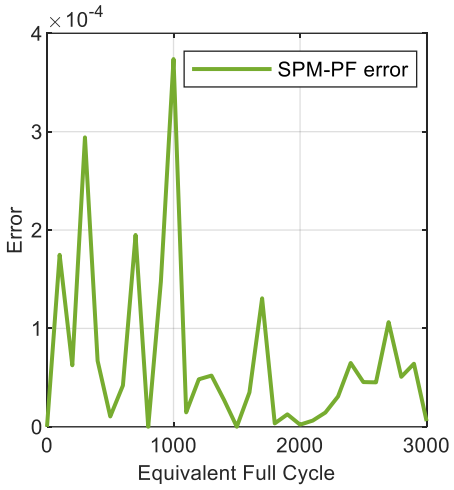

(b) Error of SPM-PF.

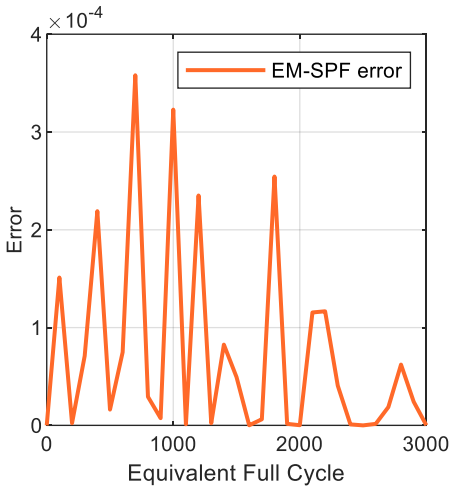

(c) Error of EM-SPF.

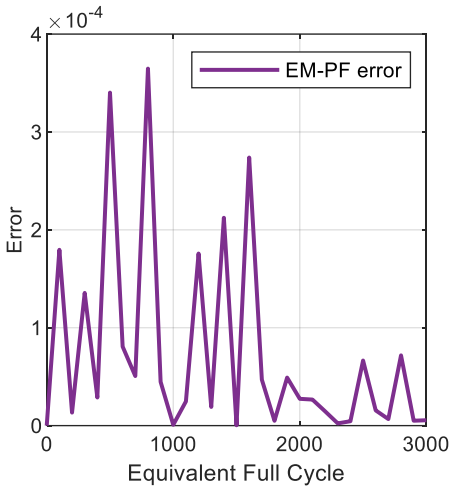

(d) Error of EM-PF.

Figure 4. 5 Error prediction for LiBs at $T_s = 1000$ cycle.

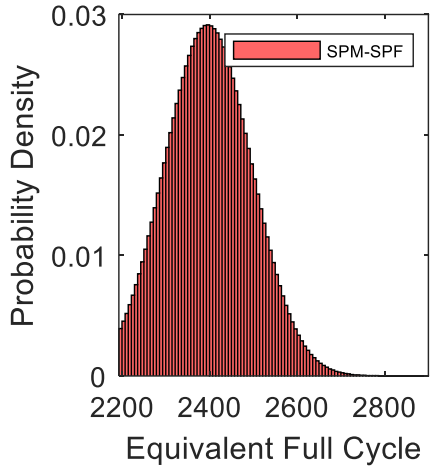

(a) PDF of SPM-SPF.

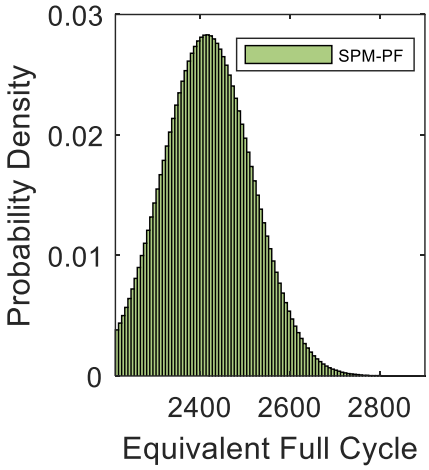

(b) PDF of SPM-PF.

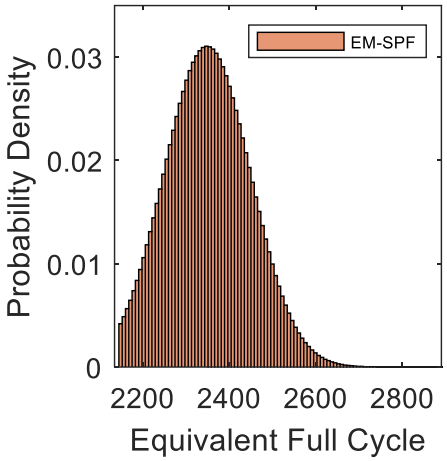

(c) PDF of EM-SPF.

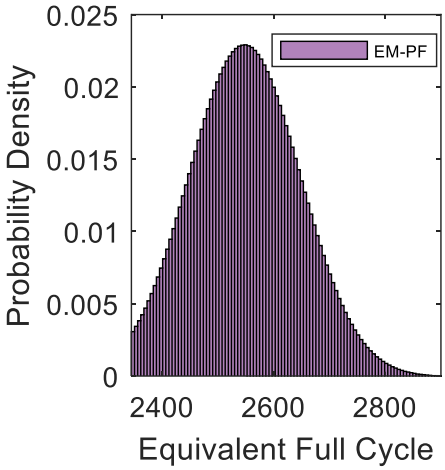

(d) PDF of EM-SPF.

Figure 4. 6 PDF RUL results at T_s = 1000 cycles for LiB.

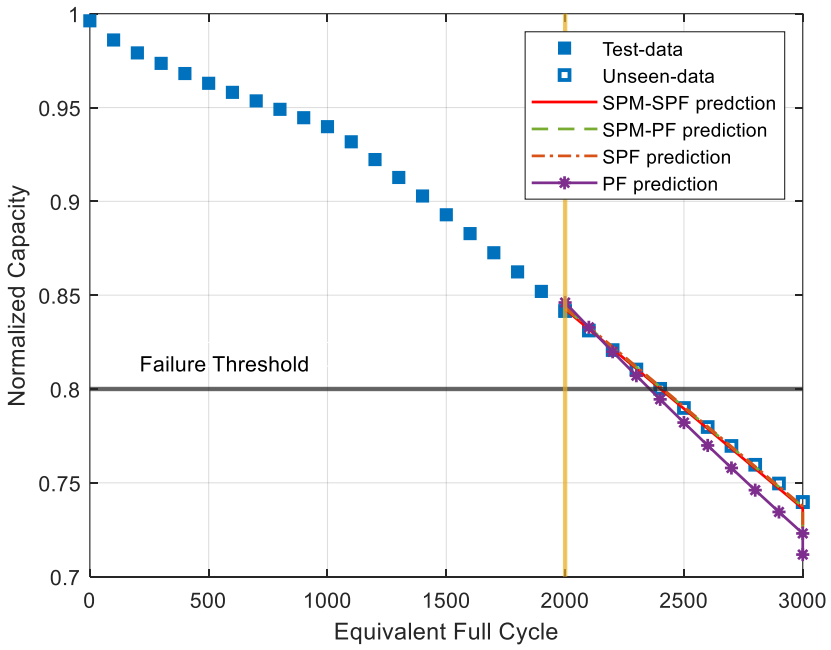

Figure 4. 7 Prediction RUL results at $T_s = 2000$ cycles for LiB.

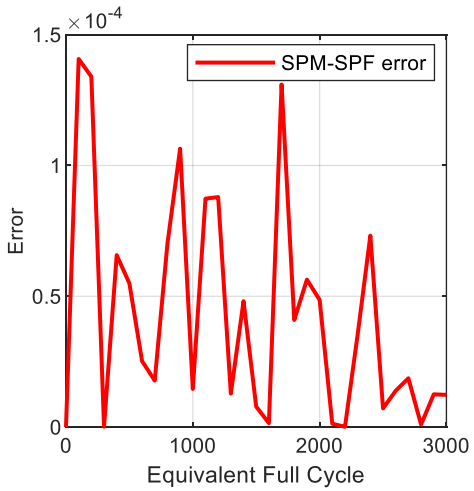

(a) Error of SPM-SPF.

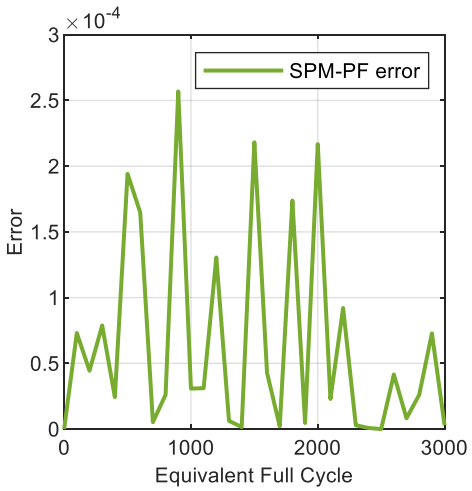

(b) Error of SPM-PF.

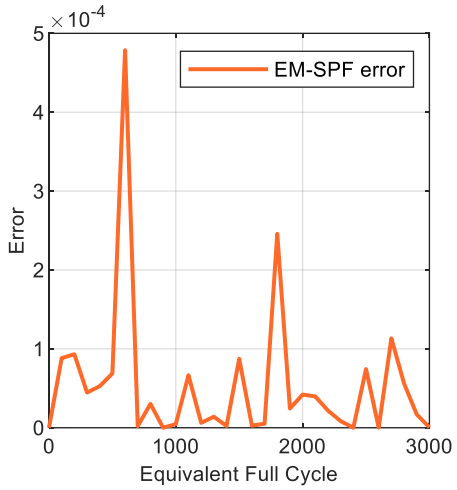

(c) Error of EM-SPF.

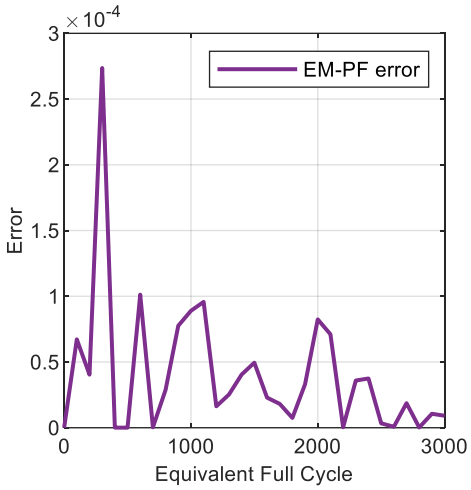

(d) Error of EM-PF.

Figure 4. 8 Error prediction for LiBs at $T_s = 2000$ cycle.

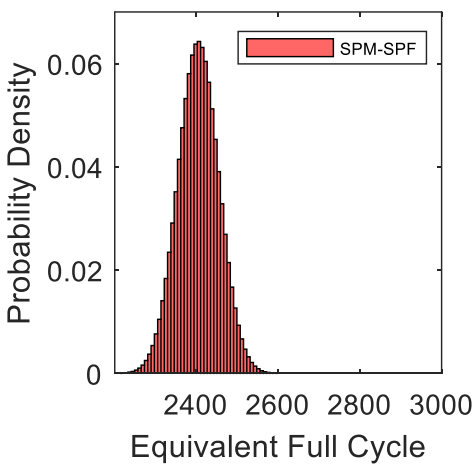

(a) PDF of SPM-SPF.

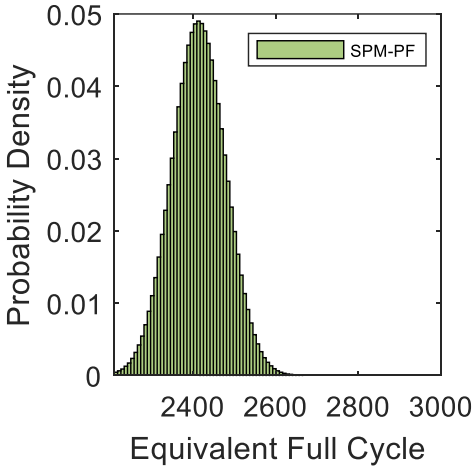

(b) PDF of SPM-PF.

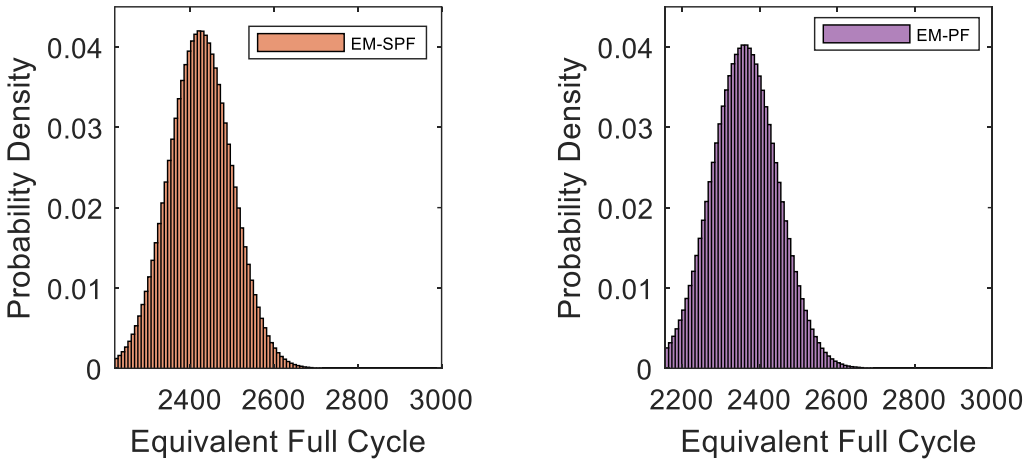

(c) PDF of EM-SPF. (d) PDF of EM-SPF.

Figure 4. 9 PDF RUL results at $T_s = 2000$ cycles for LiB.

Table 4. 2 RUL prediction results for LiB.

Algorithm	Starting point ($\boldsymbol{T_s}$)	$\boldsymbol{EOL_{true}}$	$\boldsymbol{EOL_{prediction}}$	$\boldsymbol{AE}$	$\boldsymbol{RA}$	$\boldsymbol{RMSE}$	$\boldsymbol{MAPE}$ (%)
SPM-PF	1000	2400	2413	13	0.0054	0.005	0.45
	2000	2400	2408	8	0.0033	0.0033	0.25
SPM-SPF	1000	2400	2392	8	0.0031	0.0035	0.27
	2000	2400	2402	2	$8.e-04$	0.0023	0.14
EM-PF	1000	2400	2545	145	0.0604	0.0182	1.87
	2000	2400	2408	43	0.0179	0.0124	1.30
EM-SPF	1000	2400	2345	55	0.0229	0.0083	0.96
	2000	2400	2420	20	0.0089	0.0061	0.30

To verify the performance efficiency and accuracy of the proposed method, it is necessary to compare the results obtained from the proposed method with the latest approaches presented in previous state-of-the-art methods [103, 105, 106] conducted for the same case study. The results of the proposed methods are shown in Table 4.3. Each approach's performance was assessed by looking at the AE, RE, and RUL's $RMSE$. Table 4.3 shows that the prediction accuracy of the PF was significantly improved using the suggested physics model base on NLLS, SPM-based SPF method and eSPM based on ASIR PF, compared to the proposed SEM-PF approach, demonstrating the robustness of the proposed approach. As far as the application of the RUL [108] presents a novel approach to predicting the RUL of LiBs. The proposed method is based on a physics-based model that incorporates the battery's electrochemical behaviour to estimate its SOH. The method uses a non-linear least squares (NLLS) algorithm with dynamic bounds to estimate the model parameters and their uncertainty. This approach allows the model to be updated in real-time as new data becomes available, making it suitable for online prognostics. The results show that the method can accurately predict the RUL of the LiBs with a mean absolute percentage error of less than 5%. Through this work, it has been concluded that the proposed SPF algorithm, given its higher robustness, stability, and accuracy prediction compared to the non-linear least squares algorithm. The authors in [105] introduce a novel PF framework that utilises a simplified electrochemical model to predict the RUL of LiBs. The model's parameters can be identified and used as state variables in the PF algorithm by applying specially designed current excitations to the battery. The prediction method is concerned; its approach is complicated compared with the proposed method. This is because it relies on five physical parameters related to SEM as health indicators for RUL prediction and then incorporates the PF method to generate the proposed distribution. The state variables in the new PF algorithm are selected based on battery health characteristics rather than meaningless adjustment coefficients. Trends in health-related features influenced the development of the new state equation, which makes the RUL prediction more robust by introducing the mechanism of the battery to overcome the particle deficiency problem. Nevertheless, this is difficult to do because its method is based on presenting the posterior information. An SEM-PF method can be used to draw out degradation parameters from

experimental data, and it is shown that they are associated with the battery SOH measured in the experiment. Another example [106] presents an electrochemical model technique to estimate the SOH of LMO-NMC battery cells using emulated in-situ vehicle data. The SOH estimate is used in an algorithm to predict the RUL of the battery. The SOH is determined by estimating the number of moles of cyclable lithium (n_{Li}) and battery internal resistance (R), which are identified through charging events using an enhanced-single particle model. Finally, the estimated eSPM parameters are used to make a composite SOH metric that can be used to make an RUL predictor based on classic ASIR PF that can predict the RUL based on the evolution of the SOH metric. However, we adopted the proposed SPF algorithm, given its higher robustness, stability, and accuracy prediction compared to classical particle filters. The main idea of the proposed method is to operate the algorithm based on the current degradation transaction values of equations (3.21-3.22) and then rely on the output from the proposed algorithm to reconfigure the approximation of the probability function. Thus, the computational complexity time of the SPF algorithm is longer than the classic PF algorithm because it finds the maximum probability estimates in nonlinear space state models.

Table 4. 3 Comparative results.

Method	**AE**	**RE**	***RMSE***
NLLS [108]			0.007
SEM-PF [110]	12	0.005	-
eSPM based on ASIR PF [[111]	–	0.8	-
Proposed SPM-based SPF	8	0.0033	0.0018

4.9 RUL Prediction Using ($2C-rate$) Batteries

The second dataset used in this work is a battery capacity fading data set at a different constant current rate (2C-rate) to verify the accuracy of the proposed prognostic framework prediction. At $T_s = 1000$ cycle, the RUL results for LiB data are shown in Figure 4.10. As shown in Figure 4.4 and Figure 4.7, an identical conclusion to that above can be deduced from

Figure 4.11, which shows the robustness and substantial accuracy of the proposed SPM-based SPF algorithm. Similar to the RUL results obtained in Section 4.7, the accuracy of the prediction RUL results, and the RUL's PDF obtained by the proposed SPM-SPF approach, is closer to the actual RUL than that provided by the SPM-PF (see Figure 4.12). The proposed method reduces the prediction error, RE, and RMSE by seven cycles compared to the PF utilizing 15 cycles. Table 4.4 shows a summary of the results of RUL prediction approaches for LiB data, demonstrating that the proposed method has a higher prediction accuracy than the other methods provided to predict RUL. For instance, at $T_s = 1000$, the AE predicted by SPM-PF, EM-SPF and EM-PF are 15, 25, and 40, respectively, and are thus much higher than the predicted value of the SPM-SPF approach. As such, the same conclusions can be drawn, as discussed in the previous section. In the context of the SPM-PF, SPM-SPF, EM-PF, and EM-SPF algorithms, the results suggest that the proposed SPM-SPF framework is the most accurate of the four, with a MAPE of less than 0.25%. On the other hand, the SPM-PF algorithm has a maximum MAPE is around 0.5%, which is still relatively low. The EM-SPF and EM-PF algorithms have higher maximum errors of 1.95% and 1.06%, respectively, indicating that they are less accurate than the SPM-SPF and SPM-PF algorithms.

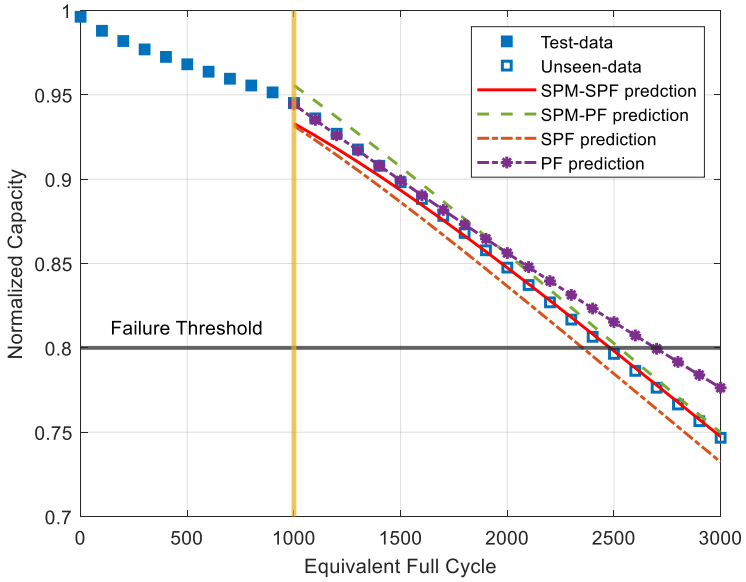

Figure 4. 10 Prediction RUL results at $T_s = 1000$ cycles for LiB at 2C rate.

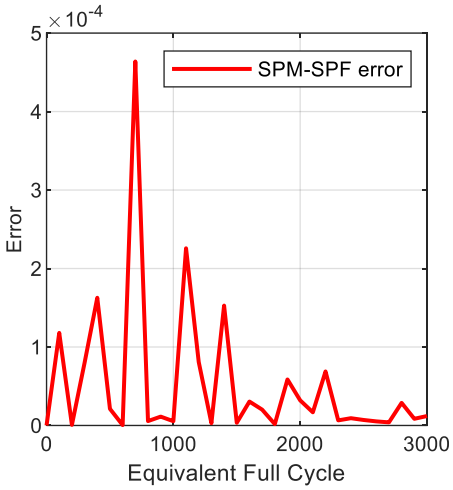

(a) Error of SPM-SPF.

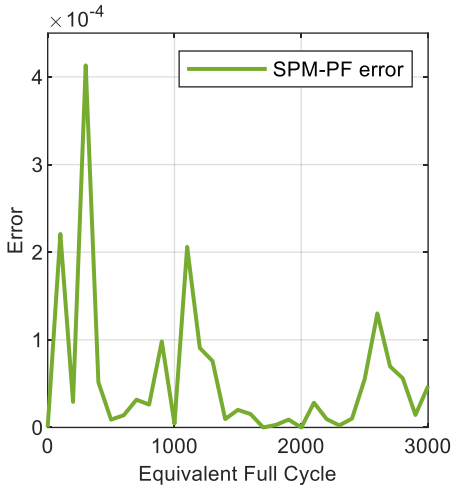

(b) Error of SPM-PF.

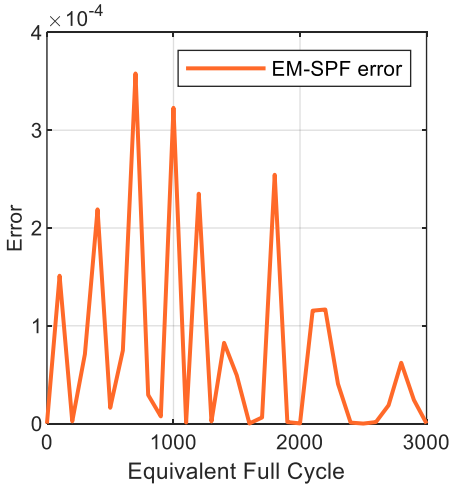

(c) Error of EM-SPF.

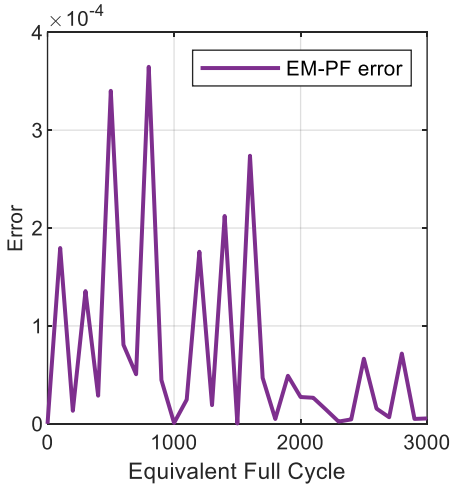

(d) Error of EM-PF.

Figure 4. 11 Error prediction for LiBs at $T_s = 1000$ cycle.

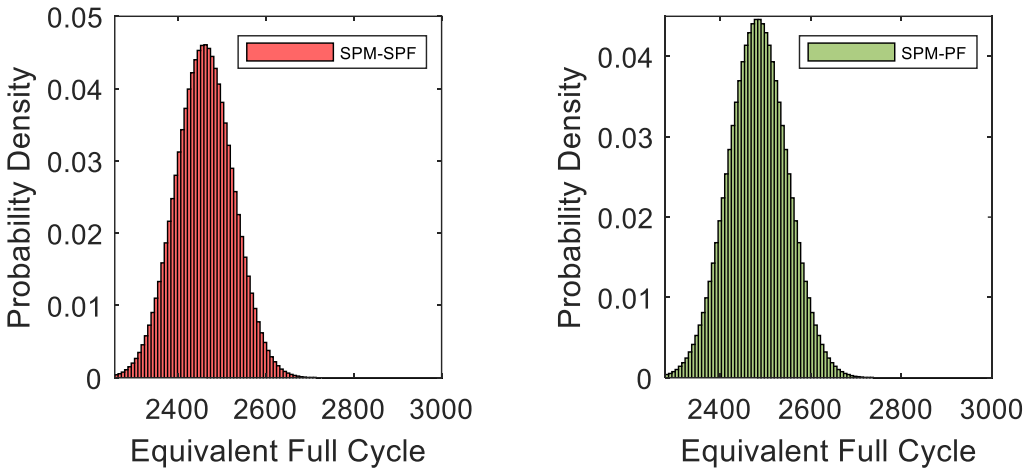

(a) PDF of SPM-SPF. (b) PDF of SPM-PF.

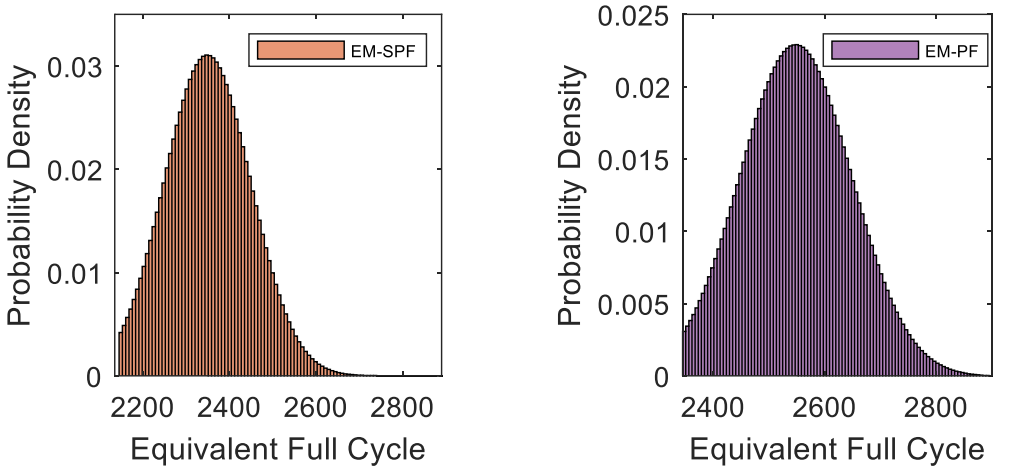

(c) PDF of EM-SPF. (d) PDF of EM-SPF.

Figure 4. 12 PDF RUL results at $T_s = 1000$ cycles for LiB.

Table 4. 4 RUL prediction results for LiB at 2C-rate.

Algorithm	Starting point (T_s)	EOL_{true}	$EOL_{prediction}$	AE	RA	$RMSE$	$MAPE$(%)
	1000	2400	2415	15	0.00417	0.0096	0.51

SPM-PF	2000	2400	2393	9	0.0033	0.0033	0.27
SPM-SPF	1000	2400	2410	10	0.0042	0.0072	0.24
	2000	2400	2403	3	0.0015	0.0001	0.11
EM-PF	1000	2400	2440	40	0.0833	0.193	1.95
	2000	2400	2420	20	0.005	0.00171	1.45
EM-SPF	1000	2400	2425	25	0.00617	0.0096	1.06
	2000	2400	2386	14	0.05	0.0047	0.67

4.10 RUL Prediction Using Different Current Profile

As mentioned earlier, the model coefficients may be incorrectly calculated because initial coefficients change with a change of profile current load. Using a distinct set of cells for training and evaluating the model, the model coefficients can be restricted to predetermined ranges [43]. To study the effects of coefficient boundaries on RUL prediction and capacity, we applied a different current profile drive cycle (UDDS) [37]. Figure 4.13 shows in red the predicted curve with an initial amplitude of about 0.936, while the same curve in Figure 4.10 has an initial amplitude of around 0.95. This indicates that initial coefficients change with profile current load, so initial coefficients must be tracked correctly to obtain a correct and reliable prediction. Furthermore, this may be led to an unexpected effect, especially in online prediction RUL. Moreover, as shown in Figures 4.13–4.15, more precise SOH estimations are provided in the suggested SPM-SPF techniques, which improves the RUL prediction. The RUL prediction error and RUL PDF width both show evidence of this precision.

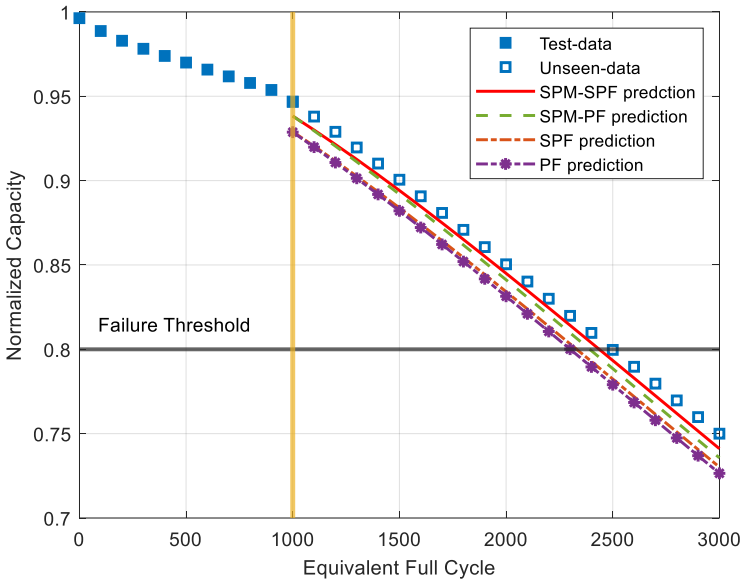

Figure 4. 13 Prediction RUL results at 1000 cycles for LiB at UDDS profile current.

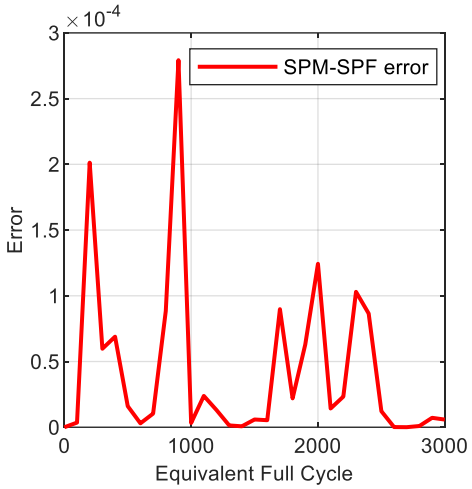

(a) Error of SPM-SPF.

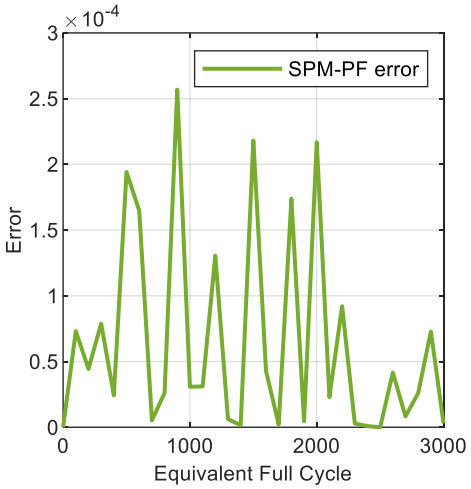

(b) Error of SPM-PF.

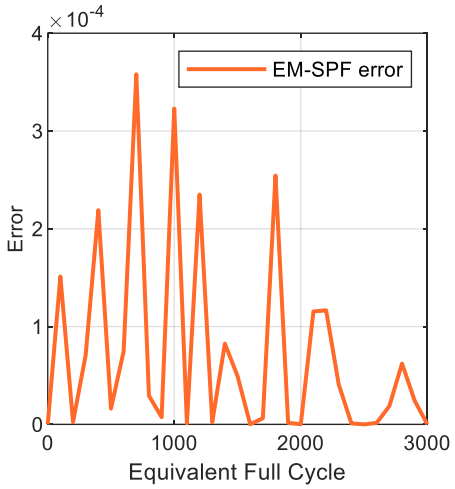

(c) Error of EM-SPF.

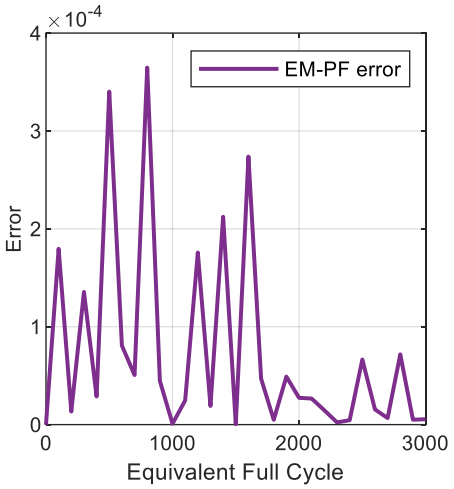

(d) Error of EM-PF.

Figure 4. 14 Error prediction for LiBs at $T_s = 1000$ cycle.

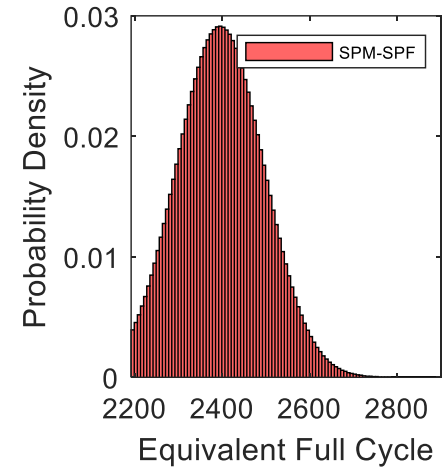

(a) PDF of SPM-SPF.

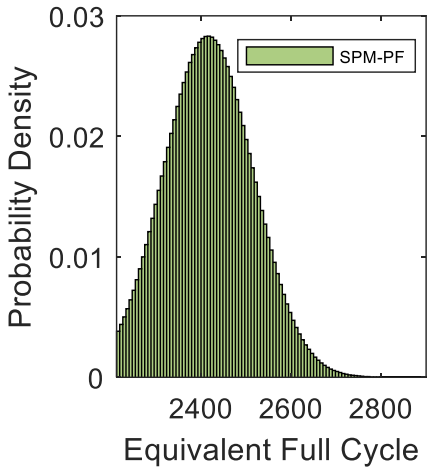

(b) PDF of SPM-PF.

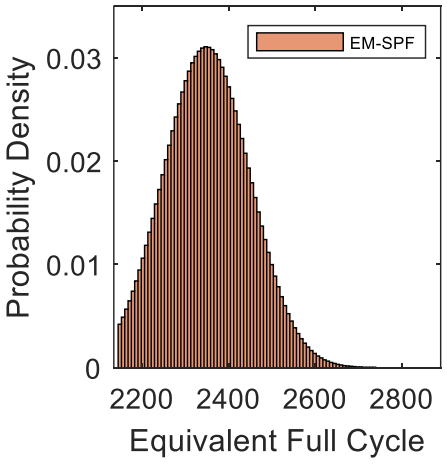

(c) PDF of EM-SPF.

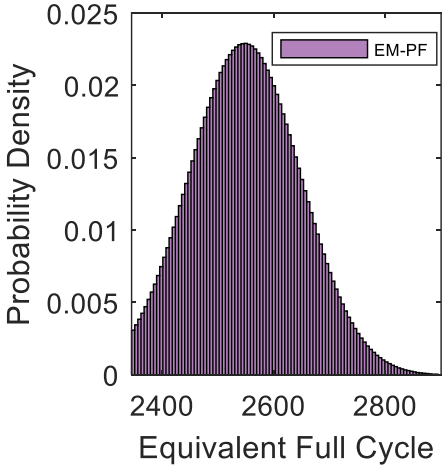

(d) PDF of EM-SPF.

Figure 4. 15 PDF RUL results at $T_s = 1000$ cycles for LiB.

4.11 Verify the robustness of the proposed framework under Gaussian white noise.

Measurement and system noises can significantly influence the quality of battery data. Therefore, it is important to develop a robust battery monitoring system, which can estimate RUL with noisy input data. The proposed SPM-SPF is capable of predicting RUL with noisy input data. Additive Gaussian White Noises (AGWN) with a signal-to-noise ratio (SNR) of 40 is introduced in the measured value further to demonstrate the dependability and robustness of the proposed SPM-SPF framework. To understand the actual life of the battery with the noise added, then employ a ground truth model. This model, which has a pristine version of the data, allows us to compare the actual, noise-free RUL against the RUL predicted by our algorithm. In this case, the ground truth is a version of the data without the Additive AGWN. I added the AGWN specifically to simulate a real-world scenario where such noise might be present. After obtaining the RUL predictions from aging model on this noisy data, compare these predictions with the actual RUL from the noise-free data. This comparison gives a measure of the error in our predictions. The prediction error is defined as the absolute difference between the predicted RUL and the actual RUL from the noise-free data. Mathematically, if denote the actual RUL as RUL_{actual} and the predicted RUL as $RUL_{\text{predicted}}$, the prediction error E can be calculated as:

$$E = \left| RUL_{actual} - RUL_{\text{predicted}} \right| \tag{4.36}$$

Prediction errors for the RUL utilising four different prognostic capacity methods are shown in Figure 4.16 throughout the updating phase of the prediction. Compared to the capacity error obtained from the other methods, the predictive error calculated from the suggested SPM-SPF technique with the cycle passing was considerably lowered, indicating that it is more dependable (see Figure 4.17). To present a more intuitive understanding of the results, the AE, RA, RMS, and MAPE error values of the four methods are also given in Table 4.5. The prediction error estimated from the traditional methods (EM-SPF, EM-PF) is approximately 10%, while the predictive error of the SPM-PF method is around 2%, but the proposed method is less than 1%. These results show the proposed model has good robustness under the

measurement noise. The addition of measurement noise has a more pronounced effect on the prediction performance of traditional (EM-SPF, EM-PF) and SPM-PF methods. However, it has only a little impact on the prediction accuracy of the proposed method, especially as its performance is essentially unaffected by the SNR = 40. Thus, these results illustrate the dynamic adjustment of the proposed framework can improve the prediction accuracy and robustness.

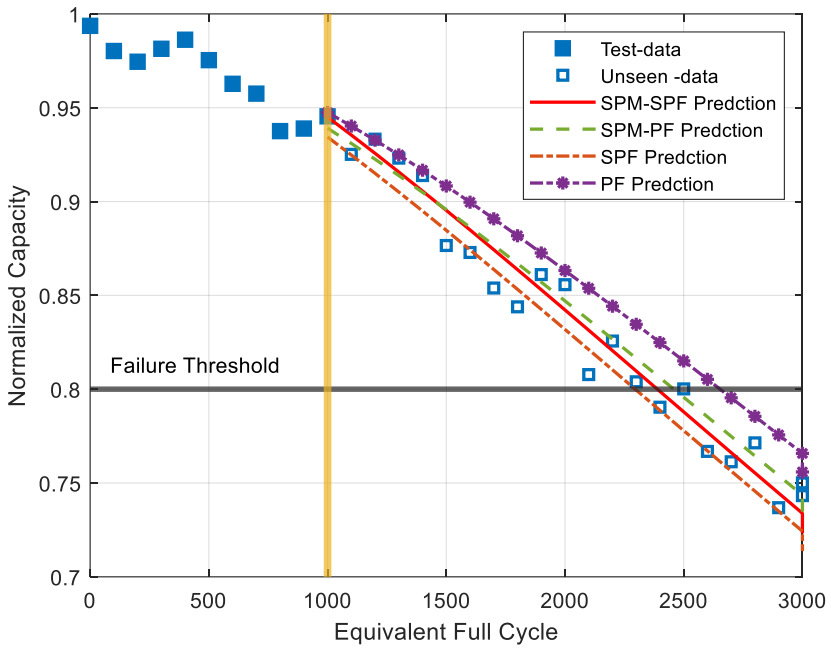

Figure 4. 16 Prediction RUL results with AWGN at $T_s = 1000$ cycles for LiBs.

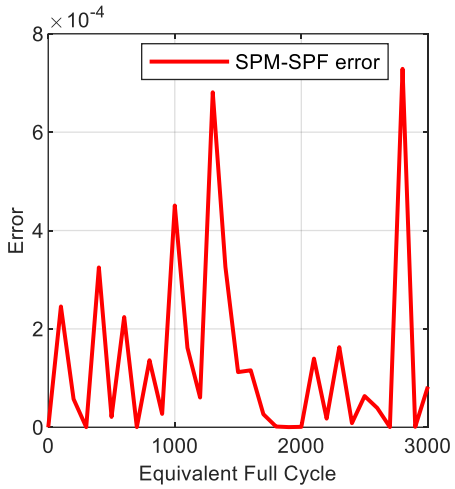

(a) Error of SPM-SPF.

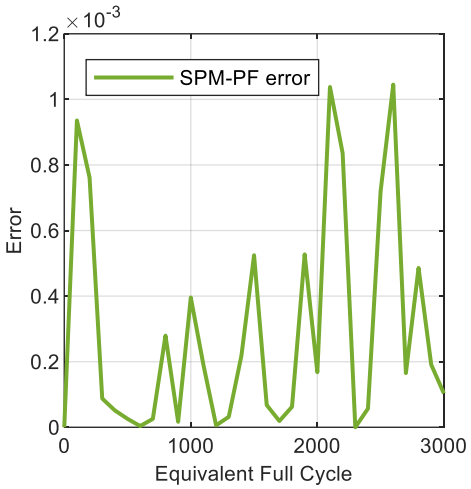

(b) Error of SPM-PF.

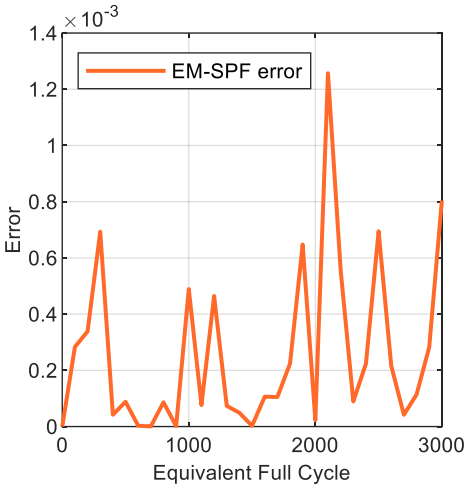

(c) Error of EM-SPF.

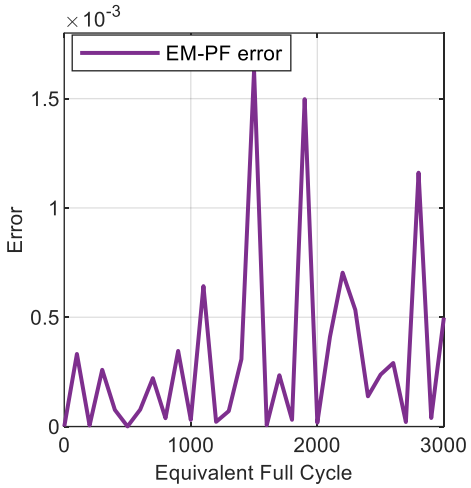

(d) Error of EM-PF.

Figure 4. 17 Error prediction for LiBs at $T_s = 1000$ cycle.

Table 4. 5 Numeric results of RUL prediction at SNR = 40.

Method	AE	RE	RMSE	$MAPE(\%)$
SPM-SPF	11	0.45%	0.0136	1.2
SPM-PF	50	2.08%	0.0156	1.68
EM-SPF	210	9.78%	0.0183	2.01
EM-PF	250	10.43%	0.0230	3.71

4.12 Summary

Two challenges arise in developing methods for predicting the RUL. Firstly, most of these approaches predominantly focus on traditional empirical degradation models, failing to consider the degradation mechanisms. Secondly, the standard PF method's stability is considerably limited by insufficient particles and uncertainty surrounding the degradation model parameters, which are further bound by the availability of adequate and dependable data. As a result, these parameters can contribute to imprecise RUL predictions. To overcome these issues, this chapter utilised an SPM to extract coefficients for three main degradation phenomena ($\mathrm{LAM}_{PE}, \mathrm{LAM}_{NE}$, and LLI) from the VQ and dV/dQ curves that are directly correlated with predicting the RUL of LiBs. This approach differs from conventional methods that rely on capacity-based measurements and empirical models to predict RUL. The proposed physics-based predictive framework provides more accurate early predictions of the late-stage fading trend than the conventional capacity-based prognostic framework. The degradation parameters obtained from the single particle model are then fed into an SPF algorithm, which is adopted due to its robustness, simplicity, and computational efficiency compared to other particle filters. This proposed solution accurately represents the degradation coefficients and capacity decay of LiBs when a suitable mathematical model is available. Once the mathematical model parameters have been created using the training data and the proposed method, the most appropriate model is selected to infer the parameters of the capacity

degradation and RUL estimation on a test set containing data from cells in addition to the training cells.

The obtained results demonstrated that the proposed SPM-based SPF framework can enhance the prediction accuracy compared with the traditional capacity predictive framework, especially for prediction during the early cycle. The proposed approach depends on extrapolating individual degradation parameters associated with different degradation mechanisms, reducing the potential for unrealistic predictions during early life. The proposed approach's average RUL errors and PDF width are lower than those of conventional prognostic capacity approaches, indicating that the proposed method is more accurate and stable. Compared to an existing framework in the predictive field, such as SPM-based PF, and eSPM-ASIR-PF, we demonstrate that the proposed framework offered accurate RUL prediction. However, there is still some confusion about tracking and estimating the trend of initial degradation model parameters for online prediction. This could be because initial coefficients change with a change of profile current load. As a result, more research is needed; the initial parameters of the degradation model could be estimated correctly using artificial intelligent algorithms such as neural networks, which could improve prognostic accuracy mainly in real-time RUL prediction.

Chapter 5 Online RUL Prediction of LiBs Using a Hybrid Model

'As detailed in chapters 3 and 4, the previously discussed forecasting frameworks are contingent on developing an experimental degradation model tailored to meet specific operational demands or batteries made with certain materials. For real-time RUL prediction, LiBs frequently operate under less-than-perfect conditions. As a result, the estimated initial model parameters could be prone to inaccuracies, leading to instability and erroneous RUL predictions [3]. Hence, it's paramount to establish a resilient and adaptable model capable of effectively mapping the trends of capacity degradation and extracting model parameters under diverse operating conditions. For this reason, this chapter aims to develop our previously proposed framework for forecasting LiB RUL into an intelligent online predictive hybrid framework employing the NN and SPF, based on maximum likelihood. The exponential empirical model-based online RUL prediction approach improves with the suggested framework in two ways. First, a general NN capacity degrading model is built. The NN model is more flexible and powerful than empirical techniques, improving RUL prediction accuracy. Second, the proposed SPF updates NN model weights and biases. This approach moves particles to the high maximum likelihood region, enhancing online prediction accuracy under complex operating conditions compared to the PF method.'

5.1 Introduction

Accurate real-time PHM estimation is essential to lithium-ion battery safety and efficiency. Recent work on developing a framework to predict RUL has primarily focused on the traditional empirical degradation model due to its simplicity. Although this model works well under specific operational conditions, for online RUL prediction, it may lack the ability to describe capacity degradation, given the variability in decline between cells and others under different operational conditions. As such, this can result in inaccurate RUL prediction. Therefore, this chapter proposes a hybrid approach to improving the accuracy of online forecasting in the existing framework by integrating data-driven and model-based approaches. The proposed framework utilises the NN to model and track battery degradation trends, and it also degrades the initial values of the degradation model's transactions under different operating conditions. Furthermore, the proposed hybrid framework includes an SPF algorithm, which continuously updates the degradation NN model. Lithium-ion battery capacity degradation datasets from the Centre for Advanced Life Cycle Engineering (CALCE) were used to evaluate the proposed paradigm. The results show that the proposed hybrid framework is more accurate and improves the convergence rate compared to the traditional capacity prognostic framework. The term 'traditional' capacity framework refers to the prevalent empirical degradation model, which has been the cornerstone of battery life prediction for a considerable time. This model, while straightforward and quite effective under certain sets of conditions, is primarily based on fixed assumptions and lacks the flexibility to account for the intricacies and variability observed in LiB degradation under a range of operational scenarios.

This chapter presents an implementation of an online hybrid PHM prediction approach for LiBs, utilising a combination of a NN and SPF. The challenges associated with online RUL prediction are presented in Section 5.2. Section 5.3 showcases experimental datasets published by the CALCE, where a second-order degradation model was developed to investigate LiB degradation. The theoretical background and implementation procedures for the NN algorithm and explanation of NNs for modelling and estimating critical degradation parameters are set

out in Section 5.4. The results are presented and examined in Section 5.5, while conclusions and discussions are summarised in Section 5.6.

5.2 Proposed Hybrid Prognostic Platform for Battery Health Morning and RUL Prediction

The main aim of this chapter is to develop our previously proposed framework in chapters (3 and 4) for predicting RUL of LiBs to produce an intelligent online predictive hybrid framework using the NN and SPF based on maximum likelihood. The proposed framework improves the accuracy of online RUL prediction in the traditional method, based on the exponential empirical model, in two ways. First, a generic NN model for capacity deterioration modelling is created. The accuracy of RUL prediction can be improved by employing the NN model since it is more flexible and powerful than existing empirical methods.

Second, the proposed SPF is used to update the NN model's parameters (weights and biases). Compared to the PF method, this method improves particle distribution by moving particles to the high maximum likelihood region; this improves the accuracy of online prediction under complex operating conditions.

The proposed framework for online RUL prediction contains two main stages, as shown in Figure 5.1. In the first stage, a state-space model based on the NN degradation model is created using previously collected battery capacity fade data. To transform the continuous state-space model into a discrete counterpart, I have employed a procedure based on the Euler method, a commonly used numerical integration method for solving ordinary differential equations (ODEs). This technique was selected due to its relative simplicity, computational efficiency, and suitability for moderately complex models. The first step in discretisation involves partitioning the time variable into discrete time intervals, often called 'time steps'. We designate these time steps as Δt. Given that study concerns the RUL prediction of LiBs, it is crucial to select an appropriate Δt that efficiently captures the degradation process of the batteries while maintaining computational feasibility. Upon determining an optimal Δt, then proceed to

approximate the state transitions. A common approach to discretising state-space models is to employ the Euler approximation. This approximation works under the presumption that within small enough time steps, Δt, the change in the state variables can be represented as the product of the time step size and the rate of change of the state variables, as dictated by the state equations. Essentially, for a given state variable $'x'$ and its rate of change given by the function $f(x, u)$, the next state is approximated as:

$$x(t + \Delta t) = x(t) + \Delta t * f\big(x(t), u(t)\big) \tag{5.1}$$

The proposed SPF algorithm tracks and continuously updates the model parameters in the second stage. Finally, the RUL of LiBs is predicted by extrapolating the updated degradation model until the end of service.

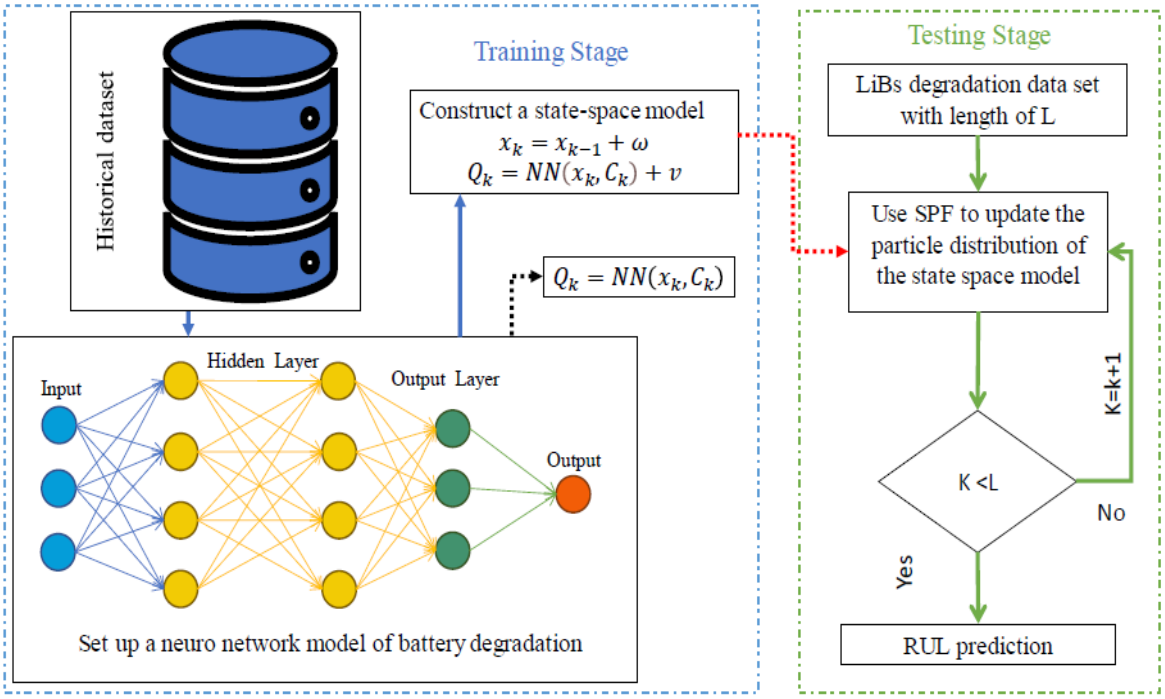

Figure 5. 1 Schematic of the proposed framework.

5.3 CALCE datas

The CALCE dataset is a collection of data related to the life cycle of products, systems, and equipment. It may include information on reliability, durability, maintenance, and other aspects of product lifecycle management. The dataset is maintained by the Center for Advanced Life Cycle Engineering at the University of Maryland [196]. It is used for research and development purposes, to support industry and government decision-making, and to advance the field of life cycle engineering.

In this work, four cell(CS35, CS36, CS37, and CS38) datasets were employed to investigate LiB degradation behaviour and demonstrate the effectiveness of the developed LiB degradation model on the accuracy of the prediction framework. The nominal capacity of the four $LiCoO_2$ pouch batteries are 1.1 Ah. The Arbin BT2000 battery testing system performed the cycling of the four $LiCoO_2$ pouch LiBs. The four cells underwent the same charging protocol: constant

CCCV under room temperature. During charging mode, the batteries are supplied with a CC rate of 0.5C until the voltage reaches a maximum of 4.2V. Then, the voltage is kept at the maximum limit until the charging CC drops below 0.05 A. During the discharge mode, CC of 0.45 A was maintained in cells until the voltage dropped to a minimum of 2.7 V. The failure threshold for these batteries was set to 0.88 Ah. For these LiBs, the Coulomb counting method was used to determine battery discharge capacity [196]. Figure.5.2 depicts the capacity degradation curve as a function of the cycle.

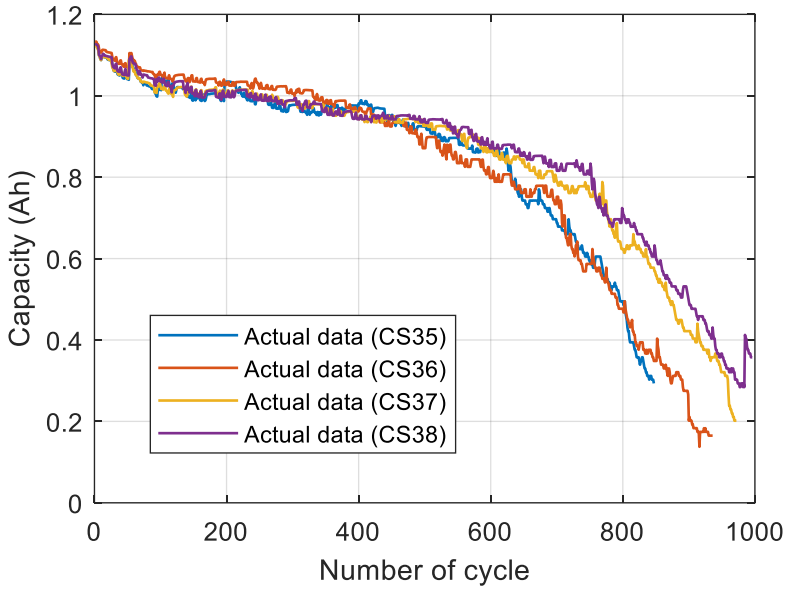

Figure 5. 2 Capacity degradation curves.

5.4 Neural network (NN) degradation model

In the proposed framework, the NN algorithm was adopted to extract a model that describes the degradation of the battery discharge capacity over time. The main goal of this approach is to identify the initial parameter values of the degradation model that can be used to predict the future capacity of the battery. The NN algorithm is trained using historical data on the battery's discharge capacity and other relevant parameters, such as temperature, usage, and age [197].

The NN algorithm then creates a model that maps the input parameters to the battery's discharge capacity.

The NN algorithm is capable of capturing complex relationships between the input parameters and the battery's discharge capacity, making it an ideal tool for modelling the degradation of the battery. The resulting model is then used to estimate the initial parameter values of the degradation model. Once the initial parameter values are estimated, they can be used to make predictions about the future degradation of the battery's discharge capacity. This information can be used to determine the optimal maintenance and replacement schedule for the battery, helping to maximise its lifespan and performance [198].

Generally, the architecture of the NN algorithm was selected as the Multi-Layer Perceptron (MLP) with two hidden layers [199]. The main structure of the NN's algorithm consists of two neuron layers connected to build an NN layer. Each neuron excludes a set of inputs from other cells connected to it proportionally to cell weights [200]. As a result, each neuron will produce a single output under the activation function, which can then spread to nearby cells. MLP can be taught simply with rapid convergence while retaining the NN's nonlinear approximation. MLP was used to simulate the dynamic and nonlinear battery deterioration trend. An MLP model's basic structure is shown in Figure 5. 3. The MLP with two hidden layers is a specific implementation of the MLP architecture that consists of three layers of artificial neurons [201]: the input layer, two hidden layers, and the output layer. The input layer receives the data on the battery's discharge capacity and other relevant parameters, such as temperature, usage, and age. The two hidden layers process the input data and pass the results to the output layer, which produces the final prediction of the battery's discharge capacity. In general, the more neurons in each hidden layer, the more complex the relationships that the model can capture [202].

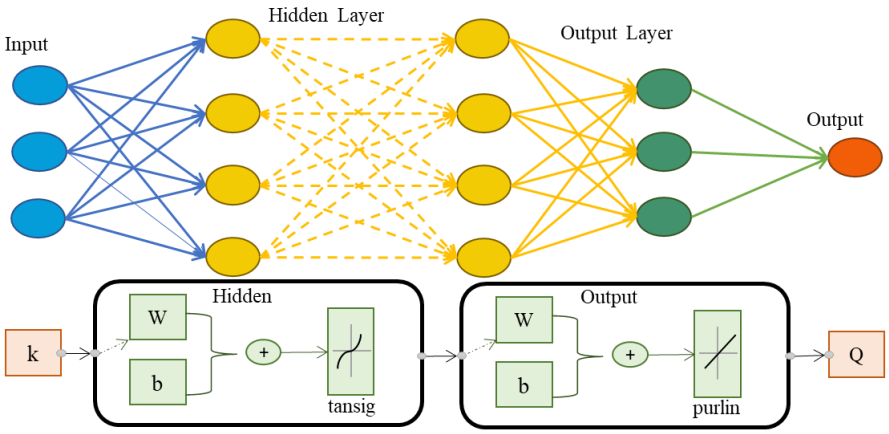

Figure 5. 3 Structure diagram of an MLP model.

In the proposed framework, the NN is used to track the trend in degradation of the battery discharge capacity as a function of the number of cycles. Afterwards, the number of the cycle (k) is fed to the input node of the NN, and the battery capacity is the output node of NN (Q). For the neurons in the hidden layer, the hyperbolic tangent sigmoid activation function, also known as tansig, is used. This activation function maps the inputs to outputs in a non-linear manner, which allows the model to capture more complex relationships between the input parameters and the output. The output node uses a linear activation function known as purelin to improve efficiency. This activation function provides a simple linear mapping of the inputs to outputs, which helps to simplify the model and reduce the computational requirements. In this way, the hidden neuron's output can be estimated as follows [99]:

$$h = tansig(IW.k + b_1) = \frac{1 - epx[-2(IW.k + b_1)]}{1 - epx[-2(IW.k + b_1)]} \tag{5.2}$$

Where IW and b_1 1 represent the input node's weight and bias, respectively. Then, the total output of the whole network can be estimated as follows:

$$Q = purlin(LW_1 \cdot h_1 + \cdots + LW_M \cdot h_M + b_2)$$

$$= LW_1 \cdot \frac{1 - epx[-2(IW_M.k + b_{11})]}{1 - epx[-2(IW_M.k + b_{11})]}$$

$$+ \cdots + LW_1 \cdot \frac{1 - epx[-2(IW_M.k + b_{1M})]}{1 - epx[-2(IW_M.k + b_{1M})]} + b_2 \quad (5.3)$$

Where LW denotes the weight associated, b_2 is the second hidden neuron bias and M represents the hidden neurons number.

5.4.1 Degradation analysis based on different models

The proposed framework based on the NN model was compared with the traditional model framework of capacity degradation modelling. For the traditional model framework, most state-of-the-art research [16–21] relies on the empirical two-exponential model to describe battery degradation status; the empirical degradation model can be expressed as in (3.24). In MATLAB's curve fitting tool, the nonlinear least square method is used to fit the parameters of the empirical degradation model (EXP model). As for the NN model, the network was designed with a different number of hidden neurons to verify the model's accuracy: the NN model with two hidden neurons (2NN) and three hidden neurons (3NN). The MATLAB nntrain tool was used to identify the parameters of the NN models. To assess the accuracy of the proposed degradation models, RMSE and R-square were used [16], both of which are explained in equations (5.4) and (5.5):

$$RMSE = \sqrt{\frac{1}{n}\sum_{i=1}^{n}\left(Q_{i,real} - Q_{i,est}\right)^2} \quad (5.4)$$

$$R^2 = 1 - \frac{\sum_{i-1}^{n}\left(Q_{i,real} - Q_{i,est}\right)^2}{\sum_{i-1}^{n}\left(Q_{i,real} - Q_{i,mean}\right)^2} \quad (5.5)$$

Where, $Q_{i,real}$ denote the actual capacity, $Q_{i,est}$ is the fitted capacity, and $Q_{i,mean}$ is the average actual capacity value.

5.4.2 Analysis of the CALCE dataset for degradation

Figures 5.4 -5.7 presents the curve-fitting outcomes for CS35 and CS37. These figures are organised in accordance with the empirical degradation model and two NN models, respectively. The models have the capability of tracking the trend of capacity loss for both batteries. The empirical degradation model and NN models were used to fit the parameters of four batteries, and the results are shown in Table I. The goodness-of-fit results for each model are shown in Table II. It can be seen that the RMSEs are lower than 0.02, and the R^2 values are greater than 0.98. This suggests that these models are well suited to the capacity degradation data. The RMSEs of the three neurons NN model are the lowest and the R^2 values are the highest of the three models for all batteries. Although this indicates that the three neurons NN model has the best-fit capability of the three models, its execution does not significantly advance; the performance of the two neurons NN and empirical degradation models, respectively, is thus sufficient in this work, as the capacity curves for these batteries are fairly smooth and track the exponential degradation trend.

Table 5. 1 Model parameter estimation result of the EXP model.

exp model (with 95% confidence bounds)				
LiB ID	$\boldsymbol{a}$	$\boldsymbol{b}$	$\boldsymbol{c}$	$\boldsymbol{d}$
CS35	-0.0017	0.0067	1.069	-0.0018
CS36	-0.0030	0.0061	1.108	-0.0002
CS37	-0.0005	0.0074	1.075	-0.0002
CS38	-0.0002	0.0081	1.074	-0.0002
exp model (with 50% confidence bounds)				
	$\boldsymbol{a}$	$\boldsymbol{b}$	$\boldsymbol{c}$	$\boldsymbol{d}$
CS35	-0.0028	0.0037	1.009	-0.0028
CS36	-0.005	0.0051	1.02	-0.0015
CS37	-0.0099	0.0064	1.035	-0.0082
CS38	-0.0018	0.0001	1.004	-0.0003

\

Table 5. 2 CALCE model goodness- of -fit analysis.

Indices	***RMSE***			***R^2***		
Model	exp	NN		exp	NN	
		2NN	3 NN		2 NN	3 NN
CS35	0.0197	0.0150	0.0142	0.9812	0.9892	0.9902
CS36	0.0181	0.0178	0.0138	0.9860	0.9864	0.9917
CS37	0.0149	0.0135	0.0126	0.9881	0.9901	0.9913
CS38	0.0169	0.0140	0.0132	0.9854	0.990	0.9910

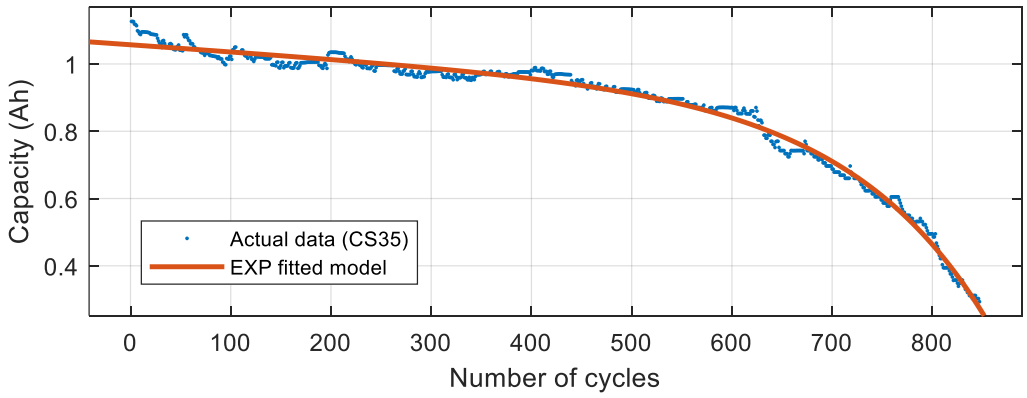

a)

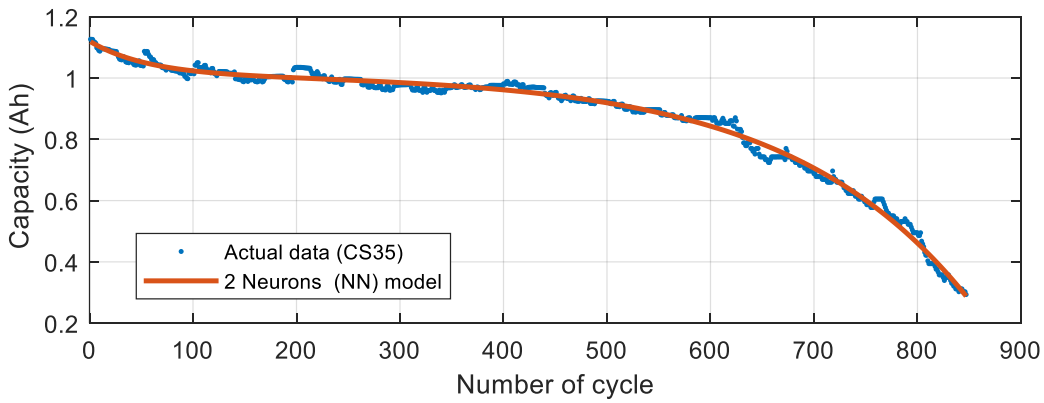

b)

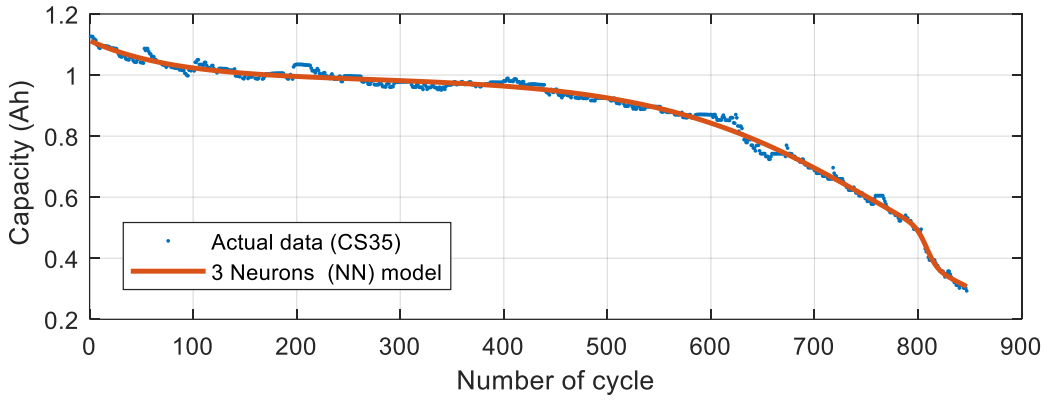

c)

Figure 5. 4 Curve fitting result for LiB CS35 dataset a) EXP model, b) 2 NN model, and c) 3 NN model.

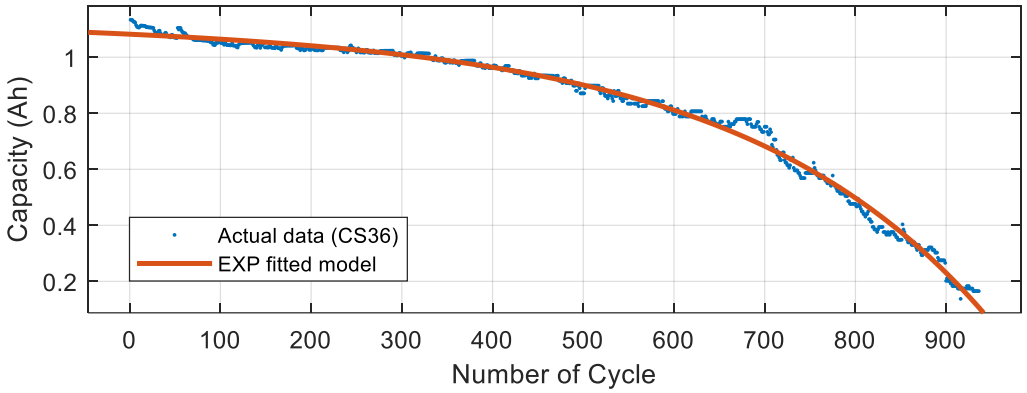

a)

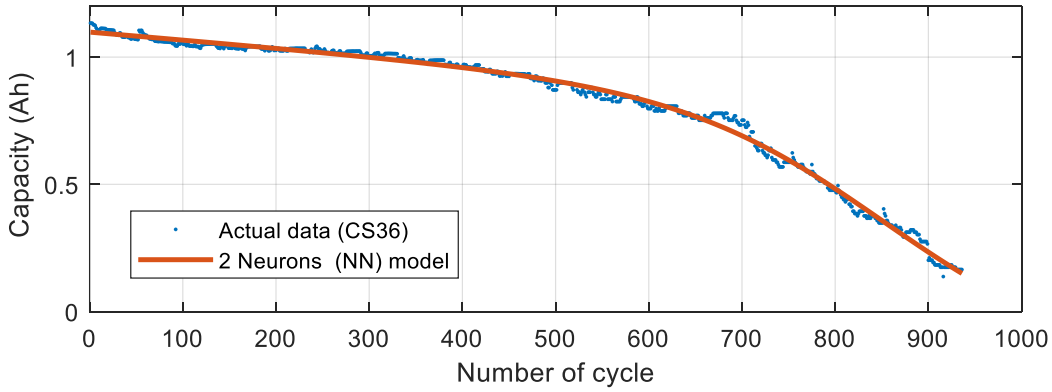

b)

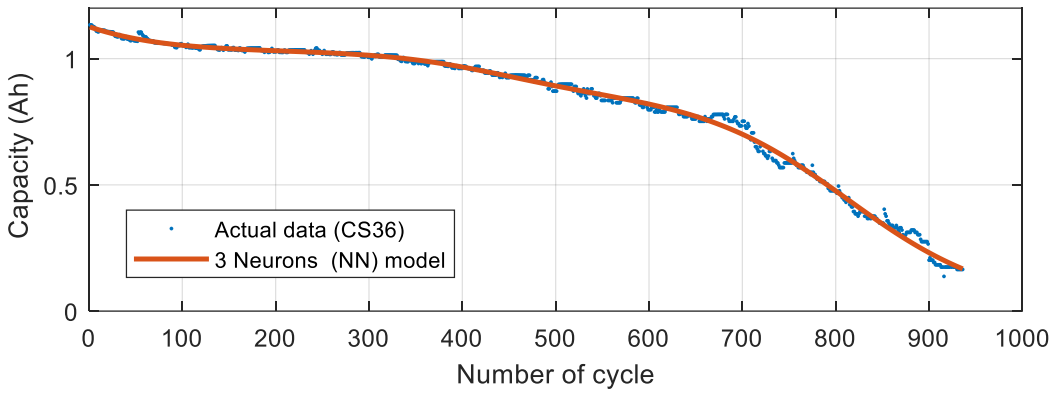

c)

Figure 5. 5 Curve fitting result for LiB CS36 dataset a) EXP model, b) 2 NN model, and c) 3 NN model.

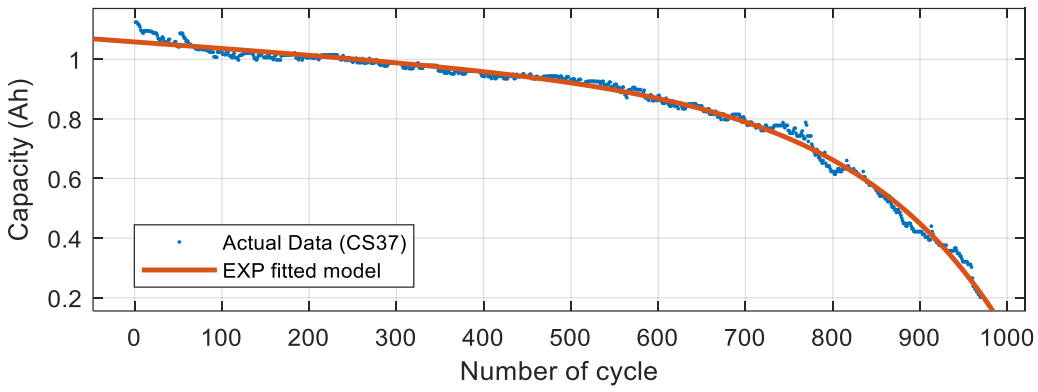

a)

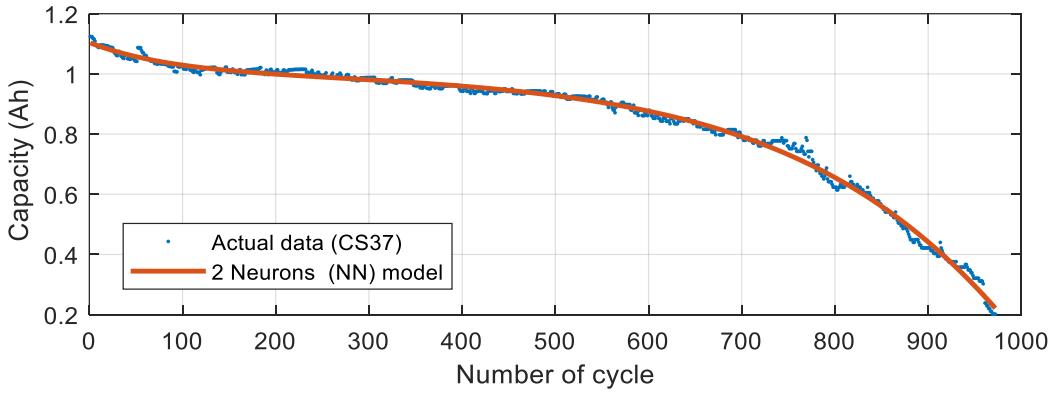

b)

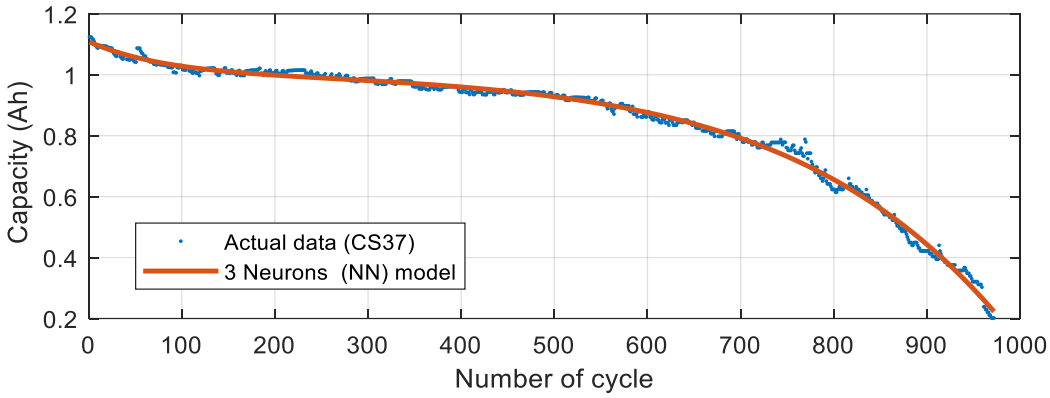

c)

Figure 5. 6 Curve fitting result for LiB CS37 dataset a) EXP model, b) 2 NN model, and c) 3 NN model.

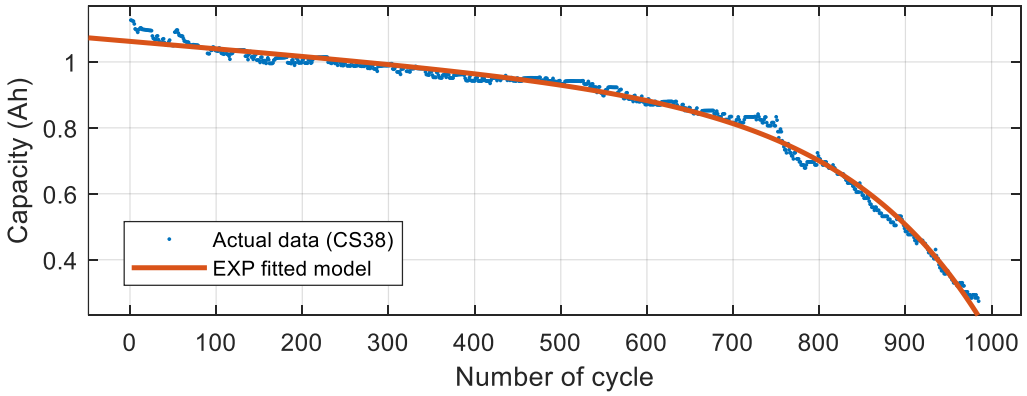

a)

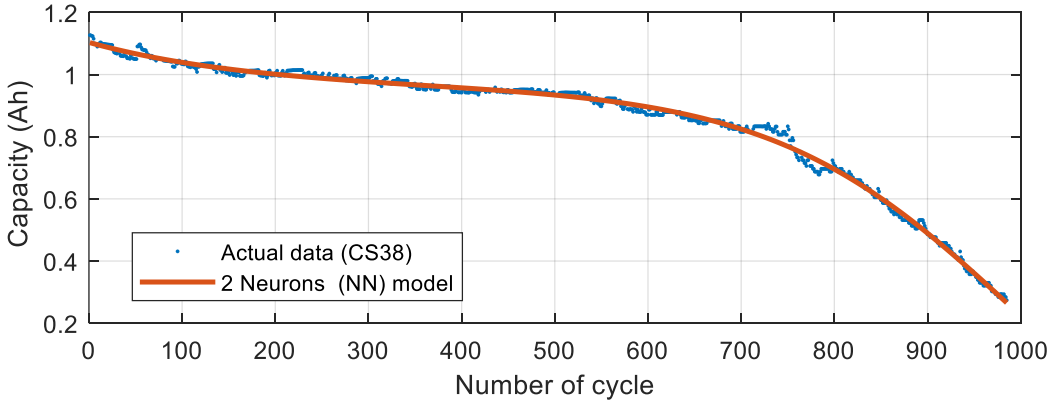

b)

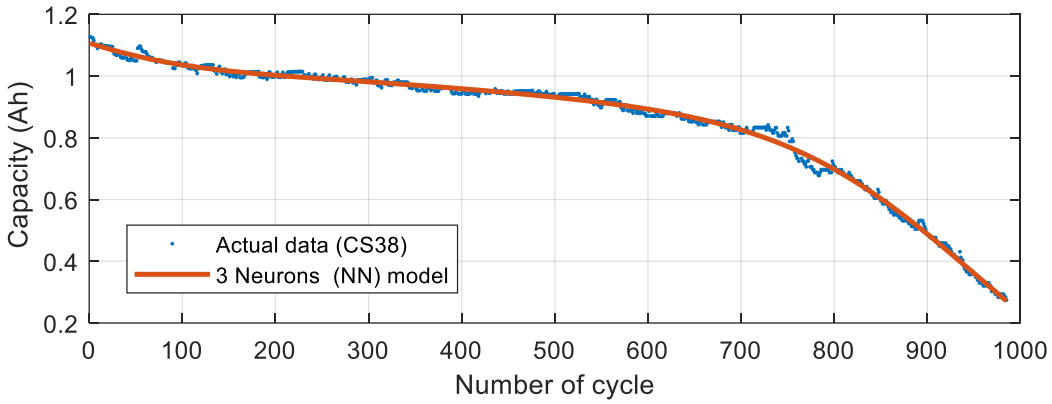

c)

Figure 5. 7 Curve fitting result for LiB CS38 dataset a) EXP model, b) 2 NN model, and c) 3 NN model.

5.5 Results and Discussion

The capacity degradation data of the CS36 and CS38 LiBs were selected as historical training data to identify information about the model's parameters. At the same time, the CS35 and CS37 batteries were selected as testing data for the accuracy of the RUL prediction performance. For the initialisation exponential empirical model, the initial parameters for the degradation model for all battery cells are shown in Table 5.2. For the NN degradation model, based on historical data, the NN model was trained to obtain its initial weights and biases.

Figures. 5.8 – 5.10 show the RUL prediction based on the traditional empirical model framework and the proposed hybrid framework of CS35 LiB. The blue line denotes the actual capacity, the predicted capacity is the red dashed line, and the orange dotted line shows the RUL PDF. The solid yellow line indicates the starting point of the prediction process. Figure 5.8 shows that the actual end of life was 557 cycles at $Ts = 300$ cycles, while the average predicted life cycle using the traditional capacity prognostic-based SPF was 565 cycles. Consequently, the conventional capacity prognostic-based SPF algorithm's AE is about 8, the maximum relative error was about 0.026, and the RMSE error was approximately 0.0532. The results show that prediction accuracy is high as the predicted RUL value is close to the real RUL value.

However, this accuracy directly depends on how precisely the initial values for the degradation model parameters are extracted.

A best-fit model with parameters bounded by 50% was used to evaluate the impact of bounds on capacity and RUL prediction (see Table 5.1). Figure. 5.9 shows that the predicted mean curve diverges further from the actual capacity curve than the curve obtained in Figure 5.8. The predicted RUL is about 620 cycles, and the AE is 63, indicating that the prediction accuracy is directly affected by the initial parameter values. Furthermore, this may be led to an unexpected effect, especially in online prediction RUL.

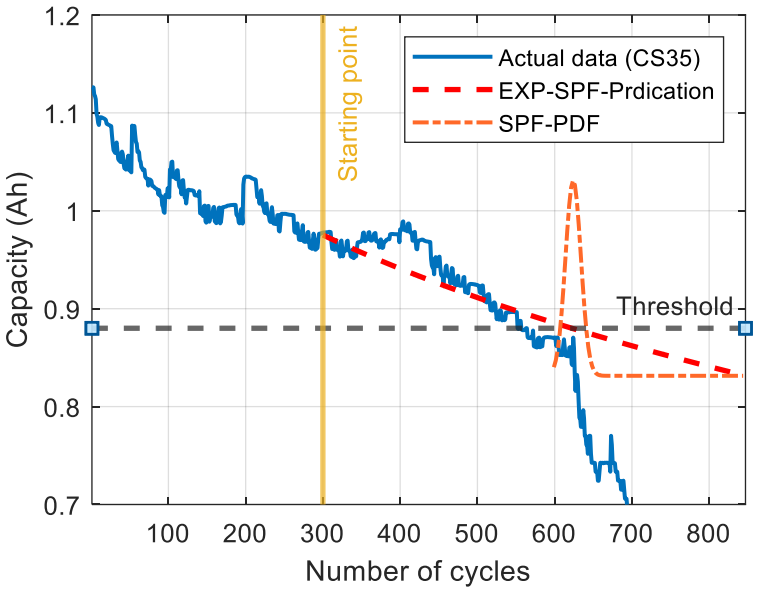

Figure 5. 8 Predicted RUL result obtained, using EXP+SPF approaches.

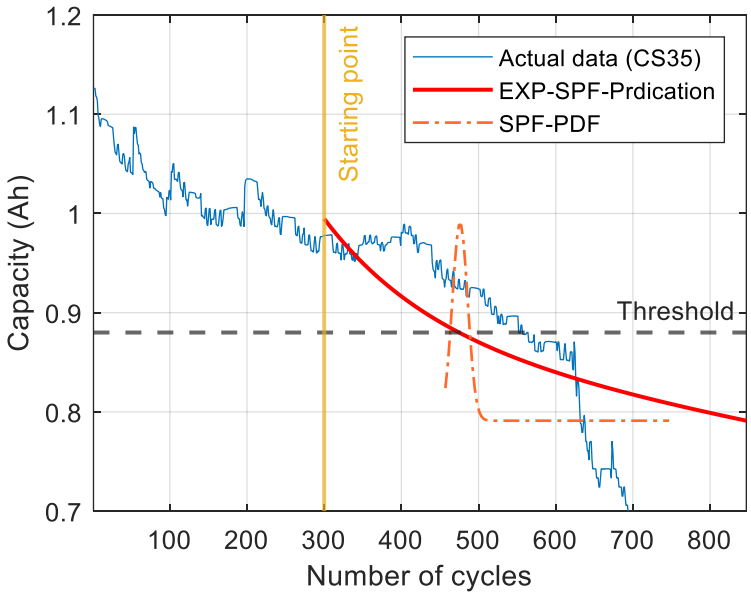

Figure 5. 9 Predicted RUL result obtained, using EXP+SPF approaches with bounded by 50%.

To this end, this work proposed a hybrid framework to predict the RUL online, Figure. 5.10 shows that the NN models' prediction curves are closer to the actual capacity degradation curve at the same predicted starting point as the conventional capacity prognostic model (Figure. 5.8).

With the NN models, RUL PDFs are narrower and taller than the empirical model. Table 5.3 illustrates the prediction errors and RUL PDF widths, suggesting the NN deterioration model is more accurate than the empirical degradation model. Since the NN model is better able to track the battery fading trend, it provides a more accurate state-space model for the RUL framework.

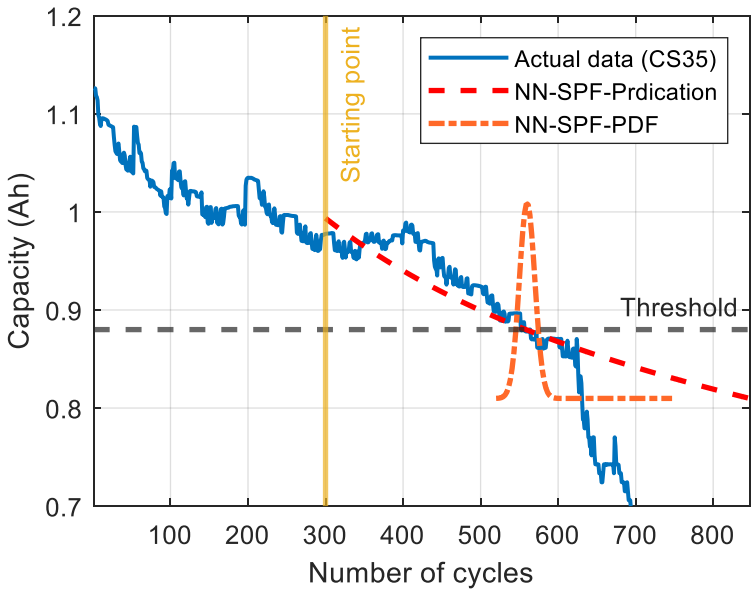

Figure 5. 10 Predicted RUL result obtained, using NN+SPF approaches.

Table 5. 3 RUL prediction results of CS35.

Algorithm	T_s	EOL_{true}	RUL_{pred}	AE	$RMSE$
Exp+SPF (95% boundary)	300	557	565	8	0.0532
	500	557	559	2	0.0218
Exp+SPF (50% boundary)	300	557	620	63	0.6606
	500	557	600	43	0.3305
NN+SPF	300	557	562	5	0.0209
	500	557	558	1	0.0198

5.5.1 Comparison With Other Published Methods

Table 5.4 lists and compares the predicted error metric of RUL obtained by the proposed method and other published methods. This comparison helps to verify the precision of the proposed approach further. The other published methods include UKF combined with error compensation (UKF+CEEMD) [116], the integration of UKF and RVM [86], the NN-Bat-PF method [99], and a combination of SVR+PF [203]. Results reveal that the suggested technique performs much better than the approaches that have previously been published in [83,109] (see Table 5.4 for details), which implies that both the universality and the precision are proven by our method.

Table 5. 4 Comparative analysis of different prediction methods for RUL.

Method	AE
(UKF+CEEMD) [116]	4
UKF and RVM [86]	3
NN-Bat-PF method [99]	2
SVR+PF [203]	2
Proposed NN+ SPF	1

5.6 Summary

This chapter has proposed a hybrid NN based on an SPF framework to predict the online RUL of LiBs. The degradation models (NN and empirical models) were trained and tested using the capacity fading dataset from CALCE. Furthermore, we used different model parameter configurations to validate the stability and effectiveness of the proposed framework. The proposed framework uses the NN algorithm to track the trend in degradation of the battery discharge capacity as a function of the number of cycles. The NN architecture consists of

multiple layers of artificial neurons, each of which is responsible for processing the input data and passing the results to the next layer. The tansig activation function is used for the hidden layer neurons, and the purelin activation function is used for the output node. This architecture provides a powerful way to capture complex relationships between the input parameters and the output and can be used to make accurate predictions about the future capacity of the battery. The comparison results clearly indicated that the proposed framework did not require a degradation pattern and could be adapted to diverse, dynamic trends, resulting in higher performance than the traditional predictive approach. In addition, the results show that the proposed framework has a more accurate RUL prediction than the conventional framework since the maximum RMSE of the proposed framework is around 0.001. The proposed approach's estimated results have been compared to those obtained using other published methods, and it was found that the proposed approach has a higher level of precision compared to the published methods.

Chapter 6 Conclusions and Future Work

6.1 Conclusion

In BMS, accurate prediction of the RUL in LiBs is a key aspect of managing their health, promoting reliable and secure systems, and reducing the need for unscheduled maintenance and costs. Recent work on RUL prediction has largely focused on refining the accuracy and reliability of the RUL prediction. However, achieving high accuracy levels in predicting the RUL of batteries requires analysing battery performance decline based on factors such as material properties, electrochemical reaction, and impedance change. Accurate prediction also depends on the tuning of particle state parameters.

Classic PF algorithm is prone to two primary issues: particle degeneracy and particle impoverishment. Particle degeneracy occurs when the weight of a small number of particles becomes significantly more significant than the others, causing a loss of diversity among the particles. Particle impoverishment happens during the resampling phase of the particle filter when a subset of particles is selected with a higher probability than the others, resulting in a loss of samples and reduced accuracy.

For this reason, the key aim of this thesis focuses on making a research contribution in the area of an online monitoring system for lithium-ion batteries that could adjust to alterations caused by varying operating conditions. Several novel approaches have been presented in this thesis.

6.1.1 Battery Lifetime Identification Using Smooth Particle Filter Technique

Here, an innovative online RUL prediction of LiBs known as the SPF algorithm is presented to overcome the limitations of many classic PF algorithms. The proposed algorithm allows for an accurate estimation of the battery's state and the uncertainty in the prediction, making it a valuable tool for battery health monitoring and management. Additionally, the proposed algorithm is computationally efficient and can be easily implemented in real-time applications. Experimental datasets published by PCoE NASA were used, and a second-order exponential

degradation model to validate the effectiveness and stability of the proposed method was developed. The results obtained clearly indicated that the proposed SPF algorithm can improve the prediction accuracy compared with the classical PF algorithm. The average RUL errors and PDF width of the SPF approach are less than in PF methods, demonstrating that the suggested method is more accurate and steadier. In addition, RUL prediction was tested with various predicted starting points to assess whether the amount of data influenced the accuracy of the prediction. The findings clearly demonstrated that the amount of data affects the accuracy of the prediction. It has also been shown that the earlier the starting point of the prediction, the higher the prediction error rate relative to the higher starting point. In fact, the predicted curve further diverges from the actual degradation curve. Overall, the SPF-based likelihood approximation method presents a significant advancement in the field of battery prognostics and offers a promising solution for improving the performance and reliability of LiBs. Further research is planned to focus on designing robust degradation models, such as the Multiphysics model, with an emphasis on accurate and reliable RUL prediction at a rapid convergence rate.

The findings and conclusions of this work have been successfully published in the following journal paper:

- **M. a. El-Dalahmeh**, M. Al-Greer, M. d. El-Dalahmeh, and M. Short, "Smooth particle filter-based likelihood approximations for remaining useful life prediction of Lithium-ion batteries," IET Smart Grid, 2021.

6.1.2 Physics-Based Modeling for Monitoring Battery Lifetime

The empirical degradation model has the advantage of being simple and easy to implement, making it suitable for real-time monitoring applications. However, it has limitations in terms of accuracy and reliability, particularly in predicting the RUL of batteries. This is because it does not account for the underlying physical processes that drive battery degradation, which can vary significantly depending on the operating conditions. To address this, a physics-informed SPF framework for RUL prediction is proposed in this work, which estimates parameters of an SPM of LiBs by extracting three main degradation mechanisms: active material loss in positive and

negative electrodes and loss of lithium inventory from the VQ and dV/dQ curves, which can then utilise to predict the LiB capacity. These parameters estimated using SPM are passed through the SPF algorithm to update the model parameters and predict the RUL of LiBs.

Overall, it has been concluded that the proposed RUL prediction framework based on combined SPM and SPF can significantly improve the RUL predictions in comparison to its predecessors. The method combines the benefits from both SPM and SPF, therefore enhancing the RUL prediction. The proposed combined SPM and SPF framework has been tested on several battery cycling and degradation datasets. The predicted RUL using the proposed framework show low RA and RMSE values in comparison to other RUL prediction methods. All datasets for battery RUL predictions show improved results by using the SPM-SPF framework. The RUL prediction has been tested on noisy data. It has been concluded that the SPM-SPF provides the best RUL predictions for noisy input data.

The findings and conclusions of this work have been successfully published in the following journal paper:

- **M.o'ath. El-Dalahmeh,** M. Al-Greer, M. d. El-Dalahmeh, and I. Bashir, "Physics-based model informed smooth particle filter for remaining useful life prediction of lithium-ion battery," Measurement, vol. 214, p. 112838, 2023/06/15/ 2023.

Online Hybrid Prognostic Health Management Prediction

For real-time RUL prediction, LiBs often operate under less-than-ideal conditions, which can result in inaccurate initial model parameters. This, in turn, can lead to unstable and inaccurate RUL predictions. Therefore, it is important to have a robust and flexible model that can accurately track the capacity degradation trends and extract model parameters even under different operating conditions.

This chapter has proposed a hybrid NN based on an SPF framework to predict the online RUL of LiBs. The degradation models (NN and empirical models) were trained and tested using the capacity fading dataset from CALCE. Furthermore, we used different model

parameter configurations to validate the stability and effectiveness of the proposed framework. The proposed framework uses the NN algorithm to track the trend in degradation of the battery discharge capacity as a function of the number of cycles. The NN architecture consists of multiple layers of artificial neurons, each of which is responsible for processing the input data and passing the results to the next layer. The tansig activation function is used for the hidden layer neurons, and the purelin activation function is used for the output node. This architecture provides a powerful way to capture complex relationships between the input parameters and the output and can be used to make accurate predictions about the future capacity of the battery.

The comparison results clearly indicated that the proposed framework was not required a degradation pattern and can be adapted to diverse, dynamic trends, resulting in higher performance than the traditional predictive approach. In addition, the results show that the proposed framework has a more accurate RUL prediction than the conventional framework since the maximum RMSE of the proposed framework is around 0.001. The proposed approach's estimated results have been compared to those obtained using other published methods, and it was found that the proposed approach has a higher level of precision compared to the published methods.

The findings and conclusions of this work have been successfully published in the following conference paper:

- **M. El-Dalahmeh**, M. Al-Greer, M. El-Dalahmeh, and I. Bashir, "Online Hybrid Prognostic Health Management Prediction Using a Neural Network and Smooth Particle Filter for Lithium-ion Batteries," in *2022 57th International Universities Power Engineering Conference (UPEC)*, 30 Aug.-2 Sept. 2022 2022, pp. 1-6.

6.2 Future Work

The research conducted in this thesis has uncovered several promising areas for further exploration in the field of prognostics. The proposed framework shows potential in predicting

the RUL of LiBs. A few areas of research could help in the future of prognostic research. These research areas have the potential to assist in refining and improving the proposed framework, making it a more reliable and accurate tool for predicting battery health. The following suggestions provide pointers towards further research for future works.

The prediction of battery RUL is primarily based on LiBs, which are composed of multiple cells connected in series and parallel to create a battery module or pack. This electrochemical process is highly variable and complex, leading to inconsistencies in performance due to differences in material composition and manufacturing guidelines. Additionally, temperature gradients within the battery pack can cause uneven aging of the cells, further complicating the prediction of RUL. The accuracy of cell-level predictions is lower than that of the battery pack due to charge unbalancing during charging and discharging, which has been addressed with the use of power electronic converters and controller circuits. However, more research is needed to investigate the issues related to inconsistencies in battery pack performance to improve the prediction of battery RUL.

The main focus of future work will be to explore the capabilities of the hybrid integration scheme. Hybrid models have shown significant progress in accurately predicting the RUL compared to model-based and data-driven techniques. The hybrid model is typically developed by combining two models or hybridizing an optimisation technique with a single model. In Section 2.5.3, several hybrid models based on the PF technique and data-driven models have been discussed. However, if two different models are combined accurately, it may lead to better outcomes, overfitting of data, and increased computational complexity. Therefore, it is crucial to investigate the practicality and feasibility of creating an intelligent hybrid model for RUL prediction. There is potential to make several improvements to the hybrid mechanism, such as incorporating more advanced similarity measures into the integration scheme. Additionally, investigating ways to reduce the computational complexity of the integration methodology will be beneficial during the instrumentation phase.

Currently, the accuracy and reliability of RUL prediction methods are evaluated through experimental work. However, real-time Internet of Things (IoT)-integrated RUL prediction has

yet to be explored. The application of IoT-based RUL prediction models, particularly data-driven approaches, involves a large volume of data, data processing, data management, and cloud storage, which can improve prognostics and health management of battery storage systems in real-time. The authors in [204] have introduced an IoT-based battery state estimation model that utilises ARM Cortex-M4 MCU and deep learning (DL) models such as LSTM, gated recurrent unit (GRU), and CNN. However, no recent publication has been on specifically IoT-integrated RUL prediction for batteries. Therefore, further investigation is necessary to develop IoT-based RUL prediction methods.

At present, RUL prediction methods have been validated using various experimental tools. However, the implementation of real-time RUL prediction with hardware-in-loop (HIL), prototype, and embedded systems has not been thoroughly investigated. Only a few recent research articles have focused on SOC estimation and have achieved satisfactory results compared to simulation results [205]. However, there is still a need for the exploration of RUL prediction for LiBs using the HIL prototype. A visual representation that outlines key suggestions and future improvements for enhancing the RUL prediction scheme is provided.

References

[1] L. Yao *et al.*, "A Review of Lithium-Ion Battery State of Health Estimation and Prediction Methods," *World Electric Vehicle Journal,* vol. 12, no. 3, p. 113, 2021.

[2] J. Tian, R. Xiong, and W. Shen, "A review on state of health estimation for lithium ion batteries in photovoltaic systems," *eTransportation,* vol. 2, p. 100028, 2019/11/01/ 2019, doi: https://doi.org/10.1016/j.etran.2019.100028.

[3] H. Meng and Y.-F. Li, "A review on prognostics and health management (PHM) methods of lithium-ion batteries," *Renewable and Sustainable Energy Reviews,* vol. 116, p. 109405, 2019/12/01/ 2019, doi: https://doi.org/10.1016/j.rser.2019.109405.

[4] W. Wu, S. Wang, W. Wu, K. Chen, S. Hong, and Y. Lai, "A critical review of battery thermal performance and liquid based battery thermal management," *Energy Conversion and Management,* vol. 182, pp. 262-281, 2019/02/15/ 2019, doi: https://doi.org/10.1016/j.enconman.2018.12.051.

[5] S. Arora, A. T. Abkenar, S. G. Jayasinghe, and K. Tammi, "Chapter 8 - Battery Management System: Charge Balancing and Temperature Control," in *Heavy-Duty Electric Vehicles*, S. Arora, A. T. Abkenar, S. G. Jayasinghe, and K. Tammi Eds.: Butterworth-Heinemann, 2021, pp. 173-203.

[6] Z. Kang, C. A.-O. Catal, and B. A.-O. Tekinerdogan, "Remaining Useful Life (RUL) Prediction of Equipment in Production Lines Using Artificial Neural Networks. LID - 10.3390/s21030932 [doi] LID - 932," (in eng), no. 1424-8220 (Electronic).

[7] R. P. Ribeiro and N. Moniz, "Imbalanced regression and extreme value prediction," *Machine Learning,* vol. 109, no. 9, pp. 1803-1835, 2020/09/01 2020, doi: 10.1007/s10994-020-05900-9.

[8] V. Sulzer *et al.*, "The challenge and opportunity of battery lifetime prediction from field data," *Joule*, vol. 5, no. 8, pp. 1934-1955, 2021/08/18/ 2021, doi: https://doi.org/10.1016/j.joule.2021.06.005.

[9] P. M. Attia *et al.*, "Review—"Knees" in Lithium-Ion Battery Aging Trajectories," *Journal of The Electrochemical Society,* vol. 169, no. 6, p. 060517, 2022/06/10 2022, doi: 10.1149/1945-7111/ac6d13.

[10] M. Aykol *et al.*, "Perspective—Combining Physics and Machine Learning to Predict Battery Lifetime," *Journal of The Electrochemical Society,* vol. 168, no. 3, p. 030525, 2021/03/16 2021, doi: 10.1149/1945-7111/abec55.

[11] L. Alzubaidi *et al.*, "Review of deep learning: concepts, CNN architectures, challenges, applications, future directions," *Journal of Big Data*, vol. 8, no. 1, p. 53, 2021/03/31 2021, doi: 10.1186/s40537-021-00444-8.

[12] K. Gao, J. A.-O. Xu, Z. A.-O. Li, Z. Cai, D. Jiang, and A. Zeng, "A Novel Remaining Useful Life Prediction Method for Capacity Diving Lithium-Ion Batteries," (in eng), no. 2470-1343 (Electronic).

[13] X. Hu, F. Feng, K. Liu, L. Zhang, J. Xie, and B. Liu, "State estimation for advanced battery management: Key challenges and future trends," *Renewable and Sustainable Energy Reviews,* vol. 114, p. 109334, 2019/10/01/ 2019, doi: https://doi.org/10.1016/j.rser.2019.109334.

[14] W. Yu, Y. Guo, S. Xu, Y. Yang, Y. Zhao, and J. Zhang, "Comprehensive recycling of lithium-ion batteries: Fundamentals, pretreatment, and perspectives," *Energy Storage Materials,* vol. 54, pp. 172-220, 2023/01/01/ 2023, doi: https://doi.org/10.1016/j.ensm.2022.10.033.

[15] P. Roy and S. K. Srivastava, "Nanostructured anode materials for lithium ion batteries," *Journal of Materials Chemistry A,* vol. 3, no. 6, pp. 2454-2484, 2015.

[16] A. Jokar, B. Rajabloo, M. Désilets, and M. Lacroix, "Review of simplified Pseudo-two-Dimensional models of lithium-ion batteries," *Journal of Power Sources,* vol. 327, pp. 44-55, 2016/09/30/ 2016, doi: https://doi.org/10.1016/j.jpowsour.2016.07.036.

[17] G. L. Plett, *Battery management systems, Volume I: Battery modeling*. Artech House, 2015.

[18] L. Zhang, H. Peng, Z. Ning, Z. Mu, and C. Sun, "Comparative research on RC equivalent circuit models for lithium-ion batteries of electric vehicles," *Applied Sciences,* vol. 7, no. 10, p. 1002, 2017.

[19] N. Tian, Y. Wang, J. Chen, and H. Fang, "On parameter identification of an equivalent circuit model for lithium-ion batteries," 2017: IEEE, pp. 187-192.

[20] H. W. You, J. I. Bae, S. J. Cho, J. M. Lee, and S.-H. Kim, "Analysis of equivalent circuit models in lithium-ion batteries," *AIP Advances,* vol. 8, no. 12, p. 125101, 2018.

[21] Z. Khalik, M. C. F. Donkers, and H. J. Bergveld, "Model simplifications and their impact on computational complexity for an electrochemistry-based battery modeling toolbox," *Journal of Power Sources,* vol. 488, p. 229427, 2021/03/15/ 2021, doi: https://doi.org/10.1016/j.jpowsour.2020.229427.

[22] M. D. Radin *et al.*, "Narrowing the Gap between Theoretical and Practical Capacities in Li-Ion Layered Oxide Cathode Materials," *Advanced Energy Materials,* https://doi.org/10.1002/aenm.201602888 vol. 7, no. 20, p. 1602888, 2017/10/01 2017, doi: https://doi.org/10.1002/aenm.201602888.

[23] A. Latz, T. Danner, B. Horstmann, and T. Jahnke, "Microstructure-and Theory-Based Modeling and Simulation of Batteries and Fuel Cells," *Chemie Ingenieur Technik,* vol. 91, no. 6, pp. 758-768, 2019.

[24] M. Doyle, T. F. Fuller, and J. Newman, "Modeling of galvanostatic charge and discharge of the lithium/polymer/insertion cell," *Journal of the Electrochemical society*, vol. 140, no. 6, p. 1526, 1993.

[25] J. M. Reniers, G. Mulder, S. Ober-Blöbaum, and D. A. Howey, "Improving optimal control of grid-connected lithium-ion batteries through more accurate battery and degradation modelling," *Journal of Power Sources*, vol. 379, pp. 91-102, 2018/03/01/ 2018, doi: https://doi.org/10.1016/j.jpowsour.2018.01.004.

[26] J. Li, N. Lotfi, R. G. Landers, and J. Park, "A Single Particle Model for Lithium-Ion Batteries with Electrolyte and Stress-Enhanced Diffusion Physics," *Journal of The Electrochemical Society*, vol. 164, no. 4, p. A874, 2017/02/28 2017, doi: 10.1149/2.1541704jes.

[27] K. Gopalakrishnan and G. J. Offer, "A Composite Single Particle Lithium-Ion Battery Model Through System Identification," *IEEE Transactions on Control Systems Technology*, vol. 30, no. 1, pp. 1-13, 2022, doi: 10.1109/TCST.2020.3047776.

[28] C. Liu, Y. Wang, and Z. Chen, "Degradation model and cycle life prediction for lithium-ion battery used in hybrid energy storage system," *Energy*, vol. 166, pp. 796-806, 2019/01/01/ 2019, doi: https://doi.org/10.1016/j.energy.2018.10.131.

[29] C. R. Birkl, M. R. Roberts, E. McTurk, P. G. Bruce, and D. A. Howey, "Degradation diagnostics for lithium ion cells," *Journal of Power Sources*, vol. 341, pp. 373-386, 2017/02/15/ 2017, doi: https://doi.org/10.1016/j.jpowsour.2016.12.011.

[30] J. Vetter *et al.*, "Ageing mechanisms in lithium-ion batteries," *Journal of Power Sources*, vol. 147, no. 1, pp. 269-281, 2005/09/09/ 2005, doi: https://doi.org/10.1016/j.jpowsour.2005.01.006.

[31] V. A. Agubra and J. W. Fergus, "The formation and stability of the solid electrolyte interface on the graphite anode," *Journal of Power Sources*, vol. 268, pp. 153-162, 2014/12/05/ 2014, doi: https://doi.org/10.1016/j.jpowsour.2014.06.024.

[32] M. Gauthier *et al.*, "Electrode–Electrolyte Interface in Li-Ion Batteries: Current Understanding and New Insights," *The Journal of Physical Chemistry Letters*, vol. 6, no. 22, pp. 4653-4672, 2015/11/19 2015, doi: 10.1021/acs.jpclett.5b01727.

[33] P. Lu, C. Li, E. W. Schneider, and S. J. Harris, "Chemistry, Impedance, and Morphology Evolution in Solid Electrolyte Interphase Films during Formation in Lithium Ion Batteries," *The Journal of Physical Chemistry C*, vol. 118, no. 2, pp. 896-903, 2014/01/16 2014, doi: 10.1021/jp4111019.

[34] P. Verma, P. Maire, and P. Novák, "A review of the features and analyses of the solid electrolyte interphase in Li-ion batteries," *Electrochimica Acta*, vol. 55, no. 22, pp. 6332-6341, 2010/09/01/ 2010, doi: https://doi.org/10.1016/j.electacta.2010.05.072.

[35] Z. Zhuo *et al.*, "Breathing and oscillating growth of solid-electrolyte-interphase upon electrochemical cycling," *Chemical Communications*, 10.1039/C7CC07082A vol. 54, no. 7, pp. 814-817, 2018, doi: 10.1039/C7CC07082A.

[36] E. Peled, D. Golodnitsky, and G. Ardel, "Advanced Model for Solid Electrolyte Interphase Electrodes in Liquid and Polymer Electrolytes," *Journal of The Electrochemical Society,* vol. 144, no. 8, p. L208, 1997/08/01 1997, doi: 10.1149/1.1837858.

[37] A. Barré, B. Deguilhem, S. Grolleau, M. Gérard, F. Suard, and D. Riu, "A review on lithium-ion battery ageing mechanisms and estimations for automotive applications," *Journal of Power Sources,* vol. 241, pp. 680-689, 2013/11/01/ 2013, doi: https://doi.org/10.1016/j.jpowsour.2013.05.040.

[38] R. Xiong, Y. Pan, W. Shen, H. Li, and F. Sun, "Lithium-ion battery aging mechanisms and diagnosis method for automotive applications: Recent advances and perspectives," *Renewable and Sustainable Energy Reviews,* vol. 131, p. 110048, 2020/10/01/ 2020, doi: https://doi.org/10.1016/j.rser.2020.110048.

[39] M. Broussely, S. Herreyre, P. Biensan, P. Kasztejna, K. Nechev, and R. J. Staniewicz, "Aging mechanism in Li ion cells and calendar life predictions," *Journal of Power Sources,* vol. 97-98, pp. 13-21, 2001/07/01/ 2001, doi: https://doi.org/10.1016/S0378-7753(01)00722-4.

[40] S. F. Schuster *et al.*, "Nonlinear aging characteristics of lithium-ion cells under different operational conditions," *Journal of Energy Storage,* vol. 1, pp. 44-53, 2015/06/01/ 2015, doi: https://doi.org/10.1016/j.est.2015.05.003.

[41] M. R. Palacín, "Understanding ageing in Li-ion batteries: a chemical issue," *Chemical Society Reviews,* 10.1039/C7CS00889A vol. 47, no. 13, pp. 4924-4933, 2018, doi: 10.1039/C7CS00889A.

[42] P. Bernard, H. Martinez, C. Tessier, E. Garitte, S. Franger, and R. Dedryvere, "Role of Negative Electrode Porosity in Long-Term Aging of NMC//Graphite Li-Ion Batteries," *Journal of The Electrochemical Society,* vol. 162, no. 13, p. A7096, 2015/09/04 2015, doi: 10.1149/2.0151513jes.

[43] R. Narayanrao, M. M. Joglekar, and S. Inguva, "A Phenomenological Degradation Model for Cyclic Aging of Lithium Ion Cell Materials," *Journal of The Electrochemical Society,* vol. 160, no. 1, p. A125, 2012/11/19 2013, doi: 10.1149/2.013302jes.

[44] Q. Liu *et al.*, "Understanding undesirable anode lithium plating issues in lithium-ion batteries," *RSC Advances,* 10.1039/C6RA19482F vol. 6, no. 91, pp. 88683-88700, 2016, doi: 10.1039/C6RA19482F.

[45] A. M. Grillet *et al.*, "Conductivity Degradation of Polyvinylidene Fluoride Composite Binder during Cycling: Measurements and Simulations for Lithium-Ion Batteries," *Journal of The Electrochemical Society,* vol. 163, no. 9, p. A1859, 2016/07/02 2016, doi: 10.1149/2.0341609jes.

[46] X. Lin, K. Khosravinia, X. Hu, J. Li, and W. Lu, "Lithium Plating Mechanism, Detection, and Mitigation in Lithium-Ion Batteries," *Progress in Energy and*

Combustion Science, vol. 87, p. 100953, 2021/11/01/ 2021, doi: https://doi.org/10.1016/j.pecs.2021.100953.

[47] Y. Li *et al.*, "Data-driven health estimation and lifetime prediction of lithium-ion batteries: A review," *Renewable and Sustainable Energy Reviews,* vol. 113, p. 109254, 2019/10/01/ 2019, doi: https://doi.org/10.1016/j.rser.2019.109254.

[48] B. Pang, L. Chen, and Z. Dong, "Data-Driven Degradation Modeling and SOH Prediction of Li-Ion Batteries," *Energies*, vol. 15, no. 15, doi: 10.3390/en15155580.

[49] H. Chaoui, C. C. Ibe-Ekeocha, and H. Gualous, "Aging prediction and state of charge estimation of a LiFePO4 battery using input time-delayed neural networks," *Electric Power Systems Research,* vol. 146, pp. 189-197, 2017/05/01/ 2017, doi: https://doi.org/10.1016/j.epsr.2017.01.032.

[50] Y. Ding, C. Lu, and J. Ma, "Li-ion Battery Health Estimation Based on Multi-layer Characteristic Fusion and Deep Learning," in *2017 IEEE Vehicle Power and Propulsion Conference (VPPC)*, 11-14 Dec. 2017 2017, pp. 1-5, doi: 10.1109/VPPC.2017.8331058.

[51] Y. Zhang, Q. Tang, Y. Zhang, J. Wang, U. Stimming, and A. A. Lee, "Identifying degradation patterns of lithium ion batteries from impedance spectroscopy using machine learning," *Nature Communications*, vol. 11, no. 1, p. 1706, 2020/04/06 2020, doi: 10.1038/s41467-020-15235-7.

[52] J. Wei, G. Dong, and Z. Chen, "Remaining Useful Life Prediction and State of Health Diagnosis for Lithium-Ion Batteries Using Particle Filter and Support Vector Regression," *IEEE Transactions on Industrial Electronics,* vol. 65, no. 7, pp. 5634-5643, 2018, doi: 10.1109/TIE.2017.2782224.

[53] X. Tang, K. Liu, X. Wang, F. Gao, J. Macro, and W. D. Widanage, "Model Migration Neural Network for Predicting Battery Aging Trajectories," *IEEE Transactions on Transportation Electrification,* vol. 6, no. 2, pp. 363-374, 2020, doi: 10.1109/TTE.2020.2979547.

[54] E. Vanem, C. B. Salucci, A. Bakdi, and Ø. Å. s. Alnes, "Data-driven state of health modelling—A review of state of the art and reflections on applications for maritime battery systems," *Journal of Energy Storage,* vol. 43, p. 103158, 2021/11/01/ 2021, doi: https://doi.org/10.1016/j.est.2021.103158.

[55] A. Koul, "DEVELOPMENT OF DATA-DRIVEN METHOD FOR CAPACITY ESTIMATION AND PROGNOSIS FOR LITHIUM-ION BATTERIES," Nanyang Technological University, 2020.

[56] X. Wang, C. Gao, and M. Sun, "Probabilistic Prediction Algorithm for Cycle Life of Energy Storage in Lithium Battery," *World Electric Vehicle Journal*, vol. 10, no. 1, 2019, doi: 10.3390/wevj10010007.

[57] K. A. Severson *et al.*, "Data-driven prediction of battery cycle life before capacity degradation," *Nature Energy,* vol. 4, no. 5, pp. 383-391, 2019/05/01 2019, doi: 10.1038/s41560-019-0356-8.

[58] P. Fermín-Cueto *et al.*, "Identification and machine learning prediction of knee-point and knee-onset in capacity degradation curves of lithium-ion cells," *Energy and AI*, vol. 1, p. 100006, 2020/08/01/ 2020, doi: https://doi.org/10.1016/j.egyai.2020.100006.

[59] D. Pan, J.-B. Liu, and J. Cao, "Remaining useful life estimation using an inverse Gaussian degradation model," *Neurocomput.*, vol. 185, no. C, pp. 64–72, 2016, doi: 10.1016/j.neucom.2015.12.041.

[60] J. Lin and M. Wei, "Remaining useful life prediction of lithium-ion battery based on auto-regression and particle filter," *International Journal of Intelligent Computing and Cybernetics*, vol. 14, no. 2, pp. 218-237, 2021, doi: 10.1108/IJICC-09-2020-0131.

[61] X. Pang *et al.*, "A lithium-ion battery remaining useful life prediction method based on the incremental capacity analysis and Gaussian process regression," *Microelectronics Reliability*, vol. 127, p. 114405, 2021/12/01/ 2021, doi: https://doi.org/10.1016/j.microrel.2021.114405.

[62] L. Zou, B. Wen, Y. Wei, Y. Zhang, J. Yang, and H. Zhang, "Online Prediction of Remaining Useful Life for Li-Ion Batteries Based on Discharge Voltage Data," *Energies*, vol. 15, no. 6, 2022, doi: 10.3390/en15062237.

[63] D. Chen *et al.*, "An Empirical-Data Hybrid Driven Approach for Remaining Useful Life prediction of lithium-ion batteries considering capacity diving," *Energy*, vol. 245, p. 123222, 2022/04/15/ 2022, doi: https://doi.org/10.1016/j.energy.2022.123222.

[64] X. Hu, L. Xu, X. Lin, and M. Pecht, "Battery Lifetime Prognostics," *Joule*, vol. 4, no. 2, pp. 310-346, 2020/02/19/ 2020, doi: https://doi.org/10.1016/j.joule.2019.11.018.

[65] S. Ansari, A. Ayob, M. S. Hossain Lipu, A. Hussain, and M. H. M. Saad, "Remaining useful life prediction for lithium-ion battery storage system: A comprehensive review of methods, key factors, issues and future outlook," *Energy Reports*, vol. 8, pp. 12153-12185, 2022/11/01/ 2022, doi: https://doi.org/10.1016/j.egyr.2022.09.043.

[66] N. Laayouj and H. Jamouli, "Lithium-ion Battery Degradation Assessment and Remaining Useful Life Estimation in Hybrid Electric Vehicle," *Renewable Energy and Sustainable Development; Vol 2, No 1 (2016): RESD Volume 2, Issue 1, June 2016*, 06/30/ 2016. [Online]. Available: http://apc.aast.edu/ojs/index.php/RESD/article/view/121.

[67] D. Z. Li, W. Wang, and F. Ismail, "A Mutated Particle Filter Technique for System State Estimation and Battery Life Prediction," *IEEE Transactions on Instrumentation and Measurement*, vol. 63, no. 8, pp. 2034-2043, 2014, doi: 10.1109/TIM.2014.2303534.

[68] M. Ahwiadi and W. Wang, "An Enhanced Mutated Particle Filter Technique for System State Estimation and Battery Life Prediction," *IEEE Transactions on Instrumentation and Measurement*, vol. 68, no. 3, pp. 923-935, 2019, doi: 10.1109/TIM.2018.2853900.

[69] J. Liu, W. Wang, and F. Ma, "A regularized auxiliary particle filtering approach for system state estimation and battery life prediction," *Smart Materials and Structures*, vol. 20, no. 7, p. 075021, 2011/06/22 2011, doi: 10.1088/0964-1726/20/7/075021.

[70] L. Chen, J. An, H. Wang, M. Zhang, and H. Pan, "Remaining useful life prediction for lithium-ion battery by combining an improved particle filter with sliding-window gray model," *Energy Reports*, vol. 6, pp. 2086-2093, 2020/11/01/ 2020, doi: https://doi.org/10.1016/j.egyr.2020.07.026.

[71] A. Guha and A. Patra, "Online Estimation of the Electrochemical Impedance Spectrum and Remaining Useful Life of Lithium-Ion Batteries," *IEEE Transactions on Instrumentation and Measurement*, vol. 67, no. 8, pp. 1836-1849, 2018, doi: 10.1109/TIM.2018.2809138.

[72] B. B. Ashoor, A. Giwa, and S. W. Hasan, "Chapter 5 - Full-Scale Membrane Distillation Systems and Performance Improvement Through Modeling: A Review," in *Current Trends and Future Developments on (Bio-) Membranes*, A. Basile, E. Curcio, and Inamuddin Eds.: Elsevier, 2019, pp. 105-140.

[73] D. U. Sauer and H. Wenzl, "Comparison of different approaches for lifetime prediction of electrochemical systems—Using lead-acid batteries as example," *Journal of Power Sources*, vol. 176, no. 2, pp. 534-546, 2008/02/01/ 2008, doi: https://doi.org/10.1016/j.jpowsour.2007.08.057.

[74] M. V. Micea, L. Ungurean, G. N. Cârstoiu, and V. Groza, "Online State-of-Health Assessment for Battery Management Systems," *IEEE Transactions on Instrumentation and Measurement*, vol. 60, no. 6, pp. 1997-2006, 2011, doi: 10.1109/tim.2011.2115630.

[75] I. Bloom *et al.*, "An accelerated calendar and cycle life study of Li-ion cells," *Journal of Power Sources*, vol. 101, no. 2, pp. 238-247, 2001/10/15/ 2001, doi: https://doi.org/10.1016/S0378-7753(01)00783-2.

[76] R. B. Wright *et al.*, "Calendar- and cycle-life studies of advanced technology development program generation 1 lithium-ion batteries," *Journal of Power Sources*, vol. 110, no. 2, pp. 445-470, 2002/08/22/ 2002, doi: https://doi.org/10.1016/S0378-7753(02)00210-0.

[77] K.-H. Tseng, J.-W. Liang, W. Chang, and S.-C. Huang, "Regression Models Using Fully Discharged Voltage and Internal Resistance for State of Health Estimation of Lithium-Ion Batteries," *Energies*, vol. 8, no. 4, pp. 2889-2907doi: 10.3390/en8042889.

[78] L. Yang, L. Zhao, X. Su, and S. Wang, "A lithium-ion battery RUL prognosis method using temperature changing rate," in *2016 IEEE International Conference on Prognostics and Health Management (ICPHM)*, 20-22 June 2016 2016, pp. 1-7, doi: 10.1109/ICPHM.2016.7542866.

[79] L. Jide, W. Longfei, M. M. Pour, Y. Mekonnen, and A. I. Sarwat, "Modeling discharge characteristics for predicting battery remaining life," in *2017 IEEE*

Transportation Electrification Conference and Expo (ITEC), 22-24 June 2017 2017, pp. 468-473, doi: 10.1109/ITEC.2017.7993316.

[80] Y. Chang and H. Fang, "A hybrid prognostic method for system degradation based on particle filter and relevance vector machine," *Reliability Engineering & System Safety*, vol. 186, pp. 51-63, 2019.

[81] W. He, N. Williard, M. Osterman, and M. Pecht, "Prognostics of lithium-ion batteries based on Dempster–Shafer theory and the Bayesian Monte Carlo method," *Journal of Power Sources*, vol. 196, no. 23, pp. 10314-10321, 2011/12/01/ 2011, doi: https://doi.org/10.1016/j.jpowsour.2011.08.040.

[82] Q. Qin, S. Zhao, S. Chen, D. Huang, and J. Liang, "Adaptive and robust prediction for the remaining useful life of electrolytic capacitors," *Microelectronics Reliability*, vol. 87, pp. 64-74, 2018, doi: 10.1016/j.microrel.2018.05.020.

[83] B. Arachchige, S. Perinpanayagam, and R. Jaras, "Enhanced Prognostic Model for Lithium Ion Batteries Based on Particle Filter State Transition Model Modification," *Applied Sciences*, vol. 7, no. 11, 2017, doi: 10.3390/app7111172.

[84] L. Wu, X. Fu, and Y. Guan, "Review of the Remaining Useful Life Prognostics of Vehicle Lithium-Ion Batteries Using Data-Driven Methodologies," *Applied Sciences*, vol. 6, no. 6, 2016, doi: 10.3390/app6060166.

[85] W. L. Burgess, "Valve Regulated Lead Acid battery float service life estimation using a Kalman filter," *Journal of Power Sources*, vol. 191, no. 1, pp. 16-21, 2009, doi: 10.1016/j.jpowsour.2008.12.123.

[86] X. Zheng and H. Fang, "An integrated unscented kalman filter and relevance vector regression approach for lithium-ion battery remaining useful life and short-term capacity prediction," *Reliability Engineering & System Safety*, vol. 144, pp. 74-82, 2015/12/01/ 2015, doi: https://doi.org/10.1016/j.ress.2015.07.013.

[87] B. Saha, K. Goebel, S. Poll, and J. Christophersen, "Prognostics Methods for Battery Health Monitoring Using a Bayesian Framework," *IEEE Transactions on Instrumentation and Measurement*, vol. 58, no. 2, pp. 291-296, 2009, doi: 10.1109/tim.2008.2005965.

[88] D. An, J.-H. Choi, and N. H. Kim, "Prognostics 101: A tutorial for particle filter-based prognostics algorithm using Matlab," *Reliability Engineering & System Safety*, vol. 115, pp. 161-169, 2013/07/01/ 2013, doi: https://doi.org/10.1016/j.ress.2013.02.019.

[89] X. Su, S. Wang, M. Pecht, P. Ma, and L. Zhao, "Prognostics of lithium-ion batteries based on different dimensional state equations in the particle filtering method," *Transactions of the Institute of Measurement and Control*, vol. 39, no. 10, pp. 1537-1546, 2017/10/01 2016, doi: 10.1177/0142331216642836.

[90] L. Zhang, Z. Mu, and C. Sun, "Remaining Useful Life Prediction for Lithium-Ion Batteries Based on Exponential Model and Particle Filter," *IEEE Access*, vol. 6, pp. 17729-17740, 2018, doi: 10.1109/ACCESS.2018.2816684.

[91] M. Ahwiadi and W. Wang, "An enhanced particle filter technology for battery system state estimation and RUL prediction," *Measurement*, vol. 191, p. 110817, 2022/03/15/ 2022, doi: https://doi.org/10.1016/j.measurement.2022.110817.

[92] T. Li, T. P. Sattar, and S. Sun, "Deterministic resampling: Unbiased sampling to avoid sample impoverishment in particle filters," *Signal Processing*, vol. 92, no. 7, pp. 1637-1645, 2012/07/01/ 2012, doi: https://doi.org/10.1016/j.sigpro.2011.12.019.

[93] Y. Hu, P. Baraldi, F. Di Maio, and E. Zio, "A particle filtering and kernel smoothing-based approach for new design component prognostics," *Reliability Engineering & System Safety*, vol. 134, pp. 19-31, 2015.

[94] C. Hu, G. Jain, P. Tamirisa, and T. Gorka, "Method for estimating capacity and predicting remaining useful life of lithium-ion battery," *Applied Energy*, vol. 126, pp. 182-189, 2014/08/01/ 2014, doi: https://doi.org/10.1016/j.apenergy.2014.03.086.

[95] H. Zhang, Q. Miao, X. Zhang, and Z. Liu, "An improved unscented particle filter approach for lithium-ion battery remaining useful life prediction," *Microelectronics Reliability*, vol. 81, pp. 288-298, 2018/02/01/ 2018, doi: https://doi.org/10.1016/j.microrel.2017.12.036.

[96] X. Zhang, Q. Miao, and Z. Liu, "Remaining useful life prediction of lithium-ion battery using an improved UPF method based on MCMC," *Microelectronics Reliability*, vol. 75, pp. 288-295, 2017/08/01/ 2017, doi: https://doi.org/10.1016/j.microrel.2017.02.012.

[97] C. Musso, N. Oudjane, and F. Le Gland, "Improving Regularised Particle Filters," in *Sequential Monte Carlo Methods in Practice*, A. Doucet, N. de Freitas, and N. Gordon Eds. New York, NY: Springer New York, 2001, pp. 247-271.

[98] C. Sbarufatti, M. Corbetta, M. Giglio, and F. Cadini, "Adaptive prognosis of lithium-ion batteries based on the combination of particle filters and radial basis function neural networks," *Journal of Power Sources*, vol. 344, pp. 128-140, 2017/03/15/ 2017, doi: https://doi.org/10.1016/j.jpowsour.2017.01.105.

[99] Y. Wu, W. Li, Y. Wang, and K. Zhang, "Remaining Useful Life Prediction of Lithium-Ion Batteries Using Neural Network and Bat-Based Particle Filter," *IEEE Access*, vol. 7, pp. 54843-54854, 2019, doi: 10.1109/access.2019.2913163.

[100] Y. Chen, Y. He, Z. Li, L. Chen, and C. Zhang, "Remaining Useful Life Prediction and State of Health Diagnosis of Lithium-Ion Battery Based on Second-Order Central Difference Particle Filter," *IEEE Access*, vol. 8, pp. 37305-37313, 2020, doi: 10.1109/access.2020.2974401.

[101] A. Svensson, F. Lindsten, and T. B. Schön, "Learning Nonlinear State-Space Models Using Smooth Particle-Filter-Based Likelihood Approximations∗∗This research was supported by the Swedish Foundation for Strategic Research (SSF) via the projects ASSEMBLE (contract number: RIT15-0012) and Probabilistic Modeling and Inference for Machine Learning (contract number: ICA16-0015), and the Swedish Research Council (VR) via the projects NewLEADS - New Directions in Learning

Dynamical Systems (contract number: 621-2016-06079) and Learning of Large-Scale Probabilistic Dynamical Models (contract number: 2016-04278)," *IFAC-PapersOnLine*, vol. 51, no. 15, pp. 652-657, 2018/01/01/ 2018, doi: https://doi.org/10.1016/j.ifacol.2018.09.216.

[102] A. Tomaszewska *et al.*, "Lithium-ion battery fast charging: A review," *eTransportation*, vol. 1, p. 100011, 2019/08/01/ 2019, doi: https://doi.org/10.1016/j.etran.2019.100011.

[103] A. Downey, Y.-H. Lui, C. Hu, S. Laflamme, and S. Hu, "Physics-based prognostics of lithium-ion battery using non-linear least squares with dynamic bounds," *Reliability Engineering & System Safety*, vol. 182, pp. 1-12, 2019/02/01/ 2019, doi: https://doi.org/10.1016/j.ress.2018.09.018.

[104] J. Shi, A. Rivera, and D. Wu, "Battery health management using physics-informed machine learning: Online degradation modeling and remaining useful life prediction," *Mechanical Systems and Signal Processing*, vol. 179, p. 109347, 2022/11/01/ 2022, doi: https://doi.org/10.1016/j.ymssp.2022.109347.

[105] Q. Liu, J. Zhang, K. Li, and C. Lv, "The Remaining Useful Life Prediction by Using Electrochemical Model in the Particle Filter Framework for Lithium-Ion Batteries," *IEEE Access*, vol. 8, pp. 126661-126670, 2020, doi: 10.1109/ACCESS.2020.3006157.

[106] K. Khodadadi Sadabadi, X. Jin, and G. Rizzoni, "Prediction of remaining useful life for a composite electrode lithium ion battery cell using an electrochemical model to estimate the state of health," *Journal of Power Sources*, vol. 481, p. 228861, 2021/01/01/ 2021, doi: https://doi.org/10.1016/j.jpowsour.2020.228861.

[107] Y. H. Lui *et al.*, "Physics-based prognostics of implantable-grade lithium-ion battery for remaining useful life prediction," *Journal of Power Sources*, vol. 485, p. 229327, 2021/02/15/ 2021, doi: https://doi.org/10.1016/j.jpowsour.2020.229327.

[108] I. Bloom *et al.*, "Differential voltage analyses of high-power, lithium-ion cells: 1. Technique and application," *Journal of Power Sources*, vol. 139, no. 1, pp. 295-303, 2005/01/04/ 2005, doi: https://doi.org/10.1016/j.jpowsour.2004.07.021.

[109] C. Su and H. J. Chen, "A review on prognostics approaches for remaining useful life of lithium-ion battery," *IOP Conference Series: Earth and Environmental Science*, vol. 93, no. 1, p. 012040, 2017/11/01 2017, doi: 10.1088/1755-1315/93/1/012040.

[110] S. Wang, S. Jin, D. Deng, and C. Fernandez, "A Critical Review of Online Battery Remaining Useful Lifetime Prediction Methods," *Frontiers in Mechanical Engineering*, Review vol. 7, 2021. [Online]. Available: https://www.frontiersin.org/articles/10.3389/fmech.2021.719718.

[111] M. S. H. Lipu *et al.*, "A review of state of health and remaining useful life estimation methods for lithium-ion battery in electric vehicles: Challenges and recommendations," *Journal of Cleaner Production*, vol. 205, pp. 115-133, 2018/12/20/ 2018, doi: https://doi.org/10.1016/j.jclepro.2018.09.065.

[112] P. Baraldi, M. Compare, S. Sauco, and E. Zio, "Ensemble neural network-based particle filtering for prognostics," *Mechanical Systems and Signal Processing,* vol. 41, no. 1, pp. 288-300, 2013/12/01/ 2013, doi: https://doi.org/10.1016/j.ymssp.2013.07.010.

[113] B. Wang, Y. Lei, N. Li, and N. Li, "A Hybrid Prognostics Approach for Estimating Remaining Useful Life of Rolling Element Bearings," *IEEE Transactions on Reliability,* vol. 69, no. 1, pp. 401-412, 2020, doi: 10.1109/TR.2018.2882682.

[114] X. Zheng, H. Wu, and Y. Chen, "Remaining useful life prediction of lithium-ion battery using a hybrid model-based filtering and data-driven approach," in *2017 11th Asian Control Conference (ASCC)*, 17-20 Dec. 2017 2017, pp. 2698-2703, doi: 10.1109/ASCC.2017.8287603.

[115] D. Liu, Y. Luo, J. Liu, Y. Peng, L. Guo, and M. Pecht, "Lithium-ion battery remaining useful life estimation based on fusion nonlinear degradation AR model and RPF algorithm," *Neural Computing and Applications,* vol. 25, no. 3, pp. 557-572, 2014/09/01 2014, doi: 10.1007/s00521-013-1520-x.

[116] Y. Chang, H. Fang, and Y. Zhang, "A new hybrid method for the prediction of the remaining useful life of a lithium-ion battery," *Applied Energy,* vol. 206, pp. 1564-1578, 2017/11/15/ 2017, doi: https://doi.org/10.1016/j.apenergy.2017.09.106.

[117] P. Sharma and B. J. Bora, "A Review of Modern Machine Learning Techniques in the Prediction of Remaining Useful Life of Lithium-Ion Batteries," *Batteries,* vol. 9, no. 1, doi: 10.3390/batteries9010013.

[118] J. S. Edge *et al.*, "Lithium ion battery degradation: what you need to know," *Physical Chemistry Chemical Physics,* vol. 23, no. 14, pp. 8200-8221, 2021.

[119] W. Li, J. Chen, K. Quade, D. Luder, J. Gong, and D. U. Sauer, "Battery degradation diagnosis with field data, impedance-based modeling and artificial intelligence," *Energy Storage Materials,* vol. 53, pp. 391-403, 2022/12/01/ 2022, doi: https://doi.org/10.1016/j.ensm.2022.08.021.

[120] V. Elvira and L. Martino, "Advances in importance sampling," *arXiv preprint arXiv:2102.05407,* 2021.

[121] D. H. Yi and C. S. Park, "Model selection for parameter identifiability problem in Bayesian inference of building energy model," *Energy and Buildings,* vol. 245, p. 111059, 2021/08/15/ 2021, doi: https://doi.org/10.1016/j.enbuild.2021.111059.

[122] R. van de Schoot *et al.*, "Bayesian statistics and modelling," *Nature Reviews Methods Primers,* vol. 1, no. 1, p. 1, 2021/01/14 2021, doi: 10.1038/s43586-020-00001-2.

[123] C. Fu, J.-J. Sinou, W. Zhu, K. Lu, and Y. Yang, "A state-of-the-art review on uncertainty analysis of rotor systems," *Mechanical Systems and Signal Processing,* vol. 183, p. 109619, 2023.

[124] Y. Huang, C. Shao, B. Wu, J. L. Beck, and H. Li, "State-of-the-art review on Bayesian inference in structural system identification and damage assessment," *Advances in Structural Engineering,* vol. 22, no. 6, pp. 1329-1351, 2019.

[125] A. J. Haug, *Bayesian estimation and tracking: a practical guide*. John Wiley & Sons, 2012.

[126] S. Särkkä, *Bayesian filtering and smoothing*. Cambridge university press, 2013.

[127] S. Theodoridis, "Chapter 13 - Bayesian Learning: Approximate Inference and Nonparametric Models," in *Machine Learning (Second Edition)*, S. Theodoridis Ed.: Academic Press, 2020, pp. 647-730.

[128] I. Redko, A. Habrard, E. Morvant, M. Sebban, and Y. Bennani, "1 - State of the Art of Statistical Learning Theory," in *Advances in Domain Adaptation Theory*, I. Redko, A. Habrard, E. Morvant, M. Sebban, and Y. Bennani Eds.: Elsevier, 2019, pp. 1-19.

[129] M. Hinne, Q. F. Gronau, D. van den Bergh, and E.-J. Wagenmakers, "A conceptual introduction to Bayesian model averaging," *Advances in Methods and Practices in Psychological Science,* vol. 3, no. 2, pp. 200-215, 2020.

[130] R. van de Schoot *et al.*, "Bayesian statistics and modelling," *Nature Reviews Methods Primers,* vol. 1, no. 1, p. 1, 2021.

[131] S. Theodoridis, "Chapter 12 - Bayesian Learning: Inference and the EM Algorithm," in *Machine Learning (Second Edition)*, S. Theodoridis Ed.: Academic Press, 2020, pp. 595-646.

[132] K. Dedecius and P. M. Djurić, "Chapter 4 - Bayesian Approach to Collaborative Inference in Networks of Agents," in *Cooperative and Graph Signal Processing*, P. M. Djurić and C. Richard Eds.: Academic Press, 2018, pp. 131-145.

[133] J. Degen and J. Tonhauser, "Prior beliefs modulate projection," *Open Mind,* vol. 5, pp. 59-70, 2021.

[134] I. Elbatal, N. Alotaibi, S. A. Alyami, M. Elgarhy, and A. R. El-Saeed, "Bayesian and non-Bayesian estimation of the Nadaraj ah–Haghighi distribution: using progressive Type-1 censoring scheme," *Mathematics,* vol. 10, no. 5, p. 760, 2022.

[135] F. Lindgren, H. Rue, and J. Lindström, "An explicit link between Gaussian fields and Gaussian Markov random fields: the stochastic partial differential equation approach," *Journal of the Royal Statistical Society: Series B (Statistical Methodology),* https://doi.org/10.1111/j.1467-9868.2011.00777.x vol. 73, no. 4, pp. 423-498, 2011/09/01 2011, doi: https://doi.org/10.1111/j.1467-9868.2011.00777.x.

[136] J. Yingyan, B. Giovanna, and G. Paolo, "A Bayesian definition of 'most probable' parameters," *Geotechnical Research,* vol. 5, no. 3, pp. 130-142, 2018, doi: 10.1680/jgere.18.00027.

[137] A. J. Haug, "A tutorial on Bayesian estimation and tracking techniques applicable to nonlinear and non-Gaussian processes," 2005.

[138] A. M. Stefan, Q. F. Gronau, F. D. Schönbrodt, and E.-J. Wagenmakers, "A tutorial on Bayes Factor Design Analysis using an informed prior," *Behavior Research Methods*, vol. 51, no. 3, pp. 1042-1058, 2019/06/01 2019, doi: 10.3758/s13428-018-01189-8.

[139] S. M. Lynch, "Basics of bayesian statistics," *Introduction to applied bayesian statistics and estimation for social scientists*, pp. 47-75, 2007.

[140] V. Kotu and B. Deshpande, "Chapter 4 - Classification," in *Data Science (Second Edition)*, V. Kotu and B. Deshpande Eds.: Morgan Kaufmann, 2019, pp. 65-163.

[141] Y. Liu and T. Sweet, "Statistical inference: Bayesian approaches," in *International Encyclopedia of Education (Fourth Edition)*, R. J. Tierney, F. Rizvi, and K. Ercikan Eds. Oxford: Elsevier, 2023, pp. 773-783.

[142] A. Dore, M. Pinasco, and C. S. Regazzoni, "CHAPTER 9 - Multi-Modal Data Fusion Techniques and Applications," in *Multi-Camera Networks*, H. Aghajan and A. Cavallaro Eds. Oxford: Academic Press, 2009, pp. 213-237.

[143] J. V. Kujala, "Bayesian Adaptive Estimation: A Theoretical Review," in *Descriptive and Normative Approaches to Human Behavior*, vol. Volume 3, (Advanced Series on Mathematical Psychology, no. Volume 3): WORLD SCIENTIFIC, 2011, pp. 123-159.

[144] R. J. LeVeque, "Finite difference methods for differential equations," *Draft version for use in AMath*, vol. 585, no. 6, p. 112, 1998.

[145] P. Blunsom, "Hidden markov models," *Lecture notes, August*, vol. 15, no. 18-19, p. 48, 2004.

[146] S. R. Eddy, "What is a hidden Markov model?," *Nature biotechnology*, vol. 22, no. 10, pp. 1315-1316, 2004.

[147] P. Dymarski, *Hidden Markov models: Theory and applications*. BoD–Books on Demand, 2011.

[148] J. Hammersley, *Monte carlo methods*. Springer Science & Business Media, 2013.

[149] D. P. Kroese and R. Y. Rubinstein, "Monte carlo methods," *Wiley Interdisciplinary Reviews: Computational Statistics*, vol. 4, no. 1, pp. 48-58, 2012.

[150] A. Barbu and S.-C. Zhu, *Monte Carlo Methods*. Springer, 2020.

[151] A. J. Haug, "Bayesian estimation for target tracking: part I, general concepts," *WIREs Computational Statistics*, https://doi.org/10.1002/wics.1211 vol. 4, no. 4, pp. 375-383, 2012/07/01 2012, doi: https://doi.org/10.1002/wics.1211.

[152] P. J. Van Leeuwen, H. R. Künsch, L. Nerger, R. Potthast, and S. Reich, "Particle filters for high-dimensional geoscience applications: A review," *Quarterly Journal of the Royal Meteorological Society*, vol. 145, no. 723, pp. 2335-2365, 2019.

[153] M. Speekenbrink, "A tutorial on particle filters," *Journal of Mathematical Psychology*, vol. 73, pp. 140-152, 2016/08/01/ 2016, doi: https://doi.org/10.1016/j.jmp.2016.05.006.

[154] M. S. Arulampalam, S. Maskell, N. Gordon, and T. Clapp, "A tutorial on particle filters for online nonlinear/non-Gaussian Bayesian tracking," *IEEE Transactions on Signal Processing,* vol. 50, no. 2, pp. 174-188, 2002, doi: 10.1109/78.978374.

[155] R. B. Gopaluni, "A particle filter approach to identification of nonlinear processes under missing observations," *The Canadian Journal of Chemical Engineering,* vol. 86, no. 6, pp. 1081-1092, 2008.

[156] S. Maskell and N. Gordon, "A tutorial on particle filters for on-line nonlinear/non-Gaussian Bayesian tracking," *IEE Target Tracking: Algorithms and Applications (Ref. No. 2001/174),* pp. 2-1, 2002.

[157] S. Yin and X. Zhu, "Intelligent particle filter and its application to fault detection of nonlinear system," *IEEE Transactions on Industrial Electronics,* vol. 62, no. 6, pp. 3852-3861, 2015.

[158] M. Jouin, R. Gouriveau, D. Hissel, M.-C. Péra, and N. Zerhouni, "Particle filter-based prognostics: Review, discussion and perspectives," *Mechanical Systems and Signal Processing,* vol. 72-73, pp. 2-31, 2016/05/01/ 2016, doi: https://doi.org/10.1016/j.ymssp.2015.11.008.

[159] T. Li, M. Bolic, and P. M. Djuric, "Resampling methods for particle filtering: classification, implementation, and strategies," *IEEE Signal processing magazine,* vol. 32, no. 3, pp. 70-86, 2015.

[160] Y. Hu, P. Baraldi, F. Di Maio, and E. Zio, "A prognostic approach based on particle filtering and optimized tuning kernel smoothing," 2014, vol. 2, 1 ed.

[161] X. Wang, T. Li, S. Sun, and J. M. Corchado, "A survey of recent advances in particle filters and remaining challenges for multitarget tracking," *Sensors,* vol. 17, no. 12, p. 2707, 2017.

[162] Y. Zhang, L. Chen, Y. Li, X. Zheng, J. Chen, and J. Jin, "A hybrid approach for remaining useful life prediction of lithium-ion battery with Adaptive Levy Flight optimized Particle Filter and Long Short-Term Memory network," *Journal of Energy Storage,* vol. 44, p. 103245, 2021/12/15/ 2021, doi: https://doi.org/10.1016/j.est.2021.103245.

[163] J. A.-O. Elfring, E. Torta, and R. van de Molengraft, "Particle Filters: A Hands-On Tutorial. LID - 10.3390/s21020438 [doi] LID - 438," (in eng), no. 1424-8220 (Electronic).

[164] C. Snyder, "Particle filters, the "optimal" proposal and high-dimensional systems," 2011: Citeseer, pp. 1-10.

[165] S. Karppinen and M. Vihola, "Conditional particle filters with diffuse initial distributions," *Statistics and Computing,* vol. 31, no. 3, p. 24, 2021/03/03 2021, doi: 10.1007/s11222-020-09975-1.

[166] J. Yu, T. Yongli, C. Xiancha, and L. Wenjing, "Choice mechanism of proposal distribution in particle filter," in *2010 8th World Congress on Intelligent Control and*

Automation, 7-9 July 2010 2010, pp. 1051-1056, doi: 10.1109/WCICA.2010.5554874.

[167] Q. Zhang, B. Shi, and Y. Zhang, "Conditional importance sampling for particle filters," *Information Sciences*, vol. 501, pp. 388-396, 2019/10/01/ 2019, doi: https://doi.org/10.1016/j.ins.2019.06.026.

[168] M. S. Hussain, "Real-coded genetic algorithm particle filters for high-dimensional state spaces," 2014.

[169] W. A. Appiah, J. Busk, T. Vegge, and A. Bhowmik, "Sensitivity analysis methodology for battery degradation models," *Electrochimica Acta*, vol. 439, p. 141430, 2023/01/20/ 2023, doi: https://doi.org/10.1016/j.electacta.2022.141430.

[170] B. Saha and K. Goebel, "Battery data set," *NASA AMES prognostics data repository*, 2007.

[171] W. Li, H. Zhang, B. van Vlijmen, P. Dechent, and D. U. Sauer, "Forecasting battery capacity and power degradation with multi-task learning," *Energy Storage Materials*, vol. 53, pp. 453-466, 2022/12/01/ 2022, doi: https://doi.org/10.1016/j.ensm.2022.09.013.

[172] F. Calabrese, A. Regattieri, L. Botti, C. Mora, and F. G. Galizia, "Unsupervised Fault Detection and Prediction of Remaining Useful Life for Online Prognostic Health Management of Mechanical Systems," (in English), *Applied Sciences*, Technical report vol. 10, p. NA, 2020/06/15/

// 2020. [Online]. Available: https://link.gale.com/apps/doc/A638408961/AONE?u=googlescholar&sid=googleScholar&xid=e7ba0f84.

[173] J. M. Reniers, G. Mulder, and D. A. Howey, "Review and performance comparison of mechanical-chemical degradation models for lithium-ion batteries," *Journal of The Electrochemical Society*, vol. 166, no. 14, p. A3189, 2019.

[174] M. Guo, G. Sikha, and R. E. White, "Single-Particle Model for a Lithium-Ion Cell: Thermal Behavior," *Journal of The Electrochemical Society*, vol. 158, no. 2, p. A122, 2011, doi: 10.1149/1.3521314.

[175] B. Rajabloo, M. Désilets, and Y. Choquette, "Parameter estimation of single particle model using COMSOL Multiphysics® and MATLAB® optimization toolbox," 2015.

[176] H. Ekström and G. Lindbergh, "A Model for Predicting Capacity Fade due to SEI Formation in a Commercial Graphite/LiFePO₄Cell," *Journal of The Electrochemical Society*, vol. 162, no. 6, pp. A1003-A1007, 2015, doi: 10.1149/2.0641506jes.

[177] A. J. Crawford, D. Choi, P. J. Balducci, V. R. Subramanian, and V. V. Viswanathan, "Lithium-ion battery physics and statistics-based state of health model," *Journal of Power Sources*, vol. 501, p. 230032, 2021/07/31/ 2021, doi: https://doi.org/10.1016/j.jpowsour.2021.230032.

[178] F. B. Planella and W. D. Widanage, "A Single Particle Model with Electrolyte and Side Reactions for degradation of lithium-ion batteries," *Applied Mathematical Modelling,* 2022/12/10/ 2022, doi: https://doi.org/10.1016/j.apm.2022.12.009.

[179] S. J. An, J. Li, C. Daniel, D. Mohanty, S. Nagpure, and D. L. Wood, "The state of understanding of the lithium-ion-battery graphite solid electrolyte interphase (SEI) and its relationship to formation cycling," *Carbon,* vol. 105, pp. 52-76, 2016/08/01/ 2016, doi: https://doi.org/10.1016/j.carbon.2016.04.008.

[180] C. Kupper and W. G. Bessler, "Multi-Scale Thermo-Electrochemical Modeling of Performance and Aging of a LiFePO4/Graphite Lithium-Ion Cell," *Journal of The Electrochemical Society,* vol. 164, no. 2, p. A304, 2016/12/29 2017, doi: 10.1149/2.0761702jes.

[181] G. Ning and B. N. Popov, "Cycle Life Modeling of Lithium-Ion Batteries," *Journal of The Electrochemical Society,* vol. 151, no. 10, p. A1584, 2004/09/21 2004, doi: 10.1149/1.1787631.

[182] P. Ramadass, B. Haran, P. M. Gomadam, R. White, and B. N. Popov, "Development of First Principles Capacity Fade Model for Li-Ion Cells," *Journal of The Electrochemical Society,* vol. 151, no. 2, p. A196, 2004/01/08 2004, doi: 10.1149/1.1634273.

[183] I. Laresgoiti, S. Käbitz, M. Ecker, and D. U. Sauer, "Modeling mechanical degradation in lithium ion batteries during cycling: Solid electrolyte interphase fracture," *Journal of Power Sources,* vol. 300, pp. 112-122, 2015/12/30/ 2015, doi: https://doi.org/10.1016/j.jpowsour.2015.09.033.

[184] R. Fu, M. Xiao, and S.-Y. Choe, "Modeling, validation and analysis of mechanical stress generation and dimension changes of a pouch type high power Li-ion battery," *Journal of Power Sources,* vol. 224, pp. 211-224, 2013/02/15/ 2013, doi: https://doi.org/10.1016/j.jpowsour.2012.09.096.

[185] R. D. Deshpande and D. M. Bernardi, "Modeling Solid-Electrolyte Interphase (SEI) Fracture: Coupled Mechanical/Chemical Degradation of the Lithium Ion Battery," *Journal of The Electrochemical Society,* vol. 164, no. 2, pp. A461-A474, 2017, doi: 10.1149/2.0841702jes.

[186] W. Ai, B. Wu, and E. Martínez-Pañeda, "A coupled phase field formulation for modelling fatigue cracking in lithium-ion battery electrode particles," *Journal of Power Sources,* vol. 544, p. 231805, 2022.

[187] E. Bohn, T. Eckl, M. Kamlah, and R. McMeeking, "A Model for Lithium Diffusion and Stress Generation in an Intercalation Storage Particle with Phase Change," *Journal of The Electrochemical Society,* vol. 160, no. 10, p. A1638, 2013/07/27 2013, doi: 10.1149/2.011310jes.

[188] B. Wu and W. Lu, "A battery model that fully couples mechanics and electrochemistry at both particle and electrode levels by incorporation of particle

interaction," *Journal of Power Sources,* vol. 360, pp. 360-372, 2017/08/31/ 2017, doi: https://doi.org/10.1016/j.jpowsour.2017.05.115.

[189] Y. Dai, L. Cai, and R. E. White, "Simulation and analysis of stress in a Li-ion battery with a blended LiMn2O4 and LiNi0.8Co0.15Al0.05O2 cathode," *Journal of Power Sources,* vol. 247, pp. 365-376, 2014/02/01/ 2014, doi: https://doi.org/10.1016/j.jpowsour.2013.08.113.

[190] N. Legrand, B. Knosp, P. Desprez, F. Lapicque, and S. Raël, "Physical characterization of the charging process of a Li-ion battery and prediction of Li plating by electrochemical modelling," *Journal of Power Sources,* vol. 245, pp. 208-216, 2014/01/01/ 2014, doi: https://doi.org/10.1016/j.jpowsour.2013.06.130.

[191] X.-G. Yang, Y. Leng, G. Zhang, S. Ge, and C.-Y. Wang, "Modeling of lithium plating induced aging of lithium-ion batteries: Transition from linear to nonlinear aging," *Journal of Power Sources,* vol. 360, pp. 28-40, 2017/08/31/ 2017, doi: https://doi.org/10.1016/j.jpowsour.2017.05.110.

[192] J. Cannarella and C. B. Arnold, "The Effects of Defects on Localized Plating in Lithium-Ion Batteries," *Journal of The Electrochemical Society,* vol. 162, no. 7, p. A1365, 2015/04/28 2015, doi: 10.1149/2.1051507jes.

[193] H. Ge *et al.*, "Investigating Lithium Plating in Lithium-Ion Batteries at Low Temperatures Using Electrochemical Model with NMR Assisted Parameterization," *Journal of The Electrochemical Society,* vol. 164, no. 6, p. A1050, 2017/03/21 2017, doi: 10.1149/2.0461706jes.

[194] E. Walker, S. Rayman, and R. E. White, "Comparison of a particle filter and other state estimation methods for prognostics of lithium-ion batteries," *Journal of Power Sources,* vol. 287, pp. 1-12, 2015/08/01/ 2015, doi: https://doi.org/10.1016/j.jpowsour.2015.04.020.

[195] P. M. Attia, W. C. Chueh, and S. J. Harris, "Revisiting the t^{0.5} Dependence of SEI Growth," *Journal of The Electrochemical Society,* vol. 167, no. 9, p. 090535, 2020/01/07 2020, doi: 10.1149/1945-7111/ab8ce4.

[196] Q. Miao, L. Xie, H. Cui, W. Liang, and M. Pecht, "Remaining useful life prediction of lithium-ion battery with unscented particle filter technique," *Microelectronics Reliability,* vol. 53, no. 6, pp. 805-810, 2013/06/01/ 2013, doi: https://doi.org/10.1016/j.microrel.2012.12.004.

[197] Z. Cui, L. Wang, Q. Li, and K. Wang, "A comprehensive review on the state of charge estimation for lithium-ion battery based on neural network," *International Journal of Energy Research,* vol. 46, no. 5, pp. 5423-5440, 2022.

[198] J. Qu, F. Liu, Y. Ma, and J. Fan, "A neural-network-based method for RUL prediction and SOH monitoring of lithium-ion battery," *IEEE access,* vol. 7, pp. 87178-87191, 2019.

[199] B. Wu, S. Han, K. G. Shin, and W. Lu, "Application of artificial neural networks in design of lithium-ion batteries," *Journal of Power Sources,* vol. 395, pp. 128-136, 2018.

[200] S. Wang, P. Ren, P. Takyi-Aninakwa, S. Jin, and C. Fernandez, "A critical review of improved deep convolutional neural network for multi-timescale state prediction of lithium-ion batteries," *Energies,* vol. 15, no. 14, p. 5053, 2022.

[201] Y. Li, K. Li, X. Liu, Y. Wang, and L. Zhang, "Lithium-ion battery capacity estimation—A pruned convolutional neural network approach assisted with transfer learning," *Applied Energy,* vol. 285, p. 116410, 2021.

[202] S. Khaleghi *et al.*, "Online health diagnosis of lithium-ion batteries based on nonlinear autoregressive neural network," *Applied Energy,* vol. 282, p. 116159, 2021.

[203] H. Dong, X. Jin, Y. Lou, and C. Wang, "Lithium-ion battery state of health monitoring and remaining useful life prediction based on support vector regression-particle filter," *Journal of Power Sources,* vol. 271, pp. 114-123, 2014/12/20/ 2014, doi: https://doi.org/10.1016/j.jpowsour.2014.07.176.

[204] G. Crocioni, D. Pau, J. M. Delorme, and G. Gruosso, "Li-Ion Batteries Parameter Estimation With Tiny Neural Networks Embedded on Intelligent IoT Microcontrollers," *IEEE Access,* vol. 8, pp. 122135-122146, 2020, doi: 10.1109/ACCESS.2020.3007046.

[205] S. Luciani, S. Feraco, A. Bonfitto, and A. Tonoli, "Hardware-in-the-Loop Assessment of a Data-Driven State of Charge Estimation Method for Lithium-Ion Batteries in Hybrid Vehicles," *Electronics,* vol. 10, no. 22, doi: 10.3390/electronics10222828.

[206] T. L. Fantham and D. T. Gladwin, "Impact of cell balance on grid scale battery energy storage systems," *Energy Reports,* vol. 6, pp. 209-216, 2020/05/01/ 2020, doi: https://doi.org/10.1016/j.egyr.2020.03.026.

[207] X. Hu, C. Zou, C. Zhang, and Y. Li, "Technological Developments in Batteries: A Survey of Principal Roles, Types, and Management Needs," *IEEE Power and Energy Magazine,* vol. 15, no. 5, pp. 20-31, 2017, doi: 10.1109/MPE.2017.2708812.

[208] G. Dong, Z. Chen, J. Wei, and Q. Ling, "Battery Health Prognosis Using Brownian Motion Modeling and Particle Filtering," *IEEE Transactions on Industrial Electronics,* vol. 65, no. 11, pp. 8646-8655, 2018, doi: 10.1109/TIE.2018.2813964.

[209] A. E. Mejdoubi, A. Oukaour, H. Chaoui, H. Gualous, J. Sabor, and Y. Slamani, "State-of-Charge and State-of-Health Lithium-Ion Batteries' Diagnosis According to Surface Temperature Variation," *IEEE Transactions on Industrial Electronics,* vol. 63, no. 4, pp. 2391-2402, 2016, doi: 10.1109/TIE.2015.2509916.

Appendix A Battery Terminologies

A.1.1 Cell, Module and Pack

LiB cells are typically arranged in groups to form battery modules and packs and to achieve the desired high power. Batteries can be grouped in series and/or parallel; by connecting many cells in series, batteries provide the required terminal voltage by adding up the voltage potential of each cell. In a parallel configuration, the total ampere-hours can be added to achieve a higher capacity (Ah). For instance, a 2 MW/1MWh grid-connected LiB can be formed of 21,120 cells [206]. The configuration of the cells, either in series or parallel, is determined by economic, safety, and lifespan factors. Estimating the available energy and power is critical to the battery owner to control the battery's charge/discharge process and maintain battery lifetime.

A.1.2 Capacity of the LiBs

The battery's capacity is the most crucial aspect in the study of battery modelling. The battery's capacity can be defined as the amount of energy stored in a battery, typically measured in ampere-hours (Ah) or milliampere-hours (mAh).

A.1.3 C-rate

C-rate is an arbitrary metric used to quantify the charge/discharge rate relative to a LiB's maximum capacity. For instance, if the rated capacity of a LiB is 1 Ah, then a fully charged battery rated at 1C should provide 1 A for one hour. At 0.5C, the same battery should provide 500mA for two hours.

A.1.4 Depth of Discharge (DOD)

Depth of discharge is the proportion of the total energy stored in a battery that has been used, expressed as a percentage.

A.1.5 Cycle life

The number of times a battery can be charged and discharged before its capacity is significantly degraded.

A.1.6 State-of-Charge (SoC)

The SoC is the indicator of the amount of charge available in a battery compared to maximum battery capacity. The SoC can be estimated based on the average concentration of lithium ions in each electrode's solid particles.

A.1.7 State of Health (SoH)

The SoH is a measurement indicator of the current health level of battery performance compared to the battery's initial condition at the start of the battery's lifecycle. According to [207, 208], the SoH can be estimated based on the battery's capacity as it decreases or as its resistance rises. The battery's internal resistance is a significant factor in its capacity to function as a power source or sink. The battery's immediate usable power decreases as its resistance increases with time. Additionally, the battery loses Ah capacity as it ages, resulting in a decline in energy.

A.1.8 Remining Useful Life (RUL)

RUL is the term used for the quantity of cycle left between the present cycle until the battery's end of service (EoS), and this can vary from 70–80% of nominal capacity [209].

Appendix B Particle Filter Code

```
clear
close all
clc
rng(100)
way = 4;
% Decide the cycle from which prediction is to be started.
Future  Cycle=50;
csv_files = {'Cap05.csv', 'Cap06.csv', 'Cap018.csv'};
failure_threshold = 1.4;


for i = 1:length(csv_files)
   data1_df = load(csv_files{i});
   disp(['[INFO] Processing ', csv_files{i}]);
   disp(['Dataset shape: ', num2str(size(data1_df, 1)-1), '*', num2str(size(data1_df, 2))]);
   x = data1_df(2:end, 1);
   y = data1_df(2:end, 2);
   selection = 3;
   x_train = x(1:Future_Cycle);
   x_test  = x(Future_Cycle+1:end);
   y_train = y(1:Future_Cycle);
   y_test  = y(Future_Cycle+1:end);

   disp(['Number of training samples: ',   num2str(length(x_train))])
   disp(['Number of Prediction samples: ', num2str(length(x_test))])

   cita = 0.0001;
   wa   = 1;
   wb   = 0.000001;
   wc   = 10;
   wd   = 0.000001;

   li = [wa, wb, wc, wd];
   Q = zeros(4);
   F = eye(4);
   for i = 1:4
      Q(i, i)= li(i)*cita;
   end
```

```
R = 0.0001;
a = -4.037e-06  ;
b = 1.379;
c = 0.9888;
d = 0.04566878;

N = length(y);
M = 100;
X0 = [a b c d];
Xpf = zeros(selection, N);
for i = 1:selection
   Xpf(i, 1) = X0(i);
end
Xm = zeros(N, selection, M);

for i = 1:M
   for f = 1:selection
      Xm(1, f, i) = X0(f)+sqrt(Q(f, f))*normrnd(0, 1);
   end
end
Zm  = zeros(N, 1, M);
Zpf = zeros(1, N);
W   = zeros(N, M);

Zpf(1) = y(1);

for k = 2:N
   for i = 1:M
      for f = 1:selection
         Xm(k, f, i) = Xm(k-1, f, 1) + sqrt(Q(f, f))*normrnd(0, 1);
      end
   end

   sum = 0;
   for i = 1:M
      Zm(k, 1, i) = func1(k, Xm(k, 1, i), Xm(k, 2, i), Xm(k, 3, i));


      W(k, i) = exp(-(y(k)-Zm(k, 1, i))^2/2/R) + 1e-99;
      sum = sum + W(k, i);
   end
   for i = 1:M
      W(k, i) = W(k, i)/sum;
```

```
    end

    if way == 1
        outindex =  Stratified_resampling(W(k, :));
    elseif way == 2
        outindex =  Systematic_resampling(W(k, :));
    elseif way == 3
        outindex =  Multinomal_resampling(W(k,  :));
    else
        outindex =  Residual_resampling(W(k, :));
    end

    for i = 1:M
        for f =1:selection
            Xm(k, f, i) = Xm(k, f, outindex(i)+1);
        end
    end
    for i = 1:selection
        sum = 0;
        for f =1:M
            sum = sum + Xm(k, i, f);
        end
        sum = sum/M;
        Xpf(i, k) = sum;
    end
    Zpf(k) = func1(k, Xpf(1, k), Xpf(2, k),Xpf(3, k));
end

y_pred = Zpf(Future_Cycle+1:end);% - [0:0.04/(length(y_test)-1):0.04];
for i=1:length(y_pred)
    if y_pred(i) < failure_threshold
        mu = i + Future_Cycle;
        break
    end
end

sigma = 10
%    xz    = linspace(mu  - 30, x(end-20), 100);
  % yz    = 0.3*gaussian(xz,  mu,  sigma) + min(y  pred);
figure;
hold on
plot(x, y, 'b-')
plot(x_test,  y_pred, 'g-')
plot(x, failure_threshold*ones(size(y)),  'k-')
```

```
    plot(Future_Cycle*ones(size(y)), linspace(min(y_pred), max(y), length(y)), 'k-')
    %plot(xz, yz, 'r-')
    ylabel('Discharge_Capacity')
    xlabel('Cycle_Index')
    legend('true','pf', 'Thresh', 'pdf')
    grid on
    errors = [];
    for d = 1:length(y_pred)
        errors = [errors, (y_pred(d)-y_test(d))^2];
    end

    figure
    plot(x_test, errors)
    ylabel('Error')
    xlabel('Cycle_Index')
    legend('Error')
    grid on

end
%% ======================    FUNCTIONS    ======================

function y = gaussian(x, mu, sig)
    y = exp(-(x - mu).^2 / (2 * sig^2));
end


function cdf = get_cdf(weight)
    cdf = weight(1);
    for i = 2:length(weight)
        cdf = [cdf (weight(i)+cdf(i-1))];
    end
end
function y = func(x, a, b, c, d)
    y = a*exp(b*x)+c*exp(d*x);
end
function y = func1(x, a, b,c)
    y = a*(b*x)+c;
end
function out_index = Residual_resampling(weight)
    cdf = get_cdf(weight);
    N = length(weight);
    need_select = [];
    for i = 1:N
        if weight(i)<1/N
```

```
        need_select = [need_select, i-1];
    end
  end

  N    = length(weight);
  temp = 1/N*rand;

  for i = 1:N
    U(i) = temp+(i-1)/N;
  end


  out  index = zeros(100, 1);
  j = 0;

  for i = 1:N
    if j ~= N
      while j<N & U(i) > cdf(j+1)
        j = j + 1;
      end
    end

    if j<N
      out_index(i) = j;
    else
      out_index(i) = N-1;
    end
  end
end
```

Appendix C Smooth Particle Filter Code

```
clc, clear, close all

load('B0005.mat');
L = length(B0005.cycle);
type = {B0005.cycle.type}.';
s2 = 'discharge';
D = strcmp(type, s2);

for i = 1:L
   if D(i) == 1
      cap(i) = B0005.cycle(i).data.Capacity;
   end
end

cap = cap(cap>0);
cycle = length(cap);
plot(1:cycle, cap,'k-*')
xlabel('cycle'), ylabel('Capacity (Ah)'), grid on

% model
nth = 1;
tht = [2.5];
f = @(x,th) exp(-th)*x;
% f = @(x, th, )
g = @(x,th) x;
Q = @(th) 0.1;
R = @(th) .009;

T = length(cap);
y = cap';

%%

K = 168;
N = T;
thr = zeros(nth,K);

for iK = 1:K-1
```

```
    w = -Inf;
    while w == -Inf
        if iK == 1 %start with a feasible value
            thr(1) = log(rand);
        end
        [w, x_pf, wn_pf, a_pf] = particle_filter( N, @(x)...
            f(x,thr(:,iK)), @(x,th) g(x,thr(:,iK)), T, y,...
            Q(thr(:,iK)), R(thr(:,iK)), 1, 0);
    end
    obj_f = @(th) -log_likelihood(N, @(x) f(x,th), @(x)...
        f(x,thr(:,iK)), @(x) g(x,th), T, y, Q(th), Q(thr(:,iK)),...
        R(thr(:,iK)), x_pf, wn_pf, a_pf) ;
    options = optimoptions('fminunc','Algorithm','quasi-
newton','Display','none','OptimalityTolerance',0.01);
    thr(:,iK+1) = fminunc(obj_f,thr(:,iK),options);
    display(['Iteration ', num2str(iK), ', th = ',num2str(thr(1,iK+1))])
%     display('State ', num2str(x_pf))
end
function [ log_W ] = log_likelihood( N, f, q, g, T, y, Qf, Qq, R, x_pf, wn_pf, a_pf )

%LOG_LIKELIHOOD Function
new_log_w = zeros(T,N);
for t = 1:T
    for i = 1:N
        if t >= 2
            new_log_w(t,i) = log(mvnpdf(g(x_pf(:,i,t), t)',y(t,:),R))' + log(new_wn(a_pf(t,i))) -
log(wn_pf(t-1,a_pf(t,i))) + log(mvnpdf(x_pf(:,i,t)',f(x_pf(:,a_pf(t,i),t-1))',Qf))' -
log(mvnpdf(x_pf(:,i,t)',q(x_pf(:,a_pf(t,i),t-1))',Qq))';
        else
            new_log_w(t,i) = log(mvnpdf(g(x_pf(:,i,t), t)',y(t,:),R))';
        end
    end
%     new_log_w(t,:)
    new_wn = exp(new_log_w(t,:) - max(new_log_w(t,:)));
    new_wn = new_wn/sum(new_wn);

end

log_W = sum(log(1/N*sum(exp(new_log_w),2)));

end

function [ log_W, x_pf, wn_pf, a_pf, Zpf, Z_RUL] = particle_filter( N, f, g, T, y, Q, R, nx,
x_init, rul_cycle)
```

```
log_w = zeros(T,N);
wn_pf = zeros(T,N);
a_pf = zeros(T,N);
x_pf = zeros(nx,N,T);
Zpf = zeros(1,T);
Xpf = zeros(nx,T);
Z_RUL = zeros(1,T-rul_cycle-1);

Xpf_sum = zeros(4,1);
x_pf(:,:,1) = x_init(:,ones(N,1)) + Q*randn(nx,N);

Q_chol = chol(Q);

Zpf(1) = y(1);

for t = 1:T
%     t
   if t >= 2
      a_pf(t,:) = systematic_resampling(wn_pf(t-1,:),N);
%         a_pf(t,:) = Residual_resampling(wn_pf(t-1,:)) + 1;
%         a_pf(t,:)
      x_pf(:,:,t) = f(x_pf(:,a_pf(t,:),t-1)) + Q*randn(nx,N);
   end
%     x_pf(:,:,t)
%     for li = 1:N
% %         y(t,:)
% %         g(x_pf(:,li,t), t)'
%         log_w(t,li) = log(mvnpdf(g(x_pf(:,li,t), t)',y(t,:),R))';
%     end
%     log_w(t,:)

%     for i=1:N
%         log_w(t,i) = log(mvnpdf(g(x_pf(:,i,t),t)',y(t,:),R))';
%     end
%     wn_pf(t,:) = exp(log_w(t,:) - max(log_w(t,:)));
%     g(x_pf(:,:,t), t)
   for i = 1:N
      wn_pf(t,i) = exp(-(y(t,:)-g(x_pf(:,i,t),t))^2/2/R) + 1e-99;
   end
%
   wn_pf(t,:) = wn_pf(t,:)/sum(wn_pf(t,:));
```

```
    % compute sum of x_pf
%     Xpf_sum = zeros(4,1);
%     for i=1:N
%       Xpf_sum = Xpf_sum + x_pf(:,i,t);
%     end

    Xpf_sum = sum(x_pf(:,:,t), 2);
    Xpf(:,t) = Xpf_sum/N;

    % predicted capacitance
    if t >= 2
       Zpf(t) = g(Xpf(:,t),t);
    end

    if t >= rul_cycle %78
       rul_id = t-rul_cycle + 1;
       Z_RUL(rul_id) = RUL(Xpf(:,t), rul_cycle, t-rul_cycle);
%        Z_RUL(rul_id) = RUL(Xpf(:,t), rul_cycle, T-t);
    end
end

log_W = sum(log(1/N*sum(exp(log_w),2)));

end
function idx = systematic_resampling(W,N)
W = W/sum(W);
u = 1/N*rand;
idx = zeros(N,1);
q = 0;
n = 0;
for i = 1:N
    while q < u
       n = n+1;
       q = q + W(n);
    end
    idx(i) = n;
    u = u + 1/N;
end
function out_index = Residual_resampling(weight)
    weight = weight/sum(weight);
    cdf = get_cdf(weight);
    N   = length(weight);
    need_select = [];
```

```
    for i = 1:N
        if weight(i)<1/N
            need_select = [need_select, i-1];
        end
    end

    N    = length(weight);
    temp = 1/N*rand;

    for i = 1:N
        U(i) = temp+(i-1)/N;
    end

    out_index = zeros(N, 1);
    j = 0;

    for i = 1:N
        if j ~= N
            while j<N & U(i) > cdf(j+1)
                j = j + 1;
            end
        end

        if j<N
            out_index(i) = j;
        else
            out_index(i) = N-1;
        end
    end
end
```